A MODEL FOR TWO PHASE COCURRENT FLOW IN A PACKED BED

A thesis submitted for the degree of
Doctor of Philosophy
in the Faculty of Engineering
University of London

by

Arnold John Sheppard B.Sc.(Eng.) in Chem. Eng. London

Department of Chemical Engineering
and Chemical Technology
Imperial College of Science and Technology
London S.W.7.

July 1976

ABSTRACT

Previous studies of the pressure drop, liquid holdup and interfacial area during two phase upward cocurrent flow in beds of spherical particles have been interpreted in terms of a liquid distribution model. The single phase flow region is one extreme of this model where the predominant flow regime is gas and liquid travelling through separate pores within the packed bed. During two phase flow the gas and liquid phases flow mainly through the same pores.

The validity of these models has been assessed by an experimental study of the dispersion occurring in the liquid phase during its passage through the packed column. Several mathematical models of varying complexity have been developed to represent the liquid flow within the column. The parameters of these models have been determined by Transfer Function analysis of the responses to a pulse injection of dye tracer into the liquid phase.

Correlations based on dimensional analysis are given for the liquid dispersion and liquid holdup.

TO MADDY

ACKNOWLEDGEMENTS

The author wishes to thank Dr Paul Eisenklam D.Sc. for his direction of this work and for his encouragement throughout.

Facilities in the Department of Chemical Engineering and Chemical Technology were made available by kind permission of Professor A R Ubbelchde F.R.S. and Professor R W H Sargent.

Thanks are also due to the Workshop Technical staff for their help in the construction of the experimental apparatus.

Financial support in the form of a Science Research Council grant is gratefully acknowledged.

In particular, the author wishes to thank his wife Maddy for her love, encouragement and help towards finishing this work.

LIST OF CONTENTS

LIST OF FIGURES

LIST OF TABLES

NOMENCLATURE

All dimensions are in terms of SI Units

Fundamental quantities

Length	L	metre	m
Mass	M	kilogram	kg
Time	T	second	s
Temperature	θ	Kelvin	K

Derived quantities

Force	F	newton	$N = kg\ m\ s^{-2}$

Symbol	Definition	Dimensions
a	interfacial area per unit volume	L^{-1}
a_k	general coefficient in series solution (e.g. eq.4.31)	-
A	cross-sectional area of packed bed occupied by flowing liquid	L^2
A_e	exchange area per unit bed length	L
A_{sr}	cross-sectional area of packed bed occupied by stagnant liquid	L^2
b_k	general coefficient in Transfer Function representation by series solution (e.g. eq. 4.34)	-
B	pressure drop parameter in eq. A.6	-
C(t)	tracer concentration	-
C_{Ai}	concentration of component A at interface	ML^{-3}
C_{AV}	arithmetic mean solute concentration	ML^{-3}
C_{Bb}	bulk concentration of component B	ML^{-3}
$C_s(t)$	system forcing function	-
d_e	equivalent particle diameter	L
d_p	particle diameter	L
d_t	column diameter	L
D_{AS}	diffusivity of component A in solvent S	L^2T^{-1}
D_L	longitudinal Dispersion coefficient	L^2T^{-1}
e	bed voidage	-
e_i	step lengths in minimisation procedure	-
E	noise weighting function in eq. 5.21	-
f_r	friction factor	-
F(p)	theoretical system Transfer Function	-

Symbol	Definition	Dimensions
g	gravitational constant	LT^{-2}
$\underline{g}$	gradient vector in eq. 5.32	-
$g(t,k)$	impulse response	-
$G(p)$	experimental system Transfer Function	-
G_M	gas mass velocity	$MT^{-1}L^{-2}$
H	parameter for evaluating axially dispersed plug flow model in eq.5.11.	-
$\underline{\underline{H}}$	Hessian matrix	-
I_1	radiation count rate for packed bed containing air and water	counts T^{-1}
I_{11}	radiation count rate for packed bed containing air, water and carbon dioxide	counts T^{-1}
I_d	radiation count rate for dry empty column	counts T^{-1}
I_i	error integral at measurement position i in eq. 5.23.	counts T^{-1}
I_t	light intensity incident on photomultiplier	-
J	parameter for evaluating axially dispersed plug flow model in eq. 5.2.	-
k_1-k_9	constants	-
k_e	mass exchange coefficient	LT^{-1}
k_L	liquid phase mass transfer coefficient	LT^{-1}
k_r	reaction velocity constant	$M^{-1}L^3T^{-1}$
ℓ	characteristic packing length	L
L	distance between two measurement points	L
L_M	liquid mass velocity	$ML^{-2}T^{-1}$
L_v	liquid flow rate per unit volume of packed bed	T^{-1}
m_1-m_7	coefficients in split flow interaction model as in eq. 4.29.	-
$\bar{M}^r$	r^{th} weighted moment about the origin as in eq. 3.16	T^r
N_A	absorption rate of component A	$ML^{-2}T^{-1}$
N_D	Dispersion Number	-
N_T	Number of Transfer Units in stagnancy model	-
p	Laplace transform variable	T^{-1}
P	system pressure	$ML^{-1}T^{-2}$
ΔP	measured pressure gradient	$ML^{-2}T^{-2}$
ΔP_G	single phase gas frictional loss	$ML^{-1}T^{-2}$
ΔP_L	single phase liquid frictional loss	$ML^{-1}T^{-2}$
ΔP_{tp}	two phase frictional loss	$ML^{-1}T^{-2}$

Symbol	Definition	Dimensions
ΔP_{Gtp}	frictional loss for gas during two phase flow	$ML^{-1}T^{-2}$
ΔP_{Ltp}	frictional loss for liquid during two phase flow	$ML^{-1}T^{-2}$
P_e	Peclet Number	-
Q	parameter for evaluating axially dispersed plug flow model in eq. 5.4.	-
Re_G	gas Reynolds Number	-
Re^*_G	transitional gas Reynolds Number	-
Re_L	liquid Reynolds Number	-
Sc	Schmidt Number	-
t	time	T
T	specific time	T
T(p)	subsystem Transfer Function	-
u	mean void velocity	LT^{-1}
U	superficial velocity	LT^{-1}
v	noise on experimental curve	-
$\underline{v}$	parameter vector in optimisation routine	-
V	volumetric flow rate	L^3T^{-1}
x	axial distance	-
X_1	flow split parameter in split flow model	-
X_2	flow area parameter in split flow model	-
z	axial distance	L
α	stagnancy model parameter	-
γ	stagnancy model parameter	-
Δ	differential change	-
ρ	density	ML^{-3}
ϕ	holdup	-
μ	viscosity	$ML^{-1}T^{-1}$
χ	Lockhart Martinelli parameter	-
σ	standard deviation	-
ω	frequency of sinusoidal input	T^{-1}
τ	mean residence time	T

Superscripts

-	denotes Laplace transformed variable	-

Pre-Subscripts

e	error value
I	interstitial value
t	true value

Post-Subscripts

o	1st measurement point
1	2nd measurement point
f	general phase
G	gas phase
L	liquid phase
m	mixture value
s	source term
sr	stagnant region
tp	two phase

CHAPTER 1 INTRODUCTION

Generally it is commercial practice to operate packed towers for gas-liquid contacting with liquid flowing downwards under gravity and gas flowing upwards. In recent years there has been increasing interest in cocurrent operation. The capacity of columns operated cocurrently is not limited by flooding and the pressure drop at any specified values of the superficial gas and liquid velocities is less than in the case of a countercurrent column. The higher mean concentration driving force obtained during the countercurrent mode is unnecessary when gas absorption is accompanied by an irreversible reaction or in physical absorption and stripping applications where one equilibrium stage only is required for the separation.

For the design of a cocurrent gas-liquid contactor it is necessary to know for a given set of gas and liquid flowrates the pressure drop, liquid holdup, interfacial area and fluid flow regimes. Previous studies, described in detail in Chapter 2, have concentrated almost exclusively on the first three areas and a number of empirical correlations are available in the literature for determining these quantities.

Work in this Laboratory on the pressure drop, liquid holdup and interfacial area during upward cocurrent air-water flow through packed columns of spherical particles has suggested a liquid distribution model of the flow within the packed bed. Two extreme conditions of this model are single phase pore flow when the predominant gas and liquid flow is through separate channels, and two phase pore flow when both gas and liquid flow through the same channels. It should be possible to distinguish between these two extreme modes of flow from the dispersion exhibited by the liquid phase during its passage through the packed bed. In the single phase pore flow regime, changes in gas rate will have little effect on the liquid dispersion. Results similar to those reported for single phase liquid flow in a packed column should be found. In contrast, when both phases flow through the same pores, the gas rate must influence the liquid dispersion and generally an increase in liquid dispersion will occur due to the presence of the higher velocity gas phase.

The present study has been undertaken to provide data on liquid dispersion during upward cocurrent air-water flow and to assess the validity of the liquid distribution model. For this investigation a vertical column 101.6mm diameter x 1 m long was packed with 5mm diameter glass ballotini spheres

to a porosity of 35.6%. Air and water were introduced at the base of the column through a gas-liquid distributor. The range of Reynolds Numbers for the liquid and gas phases, based on the superficial fluid velocity and particle diameter, was 40 to 140 and 30 to 300 respectively. A tracer dye injected into the liquid stream entering the column was measured by a photomultiplier detector beyond the column exit. The measurements were repeated for two packed columns which differed in length by 0.835m. Differences between these two measurements were related to the dispersion occurring within the packed column. The liquid flow through the packed column was represented by three mathematical models of differing complexity. The parameters of these models were obtained by matching the theoretical and experimental Transfer Functions.

In considering the problems of analysing the passage of the gas through the packed bed a new method was developed to determine the Transfer Functions for systems where the fluid compressibility cannot be ignored.

Although the experimental results obtained in this study exhibited a fair degree of scatter they supported the concepts of the liquid distribution model. In particular, the Dispersion Numbers in the single phase and two phase regions were substantially different both in magnitude and in the way they were affected by variations in gas and liquid Reynolds Numbers. The two phase flow region occurring at high gas to liquid ratios was characterised by high axial dispersion and low liquid holdup. There was a significant gas rate effect on the liquid dispersion. Liquid dispersion in the single phase region approached the values found when liquid alone is flowing in the packed bed and was little influenced by the gas rate.

CHAPTER 2 A GENERAL REVIEW OF MODELS FOR TWO PHASE FLOW IN A PACKED BED

2.1 Flow patterns arising from visual definitions

The extensive work carried out on two phase flow in open pipes has greatly influenced subsequent investigations into two phase cocurrent flow in packed beds. Visual characterisation of various modes of flow encountered in horizontal and vertical pipes has been extended to cover packed beds. In pipes as many as seven regimes have been summarised by SCOTT (67). Although the situation is less complicated in packed beds, little agreement has been reached on either the terminology to be used or the boundaries of various flow regimes. WEEKMAN and MYERS (79) and TURPIN and HUNTINGTON (73) have both indicated in graphical form the limits of various regimes as functions of gas and liquid mass velocities, as shown in Fig.2.1 and 2.2 respectively. The general findings of WEEKMAN and MYERS (79) have subsequently been endorsed by CHARPENTIER et al (11).

Unstable transition regimes exist making a precise definition of these patterns extremely difficult when based on visual appearance alone. It is possible to have several flow patterns of the same basic phenomena which differ in visual appearance. However a change in appearance does not necessarily mean a significant change has occurred in the basic mechanism whereby momentum or material is transferred. If flow types are to be distinguished on the basis of the prevailing transport mechanism theoretical analyses and extensive data are necessary. For this reason many investigations have been limited to a visual classification. In subsequent discussions, following the suggestion of SCOTT (67) flow pattern will refer to visual classification and flow regime to flow behaviour capable of a more quantitative analysis.

WEEKMAN and MYERS (79) and TURPIN and HUNTINGTON (73) indicate three main flow patterns. The uncertainty of the boundary regions can be illustrated by comparing points on both graphs having identical gas and liquid mass velocities. Three sets of gas and liquid mass velocities were chosen such that each point fell inside the 'gas continuous' region of WEEKMAN and MYERS (79) (see Table 2.1 below). According to Fig.2.2 of TURPIN and HUNTINGTON (73) these points are in the 'bubble', 'slug' and 'spray' regions respectively. Also shown on these two Figures are points representing changes in flow mechanism according to SAADA(60) whose studies will be discussed in detail in Section 2.2.3.

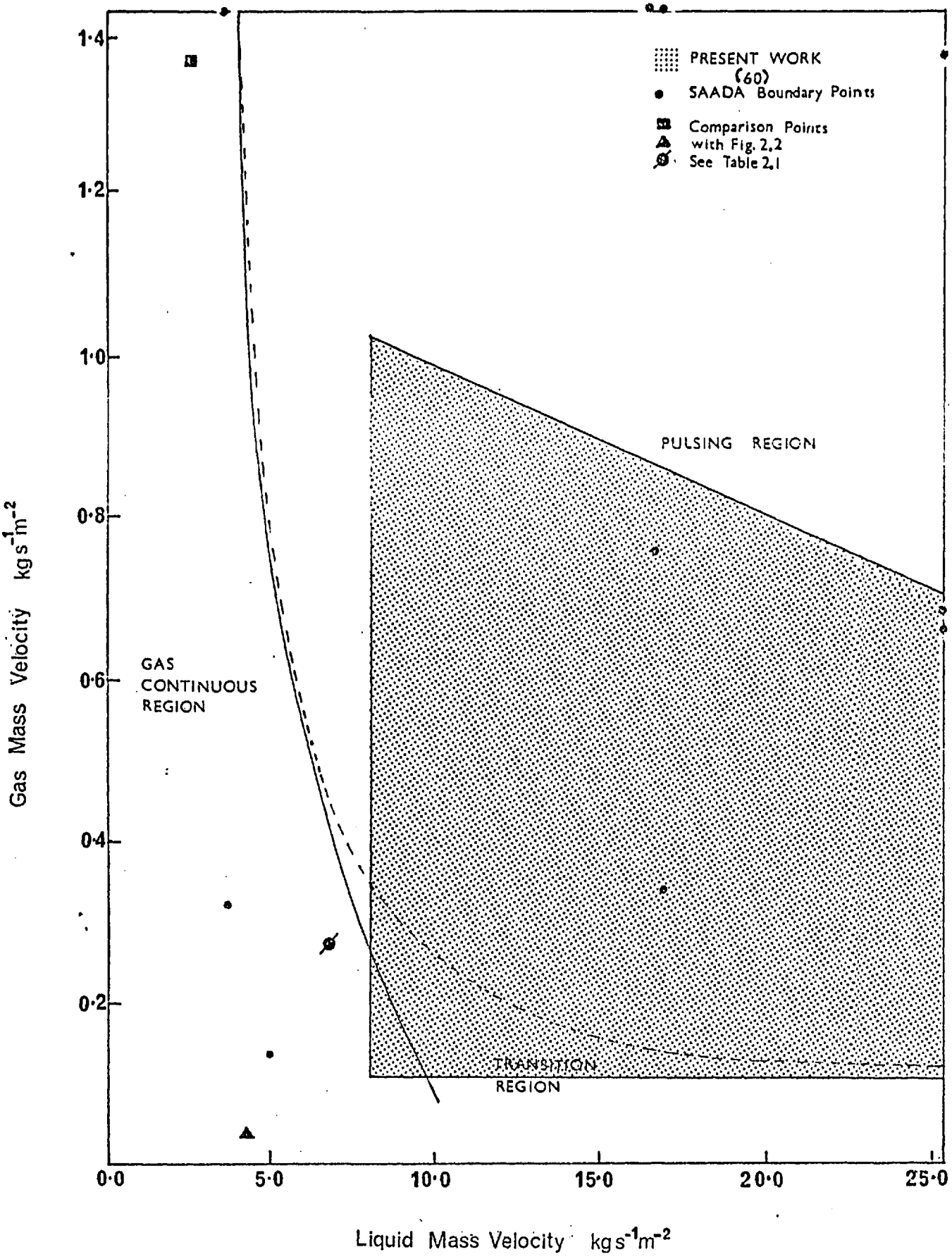

FLOW PATTERNS OF WEEKMAN & MYERS (79)

FIG. 2.1

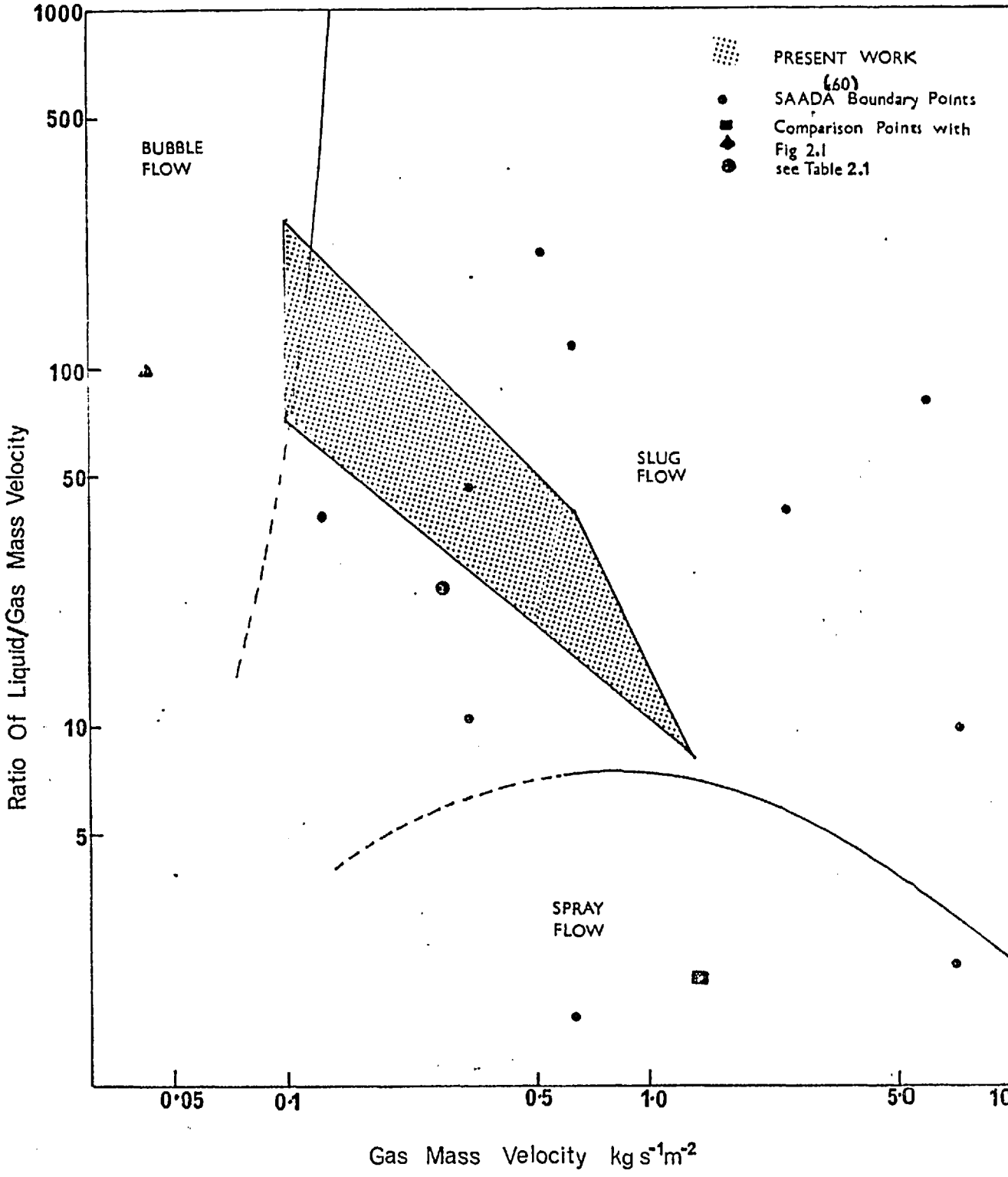

FLOW PATTERNS OF TURPIN & HUNTINGTON (73)

FIG 2.2

G_M Gas Mass Velocity $kgs^{-1}m^{-2}$	L_M Liquid Mass Velocity $kgs^{-1}m^{-2}$	L_{M/G_M}	Symbol	Classification	
				WEEKMAN (79)	TURPIN (73)
0.0405	4.05	100	▲	All in Gas	Bubble
0.27	6.75	25	◢	Continuous	Slug
1.35	2.70	2	■	Region	Spray

Table 2.1 Comparison Points between WEEKMAN & MYERS (79) and TURPIN & HUNTINGTON (73)

In spite of this apparent lack of agreement as to the exact regions where various flow patterns may be encountered, it is still possible to attempt some visual definitions.

2.1.1 Slug or Pulsing Flow

The pulses which traverse the length of the column consist of liquid with a sharp leading edge and a trailing edge which tapers off in the form of a wake. The overall flow pattern is that of a non-homogeneous region of variable density. This flow pattern exists mainly at high gas and liquid flowrates but can also occur at low flowrates when the rate of one fluid, particularly if liquid, is much greater than that of the other.

2.1.2 Gas or Bubble Flow

At low liquid flow rates the liquid appears to trickle over the packing as a laminar film. Depending on the gas rate, the gas will pass through the voids either as a set of discrete bubbles of varying size; termed displacement flow, or as a continuous fluid.

2.1.3 Spray Flow

At high gas rates a continuous flow pattern is formed in which the density difference has become far less noticeable than in slug flow. The liquid film is of gradually decreasing thickness due to the progressive liquid entrainment.

In both investigations, there was no abrupt change in the pressure driving force vs fluid flow rate curves on transition between flow patterns. The direction of flow; whether upward or downward, will modify these flow patterns especially for the bubble flow region. Fig.2.1 from WEEKMAN and MYERS (79) is for cocurrent downflow. TURPIN and HUNTINGTON (73) suggest that Fig.2.2 is applicable for both upward and downward flow. During upward flow slugging will exist over a wider range of gas velocities for a given liquid velocity. The greatest differences in flow patterns due to flow direction can be expected at liquid flow rates up to the point at which the bed is flooded. BEIMESCH and KESSLER(3) studied the phase distribution within the segregated slugs which occur during downward cocurrent flow in the pulsing region. They found that the liquid portion of the slug increased in length with increasing liquid rate although the fluid hydrodynamics remained essentially unchanged and the liquid holdup was affected by variations in the gas rate.

Up to the present, little effort has been spent, apart from the work of LARKINS et al (43), on developing correlations which can predict flow patterns from a knowledge of such system variables as gas and liquid mass velocities, fluid densities and viscosities. The effect of packing size and shape is also uncertain. HUTTON and LEUNG (37) have recently suggested that further work is needed to develop such quantitative flow pattern diagrams.

2.2 Flow Models from Pressure Drop and Liquid Holdup Studies

The number and type of flow regimes which have been suggested in the main reflect the manner in which the problem has been approached. Either a flow model was assumed a priori and the experimental results fitted to this model or else the nature of the experimental results enabled a plausible model to be proposed.

2.2.1 A priori models for pressure drop measurements

The influence of LOCKHART and MARTINELLI'S(47) work on two phase flow in open pipes has led both LARKINS et al (43) and WEEKMAN and MYERS (79) to extend this type of correlation, based on a friction factor approach to packed beds. By comparison with the results for open pipes they attempted to deduce whether a phase was in the laminar or turbulent flow regime. It was not possible to consider

the phase intermixing in any detail. The gas phase was assumed to restrict the liquid phase and the two phase friction loss was stated in terms of the single phase liquid flow.

$$\text{Hence} \quad \frac{\Delta P_{tp}}{\Delta z} = \frac{2 f_r \rho_L U_L^2}{\left[e\phi_L\right]^{k_1} d_p} \qquad \ldots\ldots\ldots \quad (2.1)$$

where ΔP_{tp}	=	two phase friction loss	$ML^{-1}T^{-2}$
Δz	=	axial distance measured vertically	L
f_r	=	friction factor	
ρ_L	=	liquid density	ML^{-3}
U_L	=	superficial liquid velocity	MT^{-1}
e	=	bed voidage	
ϕ_L	=	liquid holdup i.e.fraction of free flow area occupied by the liquid	
d_p	=	particle diameter	L

The Blasius representation was used for the friction factor such that:

$$f_r = {}^{k_2}/_{Re_L}{}^{k_3}$$

where the liquid Reynolds Number Re_L is given by:

$$Re_L = \frac{\rho_L U_L d_p}{\mu_L \left[e\phi_L\right]^{k_4}} \qquad \ldots\ldots\ldots \quad (2.2)$$

where μ_L = liquid viscosity $\qquad ML^{-1}T^{-1}$

and k_1-k_4 are constants.

$$\text{Then } \Delta P_{tp} = \phi_L^{k_4 k_3 - k_1} \Delta P_L = (1 - \phi_L)^{k_4 k_3 - k_1} \Delta P_G \qquad \ldots\ldots \quad (2.3)$$

Where ΔP_L and ΔP_G are the single phase friction losses as given by the ERGUN (21) equation for single phase flow in the same bed.

The functional relationship which fitted the data the best was:

$$\log \left\{ \frac{\frac{\Delta P_{tp}}{\Delta z}}{\frac{\Delta P_L}{\Delta z} + \frac{\Delta P_G}{\Delta z}} \right\} = \frac{0.416}{(\log \chi)^2 + 0.666} \qquad \text{for } 0.05 < \chi < 30$$

$$\ldots\ldots\ldots (2.4)$$

where χ^2 is defined as $\left[\frac{\Delta P_L}{\Delta z} \Big/ \frac{\Delta P_G}{\Delta z}\right]$ in the LOCKHART-MARTINELLI(47) manner. Experimentally ΔP_{tp} was determined from:

$$\Delta P_{tp} = \Delta P + \rho_m \, g \, \Delta z \quad \text{for downward flow} \qquad \ldots\ldots \qquad (2.5)$$

ΔP was the measured pressure gradient and ρ_m was interpreted as the density of the mixture flowing within the bed.

The results obtained using eq.2.4 had a standard deviation of ±13% and suggested a laminar mode for both phases when compared with the open pipe curves of LOCKHART and MARTINELLI(47). WEEKMAN and MYERS(79), however, found agreement with the turbulent curves. Most probably this difference was accounted for by the use of an homogeneous or mean density which neglected the significant amount of liquid which was supported by the packing. In a later study REISS(57) showed that even if the density term was neglected, the majority of the data were within the 50% confidence limits of the LARKINS(43) equation. If a two phase packed bed system was analysed by an energy, rather than a force balance, CHARPENTIER(11) et al found the form of the LARKINS(43) empirical equation was suitable for trickle flow conditions. When the velocities are equal in both phases then the same equation resulted from using either approach.

SWEENY(71) has criticised the homogeneous flow model of LARKINS(43) et al because the resulting dimensionless groups involve only single phase flow properties. In his analysis, which again is based on the ERGUN(21) equation, the liquid was assumed to flow uniformly over the packing surface and that both gas and liquid were continuous but separate. The frictional pressure drop was based on the liquid velocity with respect to the packing surface using the commonly accepted relationship:

$$u_L = \frac{U_L}{e\phi_L} \qquad \ldots\ldots\ldots \qquad (2.6)$$

modified to account for the presence of a second phase. This average void velocity although useful in many situations can be criticised in pressure drop analyses in that it may bear little relation to the component of the interstitial velocity which is responsible for the drag on the packing surface.

The ratio of frictional pressure loss for liquid when in two phase flow ΔP_{Ltp} to that when flowing alone ΔP_L was shown by SWEENY(71) to be:

$$\frac{\Delta P_{Ltp}}{\Delta P_L} = \frac{1}{\phi_L^3} \quad \ldots\ldots \quad (2.7)$$

The equivalent expression for the gas phase was:

$$\frac{\Delta P_{Gtp}}{\Delta P_G} = \frac{k_5}{\phi_G^3} \quad \ldots\ldots \quad (2.8)$$

where k_5 was a complex function of the system variables but numerically equal to unity in most situations. After equating pressure drops in both phases the following equation was obtained for the total pressure drop ΔP :

$$\left[\frac{\Delta P_L}{\Delta P + \rho_L g \Delta z}\right]^{1/3} + \left[\frac{\Delta P_G}{\Delta P + \rho_G g \Delta z}\right]^{1/3} = 1 \quad \ldots\ldots \quad (2.9)$$

SWEENY (71) found that eq.2.9 and that of LARKINS(43) nearly always agreed even though they were based on different models.

REYNIER and CHARPENTIER (58) also used the ERGUN(21) equation in a stratified pore model to estimate liquid holdup in cocurrent gas/liquid downflow. This model assumed that gas and liquid flowed through the same pores but no account was taken of any frictional pressure drop at the interface. The authors claimed reasonable agreement with the experimental liquid holdup and pressure gradient results of TURPIN and HUNTINGTON(73).

HUTTON and LEUNG (37) extended the model of BUCHANAN(7) to include the effect of pressure gradient. In this model the liquid is assumed to run down inclined surfaces of length equal to a piece of packing and lose a fraction of its kinetic energy at the end of every such surface. The following relationship was developed:

$$U_L = k_6 \phi_L \ell^{1/2} \left\{\frac{1}{\rho_L}\left[\frac{dP}{dz}\right] - g\right\}^{1/2} \quad \ldots\ldots \quad (2.10)$$

where ℓ = characteristic packing length

k_6 = shape factor

Thus for a given gas-liquid system and a specific packing the liquid holdup ϕ_L depended only on the liquid velocity U_L and the pressure gradient $\frac{dP}{dz}$. The pressure gradient was again correlated by a form of the ERGUN(21) equation.

The above correlations resort to the ERGUN(21) equation for estimations of the single phase frictional pressure gradient for a phase, f, flowing alone in a similar packed bed.

$$\text{Thus} \quad \frac{\Delta P_f}{\Delta z} = \frac{\rho_f \, u_f^2}{d_p} \left[k_7 + \frac{k_8 \mu_f}{\rho_f u_f d_p} \right] \qquad \ldots\ldots \qquad (2.11)$$

This equation is strongly dependent on the experimentally determined constants k_7 and k_8 for its accuracy.

The final work reviewed is that of TURPIN and HUNTINGTON (73) who, instead of replacing the friction factor f_r by a function of the liquid Reynolds Number, obtained the following functional relationship:

$$\log_e f_r = 8.0 - 1.12 \log_e k_9 - 0.0769 (\log_e k_9)^2 + 0.0152 (\log_e k_9)^3 \qquad \ldots\ldots\ldots \qquad (2.12)$$

$$\text{where} \quad k_9 = \frac{Re_G^{1.1667}}{Re_L^{0.767}}$$

There seems little justification for the form of eq. 2.12 except that it approximates the normally accepted shape for friction factor relationships in pipes.

The two phase pressure drop was obtained from:

$$f_r = \frac{\frac{\Delta P}{\Delta z}}{2\rho_G U_G^2} d_e \qquad \ldots\ldots\ldots \qquad (2.13)$$

where the equivalent diameter d_e is given by:

$$d_e = {}^2/_3 \left[\frac{e}{1-e} \right] d_p$$

In conclusion it seems clear that pressure drop data, when analysed in this manner cannot be used to distinguish between models. It makes little difference whether the two phases are assumed to flow through the packed bed in the same pores or in separate identifiable channels.

2.2.2 Pressure Drop Data Plotted with Linear Coordinates

WEN et al (80) proposed three regimes of flow:

(i) Channeled flow at low liquid and gas rates without the necessary turbulence to mix the phases into an homogeneous pseudophase. The liquid trickled over the packing whilst the higher velocity gas stream bypassed the liquid.

(ii) At high gas rates but moderate liquid rates the flow regime was assumed to be thoroughly dispersed liquid throughout a continuous gas phase.

(iii) At high liquid rates the gas is assumed to be dispersed through the liquid.

There is a significant difference between region (i) and the other regions in that the former has separate phases whilst the other regions assume similar conditions within all the voids. This concept has been expressed more quantitatively by EISENKLAM and FORD (20). WEN(80) derived functional relationships between pressure drop and fluid flow rates for all regions; those for regions (ii) and (iii) being almost identical.

2.2.3 Pressure Drop Data Plotted with Logarithmic Coordinates

When data have been plotted on log-log coordinates break points have been found at which the constant liquid rate lines change slope. MCILVROID(49) in 1956 reported two distinct zones. The lower zone was pulsating flow occurring at high liquid to gas ratios. The other zone at high gas to liquid rates could be sub-divided depending on whether or not the column was flooded. This data may be unreliable in that both wall and end effects may be present since the measurements were taken in a 51 mm diameter column using 4 mm and 6 mm beads over a packing height of only 0.114m. Little was inferred about the possible flow regimes within each zone.

FORD(22), although concerned with upward flow, found similar zones and suggested possible flow mechanisms for regions above and below the break point in terms of a liquid distribution model. Two distinct regimes of flow termed single phase pore flow and two phase pore flow were proposed. In single phase pore flow gas and liquid

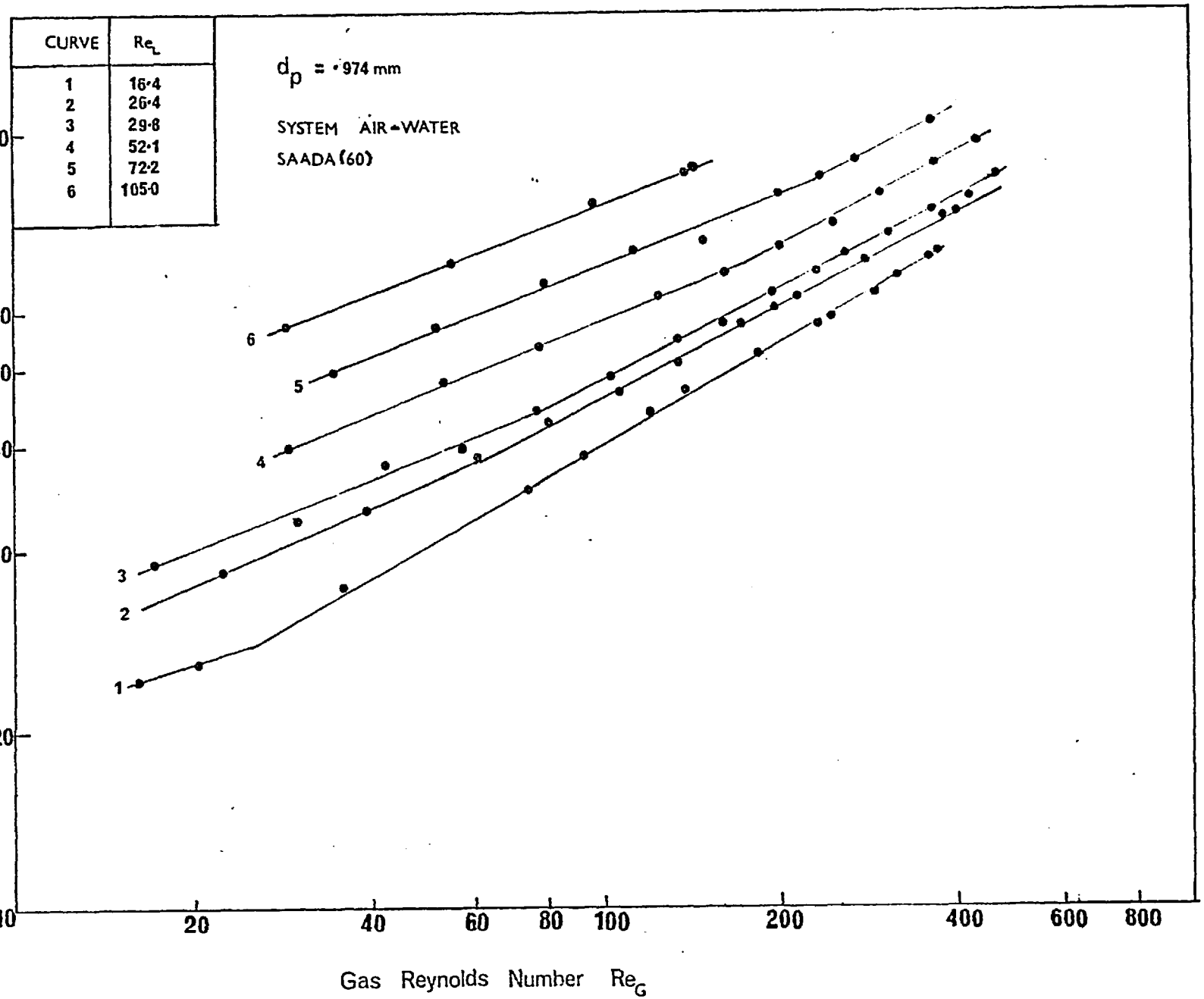

EFFECT OF GAS RATE ON TWO PHASE PRESSURE DRIVING FORCE

FIG 2.3

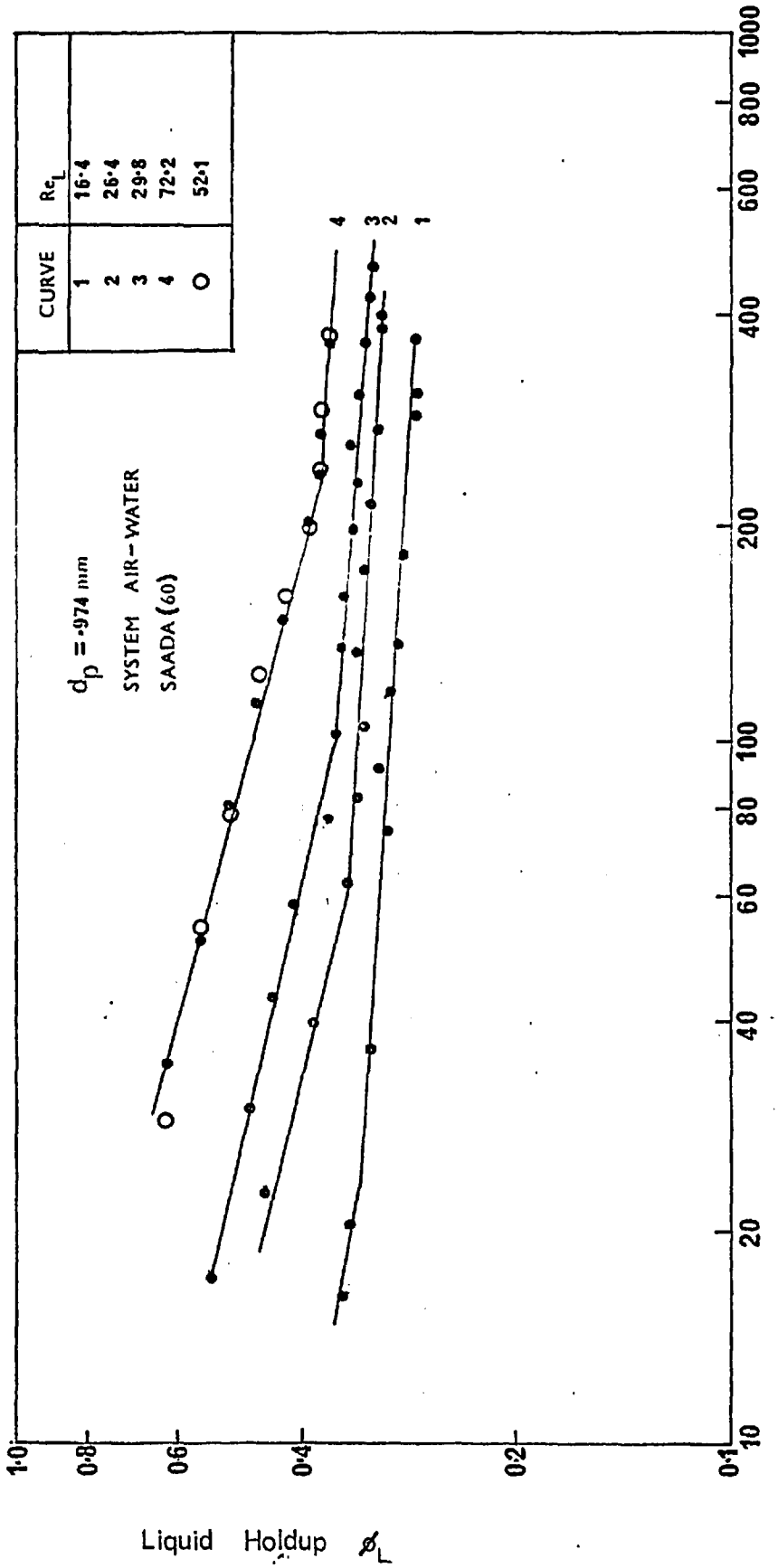

EFFECT OF GAS RATE ON LIQUID HOLDUP AT VARIOUS LIQUID FLOW RATES

FIG 2.4

have separate flow channels, although there might be some liquid flow through the pores in which the gas flow was dominant. In two phase pore flow both fluids travel in the same pores in either core or displacement flow. The dominant regime was determined from the relative flow rate curve of the liquid as a function of the liquid holdup at various pressure drops. The liquid holdup at the break point was found to be almost constant at 43% ± 3% for the reported values of Gas Reynolds Number.

SAADA(60) has since shown analytically from the reported saturation correlations of FORD(22) that this liquid holdup had to vary and verified his findings experimentally as shown in Fig.2.3. The pressure drop measurements of SAADA(60) given in Fig.2.4 also show break or transition points. These break points occur at the same Gas Reynolds Number for any particular liquid flow rate as in the holdup curves. This agreement was taken to represent a definite change in flow regime.

WEN et al (80) have also found these transition points, but suggest that the use of data with a non zero intercept produces a skewed log-log curve which erroneously indicates the presence of more than one flow regime.

EISENKLAM and FORD(20) pointed out that it is better statistically to represent this pressure drop data by two distinct lines of different slope meeting at a break point than by one curve drawn through all the data. This argument only holds however if the data should in fact be correlated linearly when using log-log coordinates. The justification for using simple power law correlations often arises as a result of dimensional analysis of the system under consideration (see section 2.2.4).

SAADA(60) suggested the following relationship for determining the Gas Reynolds Number at the break point, termed the transitional Reynolds Number Re_G^* :

$$Re_G^* = 0.44\ Re_L^2 \left[\frac{d_p}{d_t}\right]^{0.38} \qquad \ldots\ldots\ldots \qquad (2.14)$$

As shown in Fig.2.5 this relationship does not satisfactorily correlate all the data. Reanalysis of the transitional data by the present author yields the correlation:

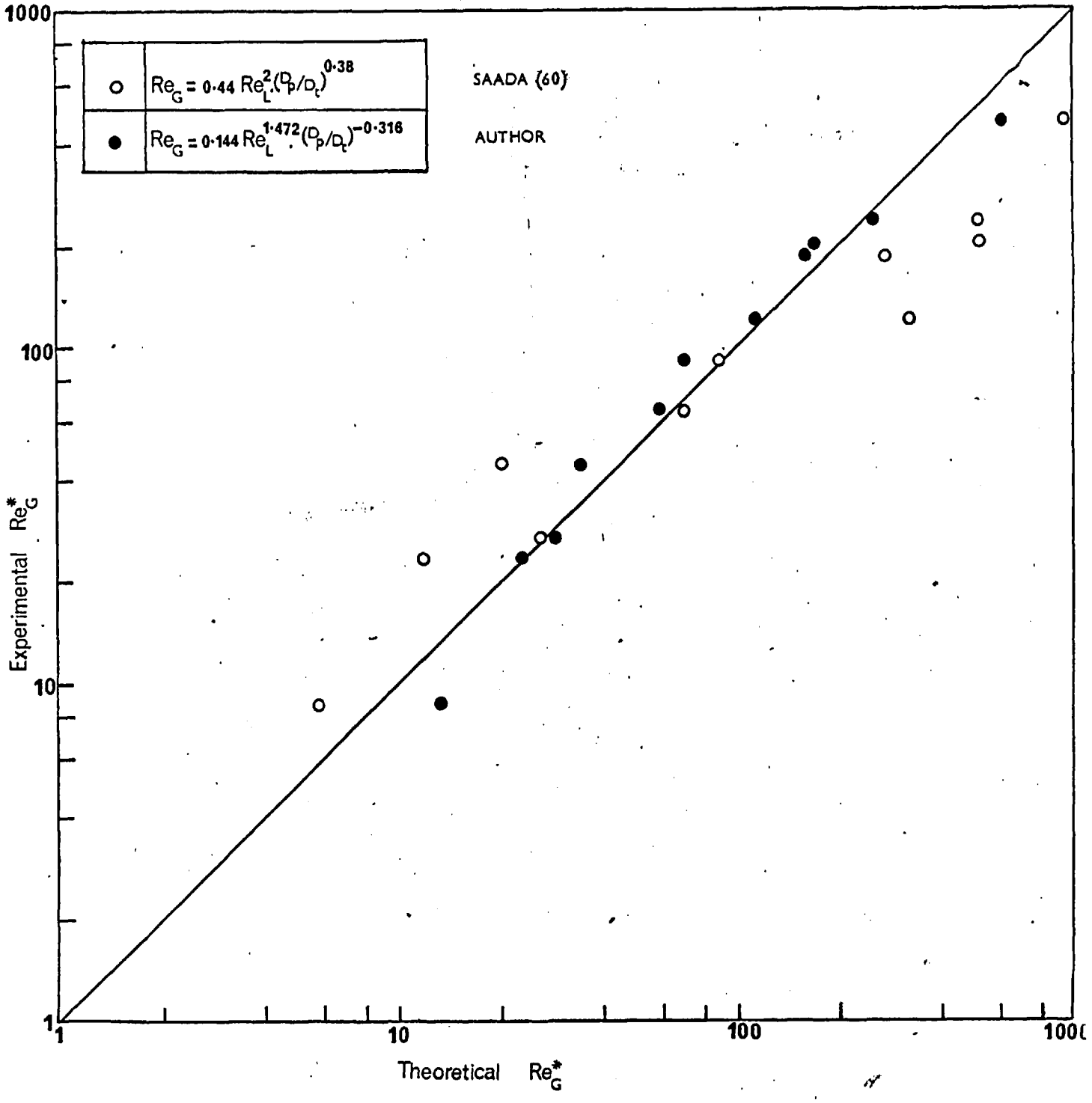

CORRELATIONS FOR TRANSITION GAS REYNOLDS NUMBER RE^*_G

FIG 2.5

$$Re_G^* = 0.144\ Re_L^{1.472}\ (d_p/d_t)^{-0.316} \quad \ldots\ldots\ (2.15)$$

It has been suggested that the transition point might be analogous to the phenomenon of flooding which occurs in counter-current flow. A plot of the data on a similar basis to that used by LOBO et al(46) to determine the onset of flooding is shown in Fig.2.6. Break points were not found by other workers because all their results were limited to the two phase region and, according to SAADA(60), did not cross the boundary line linking the transition points. However, there is some doubt as to the accuracy of such a boundary curve. A reasonable correlation of the transition points was obtained by SAADA(60) even though his ordinate of $2.45 \times 10^{-5}\ Re_G^2 d_p^{-2}$ was incorrect. The correct expression can be developed from the original work by LOBO et al (46) and is $2.39 \times 10^{-6}\ Re_G^2 d_p^{-3}$ as shown in Fig.2.6. Results given by SAADA(60) for particle sizes other than 0.974mm in diameter are therefore incorrectly plotted. In Figs. 2.1, 2.2 and 2.6 the experimental universe of the present work is indicated. Assuming the extrapolation of the boundary region shown in Fig.2.6 is valid the present results encompass both the single phase and two phase regions.

2.2.4 Correlations derived through Dimensional Analysis

Correlations obtained by fitting regression equations to a set of data are strictly only valid within the experimental universe from which the data were obtained. Although usually based on no flow model as such, these correlations are useful in that, through dimensional analysis, the important system parameters are emphasised.

FORD(22) and SAADA(60)have both given correlations for their liquid distribution model to represent flow conditions within the two distinct flow regimes of single phase and two phase pore flow.

For two phase pore flow FORD(22) suggested for 1 mm diameter spheres:

$$\frac{\Delta P}{\rho_L g \Delta z} = 0.0407\ Re_L^{0.29}\ Re_G^{0.57} \left[\mu_L/\mu_G\right]^{0.28} \quad \ldots\ (2.16)$$

SAADA(60), although restricted to an air-water system, varied the packing size to determine the effect of the group d_t/d_p. The resulting correlation was:

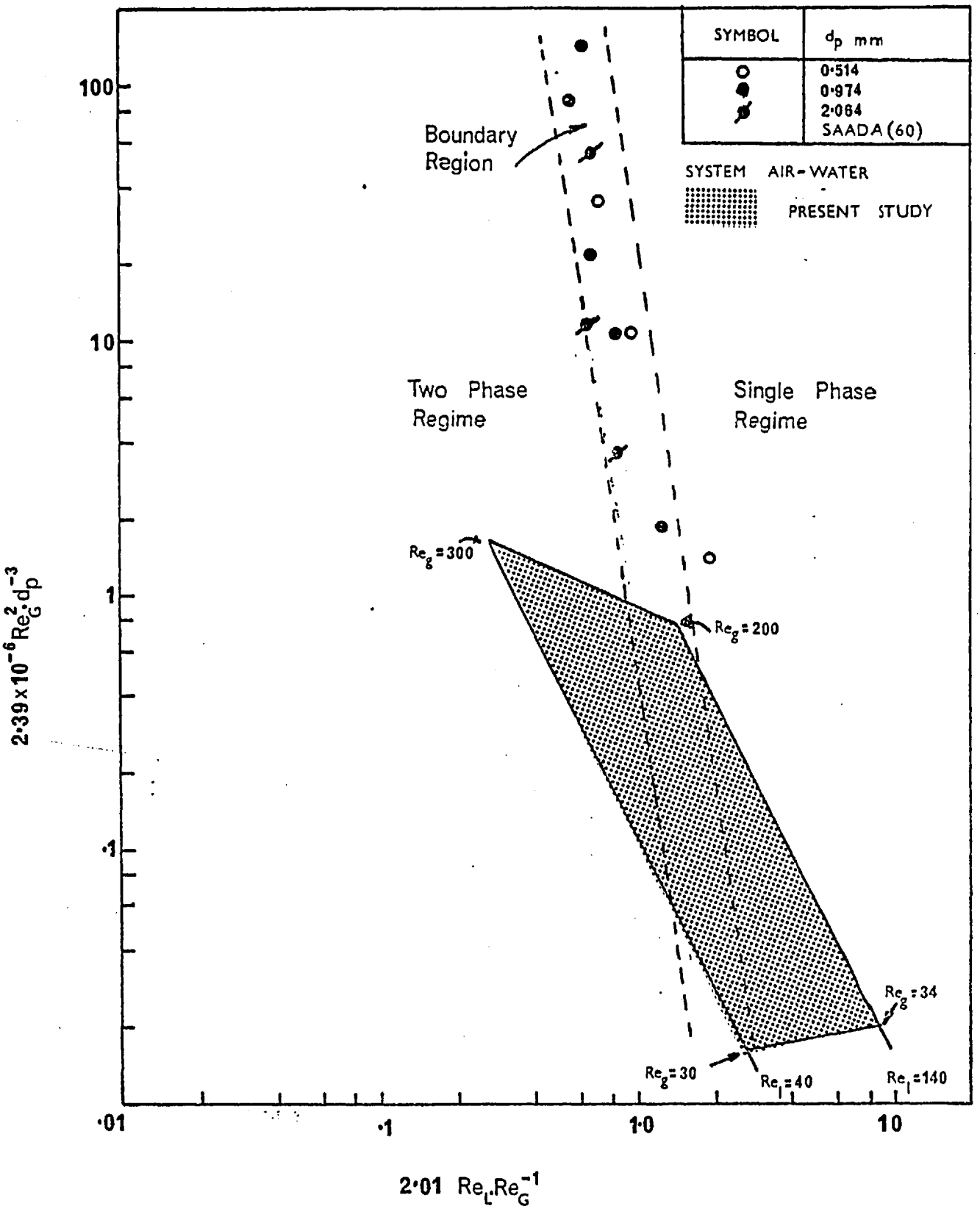

TRANSITION BOUNDARY BETWEEN FLOW REGIMES

FIG 2.6

$$\frac{\Delta P}{\rho_L g \Delta z} = 0.027\ Re_L^{0.35}\ Re_G^{0.51} \left[d_t/d_p\right]^{1.15} \quad .... \quad (2.17)$$

In single phase flow the corresponding equations were:

$$\frac{\Delta P}{\rho_L g \Delta z} = 0.485\ Re_L^{0.67}\ Re_G^{0.3} \left[\frac{\mu_L}{\mu_G}\right]^{0.8} \quad ... \quad (2.18)$$

$$\text{and } \frac{\Delta p}{\rho_L g \Delta z} = 0.024\ Re_L^{0.6}\ Re_G^{0.39} \left[d_t/d_p\right]^{1.1} \quad ... \quad (2.19)$$

The dependence of pressure drop on the gas and liquid Reynolds Numbers is in fair agreement between the two sets of equations even though there is a wide discrepancy between the transition points reported by the two workers.

2.3 Model Evaluation by Interfacial Area Measurements

The break points in the pressure drop and holdup measurements of both FORD(22) and SAADA(60) have been interpreted by them as representing a change in flow pattern which should affect the gas-liquid interfacial area. SAADA(62) by undertaking both physical and chemical absorption studies within the same column determined independent values for both the interfacial area a and the liquid phase mass transfer coefficient k_L. The interfacial area results shown in Fig.2.7 were obtained for carbon dioxide absorption in sodium hydroxide solutions and exhibit almost identical break points to those found in the previous pressure drop and holdup studies. The absolute value of these results are open to doubt as the following critical appraisal indicates.

Both DANCKWERTS(17) and ASTARITA(2) show that the absorption rate N_A when a chemical reaction occurs in the 'fast regime' can be expressed by:

$$N_A a = a(k_r C_{Bb} D_{AS})^{\frac{1}{2}} C_{Ai} \quad ..... \quad (2.20)$$

The conditions for a fast reaction regime are:

$$(k_r C_{Bb} D_{AS})^{\frac{1}{2}} << \frac{k_L C_{Bb}}{2 C_{Ai}} \quad ..... \quad (2.21)$$

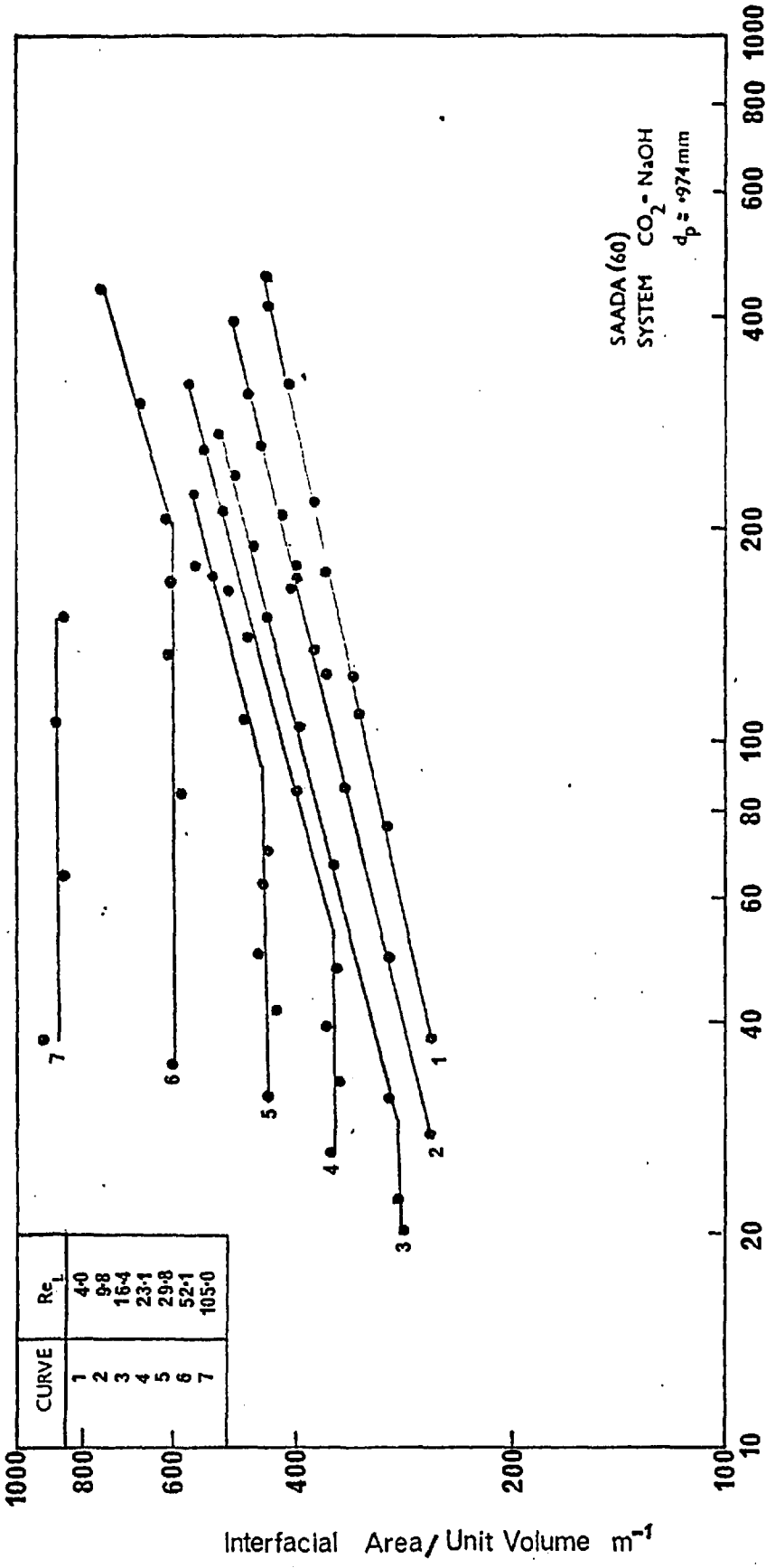

EFFECT OF GAS RATE ON GAS/LIQUID INTERFACIAL AREA AT VARIOUS LIQUID FLOW RATES

FIG 2.7

where for the CO_2/NaOH system :

k_r	is the reaction velocity constant	$M^{-1}L^3T^{-1}$
C_{Bb}	is the bulk concentration of sodium hydroxide	ML^{-3}
D_{AS}	is the diffusivity of CO_2 in the NaOH solution	L^2T^{-1}
C_{Ai}	is the concentration of CO_2 at the interface	ML^{-3}

SAADA(62) related the interfacial concentration C_{Ai} to the partial pressure of carbon dioxide in the bulk of the gas by Henry's Law neglecting the gas phase resistance. This assumption was based on the findings of YOSHIDA and MIURA(82) that the gas phase resistance in the CO_2/NaOH system was less than 10% of the overall resistance.

The average mass transfer rate was determined from eq. 2.20 using the mean values of C_{Bb} and C_{Ai} between the two extreme sampling positions within the column.

The experimental mass transfer rate in both chemical and physical absorption studies was determined from:

$$N_A a = L_v C_{av} \quad \ldots\ldots\ldots \quad (2.22)$$

where L_v is the liquid flow rate per unit volume of packed bed T^{-1}

C_{av} is the arithmetic mean concentration of solute between the two measuring points 1 and 2.

This expression is incorrect and should be replaced by:

$$N_A a = L_v (C_2 - C_1) \quad \ldots\ldots\ldots \quad (2.23)$$

The values of interfacial area reported are therefore liable to large inaccuracies.

For physical absorption SAADA(62) defined the mass transfer rate as:

$$N_A a = k_L a (C_{Ai} - C_{Ab}) \quad \ldots\ldots\ldots \quad (2.24)$$

where C_{Ab} is the bulk concentration of CO_2 in the water.

To evaluate k_L, the interfacial area was taken to be the same for both physical and chemical absorption. When the resistance to mass transfer is mainly due to the liquid phase, the age distribution of surface elements is of the greatest importance. In physical absorption surface elements of large age contribute very little to the mass transfer since they become saturated with solute. An 'average' interfacial area could therefore have little resemblance to the actual geometric area of the gas-liquid interface. In the fast regime in chemical absorption the absorption rate is almost independent of the age of surface elements. Thus the values determined for interfacial areas will not necessarily be the same in physical and chemical absorption studies even though the hydrodynamic conditions are identical. ASTARITA(2) has shown that if the chemical reaction occurs in the 'instantaneous' regime the interfacial areas will however be the same.

The condition for this regime is:

$$\left[k_r C_{Bb} D_{AS}\right]^{\frac{1}{2}} >> \frac{k_L C_{Bb}}{2 C_{Ai}} \qquad \ldots\ldots \qquad (2.25)$$

The concentration of carbon dioxide dissolved in the water, during the physical absorption studies was determined by a new radiological technique to overcome the problem of withdrawing liquid samples from the packed bed at elevated pressures. It is not clear what concentration SAADA(61) assumed this technique measured since the concentrations so determined were used in eq. 2.22 at the same time as the concentration of CO_2 in the bulk of the liquid needed in eq.2.24 was taken as zero.

The concentration of carbon dioxide in the liquid phase was defined as the moles of carbon dioxide per unit volume of solution, C_A, and determined from the relationship:

$$\frac{\text{moles of solute}}{\text{volume of solution}} = \frac{\text{moles of solute + moles of solvent}}{\text{volume of solution}} - \frac{\text{moles of solvent}}{\text{volume of solution}}$$

$$\text{or} \quad \frac{C_A}{\rho_s} = \frac{\rho_{ss}}{\rho_s} - 1 \qquad \ldots\ldots \qquad (2.26)$$

It was shown(61) that $\frac{\rho_{ss}}{\rho_s}$ could be determined from the equation:

$$\frac{\rho_{ss}}{\rho_s} = \frac{\log_e \left\{I_{11}/I_d\right\}}{\log_e \left\{I_1/I_d\right\}} \quad \ldots\ldots \quad (2.27)$$

where I_d = radiation count rate for dry empty column (counts min^{-1})

I_1 = radiation count rate for air + water in (")
packed column

I_{11} = radiation count rate for air + water + CO_2 (")
in packed column.

For the sample calculation given by SAADA(60) $\frac{\rho_{ss}}{\rho_s}$ = 1.034, and since ρ_s was taken, albeit incorrectly, as the density of water i.e. 55.5 kmol m^{-3} from eq.2.26 $C_A \simeq 1.9$ kmol m^{-3}.

The inaccuracy of the method is shown in that this concentration is greater, by a factor of 10^3, than the interfacial concentration C_{Ai} quoted by SAADA(60) in his example.

This criticism of SAADA's (60) studies, questions his contention that these results support the liquid distribution model of EISENKLAM and FORD(20).

During the last 3 years a number of other studies (24,68,70,74) have determined the effect of gas and liquid mass velocities on the interfacial areas and liquid phase mass transfer coefficient encountered during cocurrent flow. Usually the results have been specific to cocurrent downflow conditions and often the CO_2 - NaOH and CO_2 - H_2O systems have been investigated. SHENDE and SHARMA(68) and GIANETTO et al(24) both found the interfacial area increased with gas and liquid superficial velocities. The increases were most marked in the pulsing and spray flow regimes but no effects similar to those observed by SAADA(62) were observed. Values of the interfacial area as much as 3 times greater than the geometric area were reported by SPECCHIA et al(70).

Liquid phase mass transfer coefficients increased with liquid rate but UFFORD and PERONA(74) in contrast to SPECCHIA et al(70) found a

significant gas rate effect. SAADA(61) however found k_L to be independent of both gas and liquid rates. Values of a and k_L were greater in upward than downward flow. According to SPECCHIA et al(70) this was due to the increased liquid holdup during upward flow. In comparing liquid mass transfer coefficients under co- and counter-current conditions there is disagreement between UFFORD and PERONA(74) and GIANETTO et al(24). The former suggest k_L values are a factor of 3 lower in cocurrent flow whilst GIANETTO et al(24) say up to a tenfold increase can be expected.

2.4 Flow Models used in Fluid Mixing Studies

Many different mathematical models have been proposed to describe the fluid intermixing on passing through a packed bed system. A few have attempted to incorporate details of the packing structure but, due to its complexity, have met with limited success. Most models were originally developed for the simpler single phase systems, but their use in analysing continuous phases in a two phase system seems justified. Except for their effect in reducing the fluid flow area, the second phase is generally excluded from the analysis when no mass transfer or chemical reaction occurs between the phases. In this section our main consideration concerns the type of models used to represent two phase flow systems. The values obtained for the parameters of these models will however reflect the flow directions.

The most commonly used models in process analysis where axial mixing is of importance are generally based either on a Dispersion model or on a series of perfectly mixed stages. Most studies have analysed the phases independently and this review covers only liquid phase studies within a two phase system. The reasons underlying this choice are detailed in Section 6.2.

2.4.1 Axially Dispersed Plug Flow Model

This model is based on the assumption that a diffusion process in the bulk flow direction is superimposed on this bulk flow. A single parameter, termed the Dispersion Number, N_D, characterises this model where N_D is defined as:

$$N_D = \frac{D_L}{UL}$$

where	D_L	=	Dispersion Coefficient	L^2T^{-1}
	U	=	fluid pore velocity	LT^{-1}
	L	=	characteristic length	L

This model has been used with varying degrees of success by several workers. WEBER(78),in cocurrent studies, and both HOOGENDORN and LIPS(34) and SHESTOPALOV(69) et al in counter-current bubble flow conditions found the model quite adequate. KRAMERS and ALBERDA(41) however felt the model would not account for their countercurrent results and suggested this was due to a velocity profile effect. DUNN et al (18) concluded that the model was the best available even though their data showed poor reproducibility with a mean deviation of 30%. SCHWARTZ and ROBERTS(66) determined that the dispersion model appeared to be an adequate representation of liquid backmixing in trickle bed reactors. Predictions based on the dispersion model differed very little from those based on more complex two parameter models. Significant differences only occured at high degrees of backmixing and at high reactant conversions.

2.4.2 Extensions to the Dispersion Model

HARRISON et al(29) and HOOGENDORN and LIPS(34) both concluded that some form of liquid stagnancy existed due to the strong tailing of their response curves. GLASER and LICHTENSTEIN(25) characterised their axial dispersion by variability, defined as the ratio of standard deviation of residence times to the mean residence time. They were able to isolate the variability due to stagnant pools and found it diminished at high liquid rates. To accommodate this stagnancy both HOOGENDORN and LIPS(34) and HOCHMAN and EFFRON(33) suggested the liquid stream might consist of a stagnant section and a bulk flow section with cross flow between the two regions. In both instances plug flow was assumed for the flowing region. This extension correlated HOCHMAN and EFFRON's(33) results better than the simple Dispersion model. A natural extension to this model was the inclusion by VILLERMAUX and VAN SWAAIJ(76) of axial dispersion in the flowing region. The resultant 3 parameter model successfully fitted the two phase air/water data of VAN SWAAIJ et al(75).

GOTTSCHLICH(27) and GLASER and LITT(26) have both attempted to describe the stagnancy effect in greater detail by including physical models for the packed bed. GOTTSCHLICH(27) divided each interstice into a region in which the dispersion equation applied and a stagnant film around the packing into which material diffused. The area for diffusion was taken as an average of the particle surface area and the interfacial area between the stagnant and mixed regions. By considering the bed as a bundle of parallel tubes this interfacial area could be determined from the film thickness and tube geometry. The physical validity of this film was checked by comparison with the mass transfer film and both appeared to be manifestations of the same distributed film.

GLASER and LIT(26) considered the bed to consist of void channels external to the packing which included dead-end pockets holding stagnant liquid. The size and distribution of these channels and pockets were assumed to be some function of the packing material size and arrangement. Only diffusive flow occurred between the dead end pockets and the void channels, where again the flow was described by the dispersion equation. The axial velocity variation was determined by assuming the expression for laminar flow in pipes. Their results suggested that the liquid mixing caused by combination of streams of different residence times from various channels was greater than that due to dispersion within the flowing void channels themselves.

2.4.3 Series of Perfectly Mixed Stages

The free flow area normal to the direction of flow will vary as the fluid moves from one layer of particles to the next. Together with the resulting variation in fluid velocity the spaces between particles act as fluid mixing cells with jet mixer inlets promoting turbulence. The cell mixing efficiency is a function of the turbulence and retention time within the cell. However the impossibility of equating an ideal, perfectly mixed stage to a physical void space does not greatly diminish the model's usefulness or validity. In fact BUFFHAM and GIBILARO(9) show that the number of stages n can reasonably assume non integer values. This is important for low n especially in the range $0 < n < 1$.

RAGHURAMAN and VARMA(56) have expanded this simple model in a similar manner to the extensions of the basic Dispersion Model. They proposed a four parameter model consisting of a series of perfectly mixed stages in which each stage exchanged material with an associated dead region, with a fraction of the feed short circuiting each stage. For certain values of the dead space parameter, the size of the cross flow was found to have little effect on the residence time distribution of the system.

2.4.4 Probabilistic Models

Residence time distributions for flow in packed beds can also be derived from probabilistic considerations and the work of BUFFHAM et al(10) is typical. Essentially the problem is one of determining the number of times a fluid particle stops and the length of time it remains at rest as it passes through the packed bed.

Further consideration of this approach has not been undertaken since this literature review has shown that models based on the dispersion concept have received by far the widest acceptance in both single and two phase packed bed studies.

CHAPTER 3 GENERAL METHODS OF SYSTEM ANALYSIS AND MODEL PARAMETER ESTIMATION

3.1 Summary

If any quantitative analysis of the system is to be attempted a multiparameter mathematical model is needed. There are several advantages, both theoretical and experimental, to be gained from using a variation of the two point measurement technique. In particular the requirements of a system forcing function are substantially relaxed. A review of various parameter estimation techniques suggests that overall, the most suitable form of model representation and analysis is by Transfer Functions.

3.2 General Analyses of Flow Systems

A general description of any flow system is possible by the application of age distribution analyses. DANCKWERTS(16),in a classic paper, and since then NAOR and SHINNAR(53), have defined a number of distribution functions for describing the residence time of fluid elements within any system. Even though the spatial variation of the dependent variables is unknown residence time distributions, which give information about the fraction of fluid that spends a certain time within the system, are often sufficient to give adequate qualitative estimates of the system's behaviour.

The experimental determination of the age distribution functions is achieved by a stimulus - response technique using some form of tracer material in the system feed. The residence time distribution (r.t.d) function, for example, can be obtained from the variation with time of the dimensionless tracer concentration at the system outlet after injection of a tracer impulse at the system inlet.

LEVENSPIEL and TURNER(44) studied the influence of velocity profile, at the locations where tracer is injected and measured, on the interpretation of pulse response measurements in terms of the r.t.d. This work has since been extended by LEVENSPIEL et al(45) and TURNER(72) and generalised by BUFFHAM(8). LEVENSPIEL and TURNER(44) showed that if the velocity profile is not flat at the injection and measurement points, then different ways of injecting

and measurement will give different tracer curves. Only when tracer is injected in quantities proportional to the flow through each point in the injection plane and measured as the 'mixing cup' average concentration, is the r.t.d of the fluid in the vessel obtained.

However since r.t.d's themselves cannot be simply correlated with system variables, it is usual to devise some mathematical model, containing several parameters, which will closely approximate the experimental age distribution functions.

A major premise involved in process analysis is that, where necessary, the entire process can be broken down into distinguishable subsystems and that relationships exist between the subsystems, which when assembled into a whole can simulate the process. Although these subsystems do not have to correspond to any basic physical subdivisions of the real process, the danger may exist that a concept, intended merely as an analysis technique, can become endowed with a physical reality which was never intended.

3.3 System Forcing Functions

Whilst any stimulus or forcing function can, in principle, be used only a few are used in practice. One of the main reasons for the prominence of the step, impulse and sinusoidal forcing functions has been simply one of mathematical convenience in those situations where the forcing function cannot be excluded from the equations describing the system. Although the two point measurement technique described in section 3.4 alleviates this problem, a comparison of the various inputs is still justified since the choice of forcing function affects, to some degree, the ease with which the various parameter estimation techniques may be applied.

3.3.1 Step Functions

A reasonable approximation to a step function is obtained if the rise time is fast compared with the process response time. Usually the considerable quantity of tracer needed is a disadvantage. An 'up step' can however simply yield the internal age distribution function. The response from step inputs are most commonly used in systems capable of analysis in the time domain, especially those involving ordinary first order differential equations.

3.3.2 Sinusoidal Functions

Frequency response shows how a system responds to a sustained disturbance varying in a sinusoidal manner. The technique is useful in distributed parameter systems, such as packed beds where it is often difficult to invert the Laplace transform of the governing differential equations to obtain the complete time domain solution. To obtain enough points to define the frequency response a number of sinusoidal tests must be made at various frequencies. HOUGAN and WALSH(36) consider a hundred fold variation in frequency is often necessary to get a good description of the system dynamics. Although setting up a disturbance in the normal process operation, KRAMERS and ALBERDA(41) considered the main advantage of harmonic analysis was that no discontinuities are introduced and that steady cycling can be obtained. Both KRAMERS and ALBERDA(41) and CLEMENTS and SCHNELLE(15) agree on the difficulty of generating a good input sine wave and the disadvantage in some circumstances of carrying on tests long enough to remove the system transients.

3.3.3 Pulse Functions

Two distinct forms of pulse; the delta function and the imperfect or general pulse have been used. The response when the forcing function $C_s(t)$ is taken as the unit impulse or delta function is usually termed the impulse response $g(t,k)$. This response is in general a function of the time t of the response measurement and the time k at which the impulse input was applied.

If the input, $C_s(t)$ is arbitrary, it can be regarded as consisting of a succession of pulses. If the magnitude of this input at time k is $C_s(k)$ and the input lasts for time δk then, since the response to a unit impulse at time k is $g(t,k)$, the response to the pulse of value $C_s(k)\delta k$ will be $C_s(k)\delta k\, g(t,k)$ for a linear system.

Thus the system response $C_o(t)$ at any time t, will be due to all pulses applied between $k = 0$ and $k = t$.

In the limit as $\delta k \to 0$

$$C_o(t) = \int_{k=0}^{k=t} C_s(k)\, g(t,k)\, dk \qquad \ldots\ldots\ldots \qquad (3.1)$$

If the input $C_s(t)$ is the delta function which has the properties:

$$\delta(t-k) = 0 \quad t \neq k$$
$$\int_{-\infty}^{\infty} \delta(t-k) = 1 \qquad \ldots\ldots \qquad (3.2)$$

then the output $C_o(t)$ given by equation 3.1 will be the impulse response $g(t,k)$. If the differential equation describing the system is known the impulse response for the model can be obtained by setting $C_s(t) = \delta(t-k)$ in this differential equation.

The problems associated with representing a delta function accurately under experimental conditions are overcome when using an imperfect pulse with measurement at two positions as described in Section 3.4.

Defining the general pulse as a function which varies from zero for a finite time, the principal requirement, given by HOUGAN and WALSH(36), is that the system be driven sufficiently hard so that the system dynamics are excited, but not at such a rate as to exceed the system's capacity to respond.

3.4 Imperfect Pulse and Two Point Measurement Technique

When the standard impulse-response technique is used, tracer is injected at some position upstream of the test section and the response measured near to the downstream exit. The following points must be considered:

(i) The tracer injection must be described mathematically.
(ii) The effect of the detector must be known
(iii) The effect of subsystems either side of the test section, termed 'end effects' must be allowed for.

By measuring at two positions however all the above requirements can be avoided.

3.4.1 Tracer Injection

ARIS(1) showed that a mathematical description of the system forcing function was unnecessary if the transient tracer concentration was measured at two points, since it could be eliminated from the equations describing the system. Extensions of this work by BISCHOFF(4) and BISCHOFF and LEVENSPIEL(5) form the basis of the imperfect pulse technique.

3.4.2 Effect of Detection System

SCHMALZER and HOELSCHER(64) studied the effect of both the mean residence time and mixing characteristics of the detector on the apparent tracer concentration. They concluded that the mean residence time of the detector should be less than 0.1 σ (where σ is the standard deviation of the recorded pulse), if the measurements are to reflect accurately the actual tracer concentration. JOHNSON and FAN(39) showed that the detector analysis is unnecessary if the two point measurement technique is used.

From Laplace Transform theory equation 3.1 can be written:

$$\bar{C}_o(p) = \bar{C}_s(p)\ F(p) \qquad \ldots\ldots\ldots \qquad (3.3)$$

where $\bar{}$ - denotes a Laplace transformed variable such that

$$\bar{C}_o(p) = \int_o^\infty C_o(t) e^{-pt}\, dt \qquad \ldots\ldots\ldots \qquad (3.4)$$

p = Laplace Transform variable $\qquad T^{-1}$

$F(p)$ is termed the Transfer Function of the system between the two points identified by subscripts o and s.

Measurements at two positions in the test section, designated 0 and 1 would result in ${}_e\bar{C}_o(p)$ and ${}_e\bar{C}_1(p)$. The second subscript e indicates that it is not the true tracer concentration at these positions which is recorded since the measurements include the effect of the detectors.

If $T(p)$ is the Transfer Function of a detector system then ${}_t\bar{C}(p)$ the true tracer concentrations are related to the measured values by:

$$\begin{aligned} {}_e\bar{C}_o(p) &= {}_t\bar{C}_o(p)\ T_o(p) \\ {}_e\bar{C}_1(p) &= {}_t\bar{C}_1(p)\ T_1(p) \end{aligned} \qquad \ldots\ldots\ldots \qquad (3.5)$$

The experimentally measured Transfer Function ${}_eG(p)$ is given by:

$${}_eG(p) = \frac{{}_e\bar{C}_1(p)}{{}_e\bar{C}_o(p)} = \frac{{}_t\bar{C}_1(p)}{{}_t\bar{C}_o(p)} \cdot \frac{T_1(p)}{T_o(p)}$$

$$\text{or} \quad {}_eG(p) = {}_tG(p) \frac{T_1(p)}{T_o(p)} \qquad \ldots\ldots\ldots \qquad (3.6)$$

Since the ratio $T_1(p)/T_o(p)$ will be near unity for similar detectors, the error in the measured Transfer Function due to the detectors will be small.

3.4.3 End Effects

When the effects of the unpacked sections at either end of the experimental test section can be ignored, the equations describing the system are usually considerably simplified. This neglect of end effects is justifiable on theoretical grounds if we postulate the test section to be part of a doubly infinite packed bed system as shown in Fig.3.1(a). Experimentally this can be approximated by taking both measurements inside a packed bed of finite length as shown in Fig.3.1(b). Exact conditions, applicable to the Dispersion Model, are given by BISCHOFF and LEVENSPIEL(5). In a packed bed system containing two phase flow, internal concentration measurements create experimental difficulties unless radioactive tracers are used. With any other tracer measurements must be taken outside the packed bed, in the unpacked sections. Any theoretical analysis must then make some assumptions concerning the flow within these sections. One possibility is to consider the Dispersion model applicable but with different values for the Dispersion Number. Even if this is a realistic representation, the resulting relationships are so complex as to preclude their use. An alternative approach was used by OTTO and GESTRICH(54). They deliberately mixed the fluid on either side of the test section. Knowing the residence time distribution of an ideal mixer they were able to determine the residence time distribution of the test section by removing from the overall response the effect of the two mixers.

EDWARDS(19), during single phase packed bed studies, modified the classical two point technique in the following manner, as illustrated in Fig.3.2.

(i) A pulse is injected upstream of a short length of packed bed L_o and the response $C_o(t)$ is measured outside the downstream exit. (see Fig.3.2(a)).

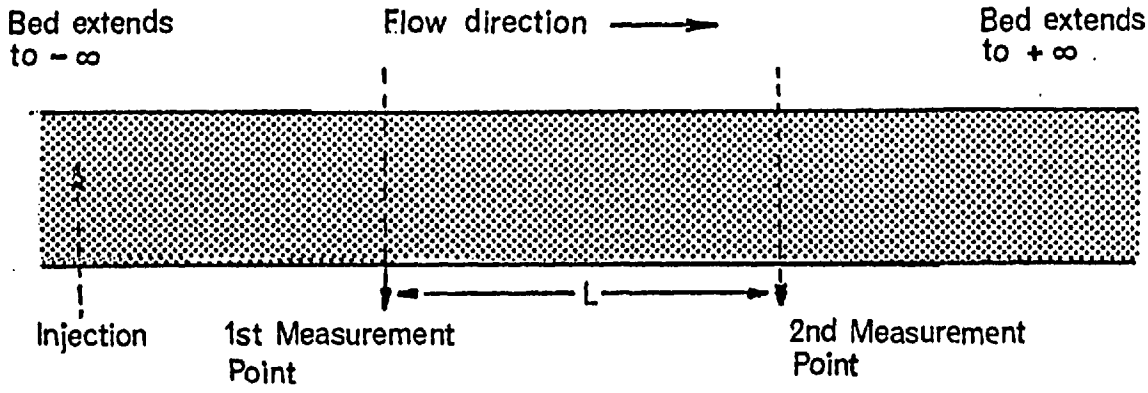

(a) Infinite Packed Bed System

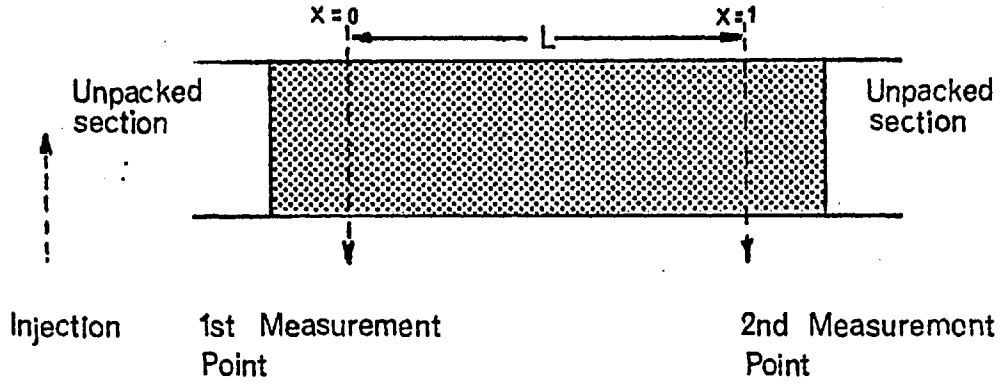

(b) Approximation in a Packed Bed of Finite Length

INJECTION AND MEASUREMENT POSITIONS WHEN END EFFECTS CAN BE NEGLECTED

FIG 3.1

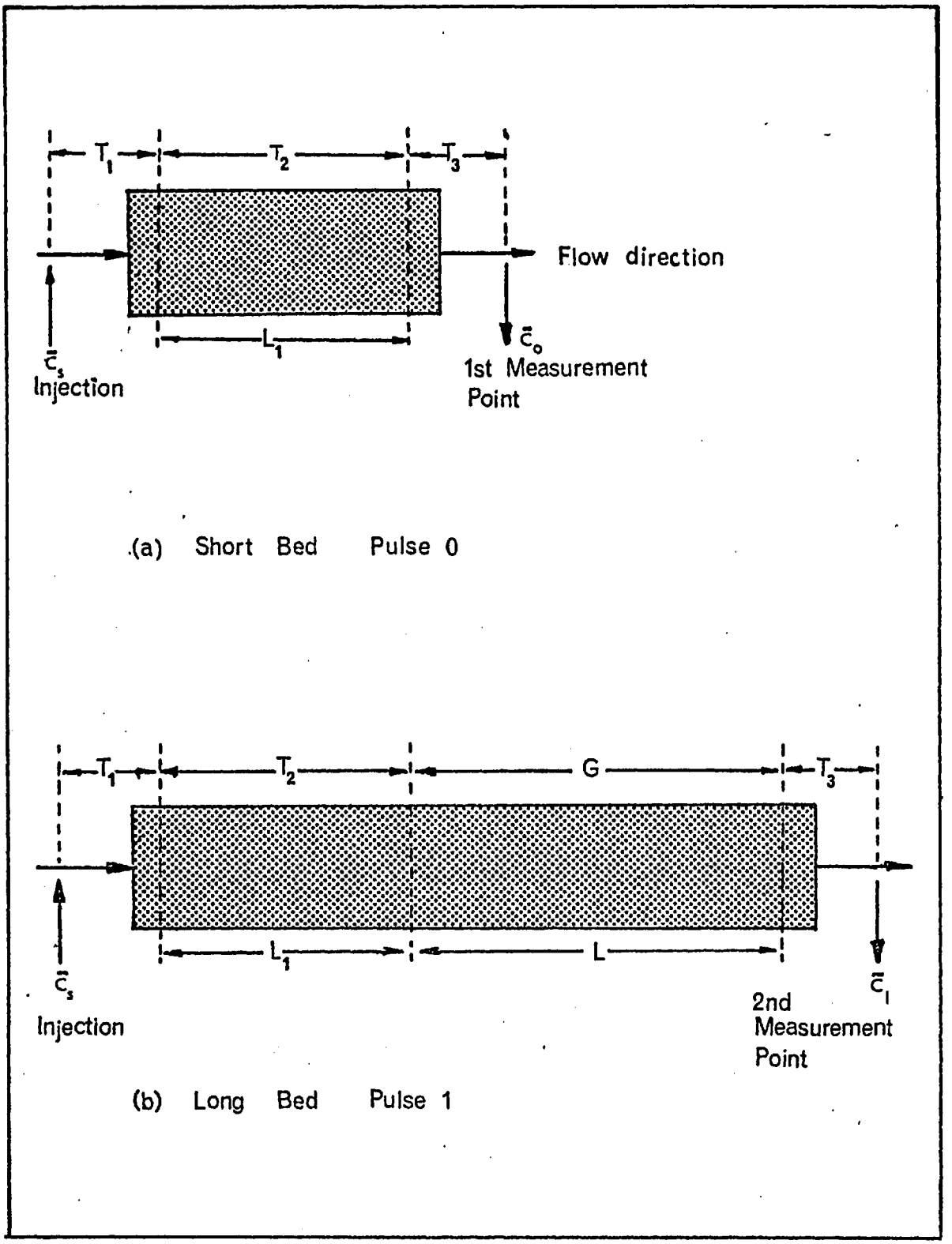

MODIFIED TWO POINT MEASUREMENT TECHNIQUE

FIG 3.2

(ii) The bed length is increased to a length L_1 and another pulse injected in the same position as before. The second outlet pulse is measured at the same distance beyond the downstream exit to give $C_1(t)$ as shown in Fig.3.2(b).

EDWARDS(19) argued that if the injection was reproducible and all subsystems linear, the end effects would be the same for both bed lengths and could therefore be ignored.

The validity of this assumption can be shown by the following analysis:

Using the subsystem Transfer Functions shown in Fig.3.2 we have

For outlet pulse designed by o

$$\bar{C}_o(p) = T_1(p) . T_2(p) . T_3(p) . \bar{C}_s(p)$$

For the longer bed length ..... (3.7)

$$\bar{C}_1(p) = T_1(p) . T_2(p) . G(p) . T_3(p) . \bar{C}_s(p)$$

where $\bar{C}_s(p)$ is the Laplace transformed pulse on injection.

$T_1(p)$ = Transfer Function of the subsystem between the injection point and some position within the bed where the upstream end conditions have no effect.

$T_3(p)$ = Transfer Function at the bed exit allowing for downstream end effects and the detector subsystem.

$T_2(p)$ = Transfer Function for a length of the short bed where end effects are absent.

$G(p)$ = Transfer Function of the <u>additional length</u> of packed bed added when the second outlet pulse was recorded.

The following assumptions are made:

(i) The subsystems between the injector and bed inlet, and the bed exit and detector are identical for both bed lengths and hence $T_1(p)$ and $T_3(p)$ are the same in both cases.

(ii) The pulse injection is reproducible.

Then from eq.3.7 we have:

$$G(p) = \frac{\bar{C}_1(p)}{\bar{C}_o(p)} \qquad \ldots\ldots\ldots \qquad (3.8)$$

3.5 Parameter Estimation Techniques

In the following sections the tracer measurements are assumed to have been recorded using the modified two point measurement technique outlined in section 3.4. Three methods of analysing and fitting models to pulse testing data have been reported in the literature. These methods are the moments method of analysis, Laplace Transform analysis and frequency response analysis. Whilst it would be desirable to estimate the model parameters from response curve matching in the time domain, this is always time consuming. Often its use is precluded by the difficulty or even impossibility of obtaining analytically the inverse of the describing Laplace Transforms.

Factors which can affect the alternative methods are:

(a) The experimental tracer response measurements may contain excessive noise.

(b) The measured output signal often registers non-zero values, termed tailing, even after long periods of time.

(c) The model chosen may not represent the physical situation exactly.

(d) The different methods attach varying importance to any one part of the response curves.

As the number of parameters in the model increases, these effects are compounded. More parameters require more information to evaluate them, and this information is known with progressively decreasing accuracy.

3.5.1 Analysis by Moments

For systems where there is a small degree of mixing, the peak of the response curve occurs near the mean velocity plane and the curve is nearly symmetrical. These features resulted in the widespread use of two parameters based on Gaussian curves, namely the mean and variance.

Defining the r^{th} moment above the origin M^r as:

$$M^r = \int_o^\infty t^r C(t)dt \quad \ldots\ldots\ldots \quad (3.9)$$

and assuming the response curve is normalised such that

$$\int_o^\infty C(t)dt = 1 \quad \ldots\ldots\ldots \quad (3.10)$$

the mean and variance are M^1 and $M^2 - \left[M^1\right]^2$ respectively.

Comparing equations 3.4 and 3.9 we see that:

$$M^o = \underset{p\to o}{Lt}\ \bar{C}(p)$$

Differentiating eq.3.4 with respect to p we obtain:

$$\frac{\partial \bar{C}(p)}{\partial p} = - \int_o^\infty tC(t)e^{-pt}dt \ldots\ldots\ldots \quad (3.11)$$

On comparison with eq.3.9 we see that

$$\underset{p\to o}{Lt}\ \frac{\partial \bar{C}(p)}{\partial p} = -M^1 \quad \ldots\ldots\ldots \quad (3.12)$$

Similarly one finds $\underset{p\to o}{Lt}\ \frac{\partial^2 \bar{C}(p)}{\partial p^2} = M^2 \quad \ldots\ldots\ldots \quad (3.13)$

Thus in general $M^r = (-1)^r \underset{p\to o}{Lt}\ \frac{\partial^r \bar{C}(p)}{\partial p^r} \quad \ldots\ldots\ldots \quad (3.14)$

Therefore the mean and variance of the model can be obtained by setting p = O in the expressions for the first and second derivatives of the Laplace Transformed tracer concentration. The model's parameters can be estimated by matching the theoretical and experimental mean and variance. In general n+1 moments will be required for an n parameter model. When the modified two point pulse technique is used, the mean and variance of the experimental concentration curves at the two points are calculated. The difference between the variances can then be related to the model parameter e.g. Dispersion Number.

In equation 3.9 the weighting t^r given to C(t) is greatest at large t when the response is known with least accuracy. Ideally the weighting function should approach zero under these conditions. This requirement already existed with the Laplace Transform when the variable p was real and positive. The use of the model's

transform for moments analysis by setting p = 0 was clearly a retrograde procedure.

If the Laplace Transform variable p is retained as real and positive in eq.3.4, then an analysis method based on Transfer Functions results.

3.5.2 Transfer Function Analysis

We can define the Transfer Function F(p) of any system, or subsystem as the ratio of the tracer concentration at the outlet $C_1(t)$ to that at the inlet $C_o(t)$ in Laplace transform space

$$\text{Thus} \quad F(p) = \frac{\int_o^\infty C_1(t)e^{-pt}\,dt}{\int_o^\infty C_o(t)e^{-pt}\,dt} \qquad \ldots\ldots \qquad (3.15)$$

Similar to the ordinary moments defined by eq.3.9 we have a set of weighted moments $\bar{M}_i^r$ such that

$$\bar{M}_i^r = \int_o^\infty t^r C_i(t)e^{-pt}\,dt \qquad \ldots\ldots \qquad (3.16)$$

$$\text{Thus} \quad F(p) = \frac{\bar{M}_1^o}{\bar{M}_o^o} \qquad \ldots\ldots \qquad (3.17)$$

Analogous to eq.3.14 the r^{th} weighted moment can be related to the derivatives with respect to p of the Laplace transformed concentration by:

$$\bar{M}^r = (-1)^r \frac{\partial^r \bar{C}(p)}{\partial p^r} \qquad \ldots\ldots \qquad (3.18)$$

Whilst the zeroth ordinary moment M^o from eq.3.9 only serves as a mass balance check the zeroth weighted moment $\bar{M}^o$ contains useful information as eq. 3.17 indicates.

The studies of MICHELSEN and OSTERGAARD(50) have suggested a number of ways in which the various weighted moments $\bar{M}^o$, $\bar{M}^1$ and $\bar{M}^2$ can be used to determine the model's parameters. In particular they discuss further restrictions on the range of p values which may be used (other than that they must be real and positive) in order that:

(a) the contribution of the tails of the response curves should be minimised.

(b) the early portion of the response should not be overemphasised.

A detailed discussion on these points is left to Chapter 5. Models with several parameters can be analysed by Transfer Functions using a range of p values, without necessarily resorting to the higher moments needed by the ordinary moments analysis.

3.5.3 Frequency Response Analysis

The basic difference between Transfer Function and Frequency Response analysis is that the Transfer Function analysis requires curve fitting along the real positive p axis, while frequency response analysis involves fitting along the imaginary axis, $j\omega$.

The frequency response $F(j\omega)$ is given by:

$$F(j\omega) = \frac{\int_{-\infty}^{\infty} C_1(t)e^{-j\omega t}\,dt}{\int_{-\infty}^{\infty} C_o(t)e^{-j\omega t}\,dt} \qquad \ldots\ldots\ldots \qquad (3.19)$$

Since both $C_1(t)$ and $C_o(t)$ are zero for $t<0$, the lower limit of the integrals can be set to zero. The frequency response can therefore be obtained from the system Transfer Function by simply replacing the Laplace Transform variable p by $j\omega$.
Using the Euler identity:

$$e^{-j\omega t} = \cos\omega t - j\sin\omega t \qquad \ldots\ldots\ldots \qquad (3.20)$$

we obtain $F(j\omega) = \dfrac{A_1 - jB_1}{A_o - jB_o}$

$$\text{where} \quad A_n = \int_o^{\infty} C_n(t)\cos\omega t\,dt$$

$$B_n = \int_o^{\infty} C_n(t)\sin\omega t\,dt \qquad \ldots\ldots\ldots \qquad (3.21)$$

The frequency response is often characterised by the gain and phase lag which are given by the modulus and argument of $F(j\omega)$ respectively.

$$\text{Gain} = \left[\frac{A_1^2 + B_1^2}{A_o^2 + B_o^2}\right]^{\frac{1}{2}}$$

$$\text{Phase Lag} = \tan^{-1}\left[\frac{A_1B_o - A_oB_1}{A_1A_o + B_1B_o}\right] \qquad \ldots\ldots\ldots \qquad (3.22)$$

Frequency response analyses have been discussed in detail by HAYS et al(31) and by CLEMENTS(13). Usually it is assumed that the frequency response is obtained from pulse tests by evaluating $F(j\omega)$ for various values of ω as suggested by CLEMENTS and SCHNELLE(15). There is however an upper limit on the values ω may take due to the oscillation of the $\cos\omega t$ and $\sin\omega t$ curves which may become zero leading to indeterminate values for the gain. Both JOHNSON et al(40) and JEFFREYSON(38) suggest empirical criteria for determining this maximum frequency. As noted by CLEMENTS(15), the success of this method depends on the accurate evaluation of the integrals given in eq.3.21. HARRISON et al(30) discuss the relative accuracy of complex Transfer Function fitting and amplitude ratio fitting to obtain the model's parameters and conclude that least squares minimisation of the complex Transfer Function has a much lower sensitivity to noise.

The function to be minimised is thus:

$$\sum_{\omega} \{\mathrm{Re}\left[F(j\omega)\right] - \mathrm{Re}\left[G(j\omega)\right]\}^2 + \sum_{\omega} \{\mathrm{Im}\left[F(j\omega)\right] - \mathrm{Im}\left[G(j\omega)\right]\}^2 \quad \ldots\ldots \quad (3.23)$$

Since both the real, Re, and imaginary, Im, parts are involved in eq.3.23 additional mathematical manipulation of the model is required. CLEMENTS(14) points out, however, that resolution problems can be overcome by using complex mode arithmetic in FORTRAN and using the appropriate FORTRAN functions to do the resolution numerically. Additionally, the results obtained by minimising the least squares error in the frequency domain are shown by CLEMENTS(13) to be the same as would be obtained by a least squares error in the time domain.

JOHNSON et al(40) compared the relative advantages and disadvantages of the three methods described above, by analysing pulse testing data obtained from radioactive tracer studies of liquid mixing on distillation trays. The data was fitted to a Gamma Distribution Model with bypassing, containing three parameters. They found the results from the Transfer Function Analysis were intermediate and significantly closer to the results of the Frequency Response method than those of the moments method.

Balancing simplicity, rapidity and reliability, they recommended the Transfer Function method of analysis. This view is also endorsed by WILLIAMS and ADLER(81) from their study of finding parameters to a complex model, describing gas mixing in a fluidized bed, by least squares fitting of the Transfer Function.

CHAPTER 4 MATHEMATICAL MODELS FOR TWO PHASE FLOW SYSTEMS BASED ON THE DISPERSION MODEL

4.1 Summary

On the basis of the review in Chapter 2, three models are derived, all based on the Axially Dispersed plug flow model. Apart from the basic axially dispersed plug flow model itself, more complex models incorporating liquid stagnancy and split flows are developed. All the models are characterised by their Transfer Functions, since this form was considered the most suitable in Chapter 3. A new technique for deriving the Transfer Functions of complex flow systems is developed.

4.2 Development of the Axially Dispersed plug flow model

Models based on the analogy between mixing during actual flow and a diffusional process are termed Dispersion models. This class of model is relevant in packed bed systems as a close approach is obtained to the idealised concept of plug flow.

Mixing can be caused by any or all of the following:

- molecular diffusion
- flow splitting around particles
- turbulent fluctuations
- convective diffusion in channels

Due to the complexity which would result from considering the rapid concentration fluctuations present during turbulent flow, it is convenient to characterise the mixing by a Dispersion coefficient, whose magnitude is determined experimentally. For a non reacting system with no source term present within the system boundaries (i.e. the two measurement positions) an unsteady mass balance yields the following:

$$\underline{u}.\,\nabla C - \nabla.(D\,\nabla C) + \frac{\partial C}{\partial t} = 0 \qquad \ldots\ldots\ldots \qquad (4.1)$$

The dispersion coefficient D will depend on both the flow regime and the properties of the fluid, the latter being prevalent at low fluid flow rates. Only axial and radial components of D will exist if axial symmetry is assumed. Two assumptions concerning the fluid velocity are made to obtain a solution to eq. 4.1:

(i) No axial dependence of u since the fluid density is assumed constant.

(ii) No radial dependence of u i.e. the velocity u constant at the mean value.

A further simplification resulting from assuming a constant velocity is that both the axial and radial dispersion coefficients are assumed independent of radial position. It is clear that the effect of the fluid's velocity profile is now included in the Dispersion coefficients.

If the radial variation in fluid concentration is negligible in comparison with axial variations, the axially dispersed plug flow model with one parameter D_L is obtained:

$$u \frac{\partial C}{\partial z} = D_L \frac{\partial^2 C}{\partial z^2} + \frac{\partial C}{\partial t} = 0 \qquad \ldots\ldots \qquad (4.2)$$

where z = axial distance measured from the upstream system boundary i.e. the 1st measurement point — L

u = average pore velocity in direction of macro flow — LT^{-1}

D_L = axial dispersion coefficient — L^2T^{-1}

The concentration C(z,t) is made dimensionless through dividing by the average fluid concentration that would result if the tracer was evenly spread throughout the system.

The system under investigation is shown diagrammatically in Fig.4.1, and has a system Transfer Function F(p) which by definition is the ratio of the Laplace transformed concentration at the second measurement point z=L to that at the first measurement point i.e. z = 0.

Setting $x = z/L$ where L is the distance between the two measurement points we have:

$$F(p) = \frac{\bar{C}\ (1,p)}{\bar{C}\ (0,p)} \qquad \ldots\ldots \qquad (4.3)$$

where $\bar{C}\ (x,p) = \int_0^\infty C(x,t)e^{-pt}\,dt \qquad \ldots\ldots \qquad (4.4)$

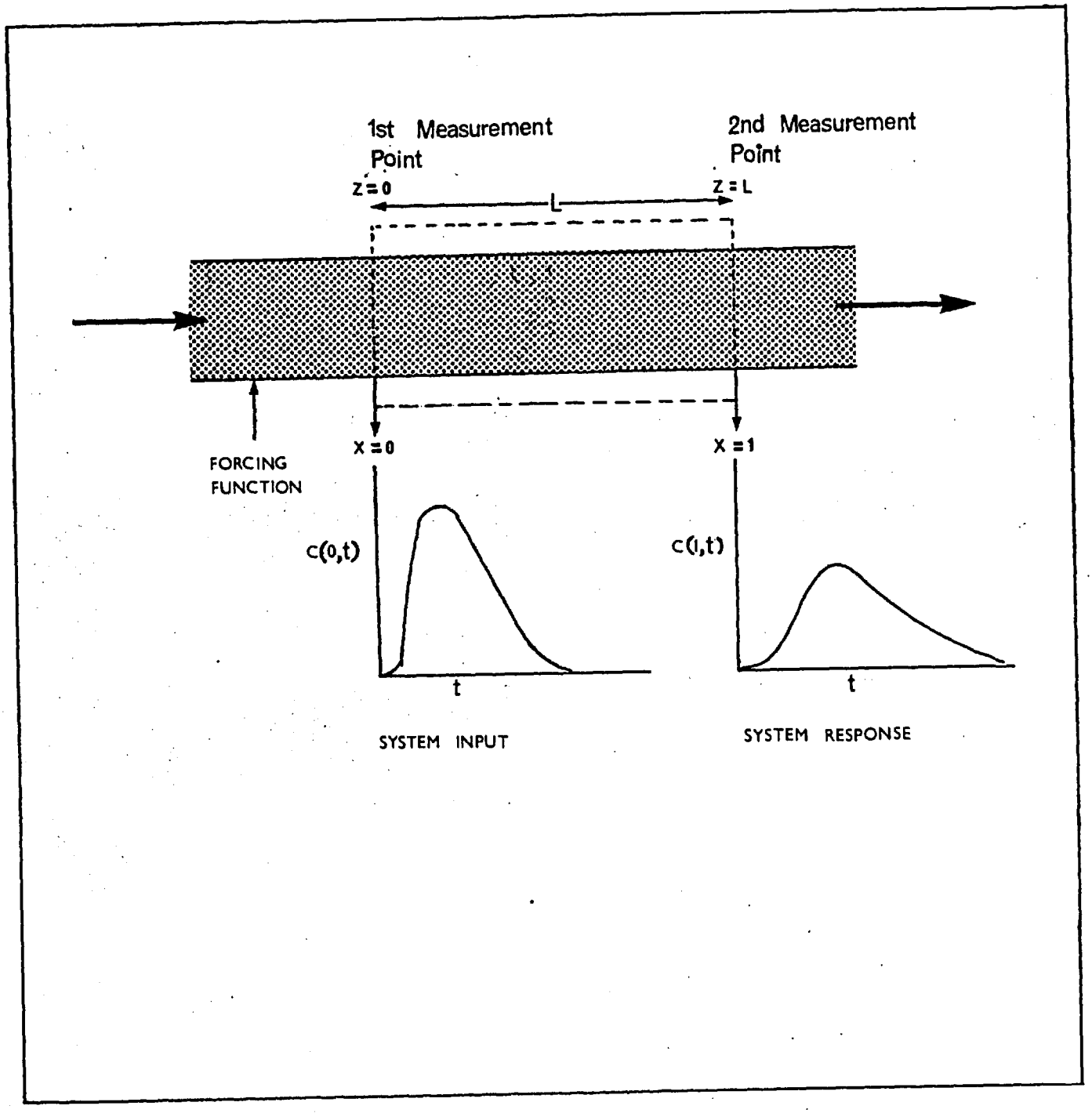

DIAGRAM OF FLOW SYSTEM WITH TYPICAL TRACER CURVES

FIG. 4.1

Equation 4.2 may be written as:

$$N_D \frac{\partial^2 C}{\partial x^2} - \frac{\partial C}{\partial x} - \tau \frac{\partial C}{\partial t} = 0 \quad \ldots\ldots \quad (4.5)$$

where $N_D = \frac{D_L}{uL}$ is the system Dispersion Number

$\tau = {}^{L}/_{u}$ is the system mean residence time.

A solution in the p domain is sought for eq.4.5 subject to the following conditions in the time domain:

$$C(x,0) = 0 \quad \text{for} \quad 0 < x < 1 \quad \ldots\ldots \quad (4.6)$$

$$C(x,t) \to 0 \quad \text{for} \quad x \text{ increasing} \quad \ldots\ldots \quad (4.7)$$

Laplace transforming eq. 4.5 and using condition 4.6 we obtain:

$$N_D \frac{d^2\bar{C}}{dx^2} - \frac{d\bar{C}}{dx} - \tau p\bar{C} = 0 \quad \ldots\ldots \quad (4.8)$$

whose solution is given by:

$$\bar{C}(x,p) = A \exp x \left[\frac{1}{2N_D}\left\{1 + (1 + 4\tau pN_D)^{\frac{1}{2}}\right\}\right] + B \exp x \left[\frac{1}{2N_D}\left\{1 - (1 + 4\tau pN_D)^{\frac{1}{2}}\right\}\right] \quad \ldots. \quad (4.9)$$

The condition that $C(x,p) \to 0$ as x increases follows from eq.4.7 and can only be met in eq. 4.9 with $A = 0$.

Thus $\bar{C}(x,p) = B \exp x \left[\frac{1}{2N_D}\left\{1 - (1 + 4\tau pN_D)^{\frac{1}{2}}\right\}\right]$ .... (4.10)

From eq.4.3 and eq.4.10 we have:

$$F(p) = \exp\left[\frac{1}{2N_D}\left\{1 - (1 + 4\tau pN_D)^{\frac{1}{2}}\right\}\right] \quad \ldots. \quad (4.11)$$

As $N_D \to 0$, from eq.4.11 $F(p) \to e^{-\tau p}$ (the plug flow Transfer Function)

The effect of varying the model's parameter N_D can be represented both in the time domain and Laplace (p) space. The latter is most convenient for complex flow models where Transfer Function inversion is difficult. The time domain solutions in this Chapter are determined by solving the differential equations describing the model by a finite difference technique. An actual experimental pulse,

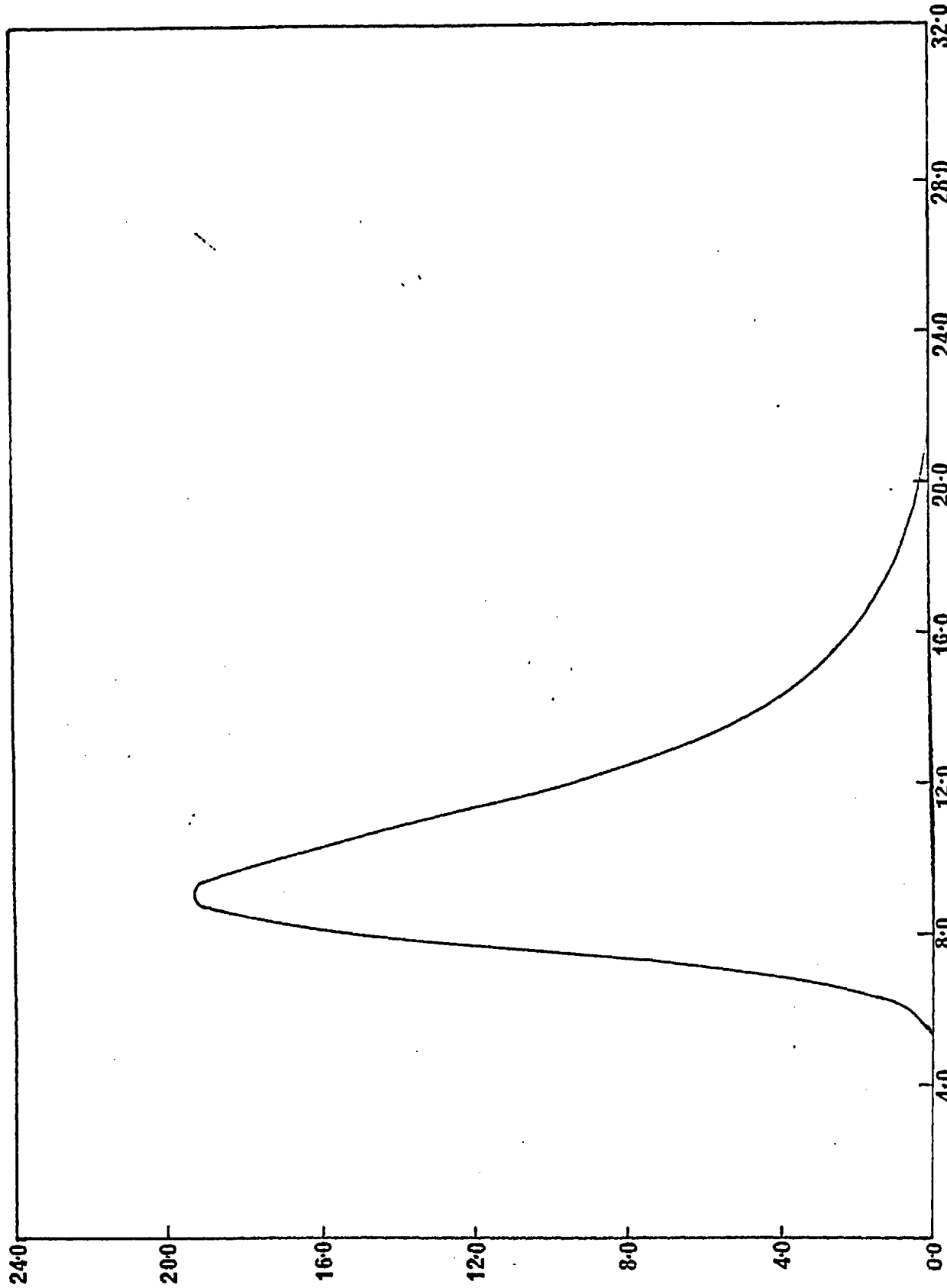

TYPICAL SYSTEM FORCING FUNCTION

FIG 4.2

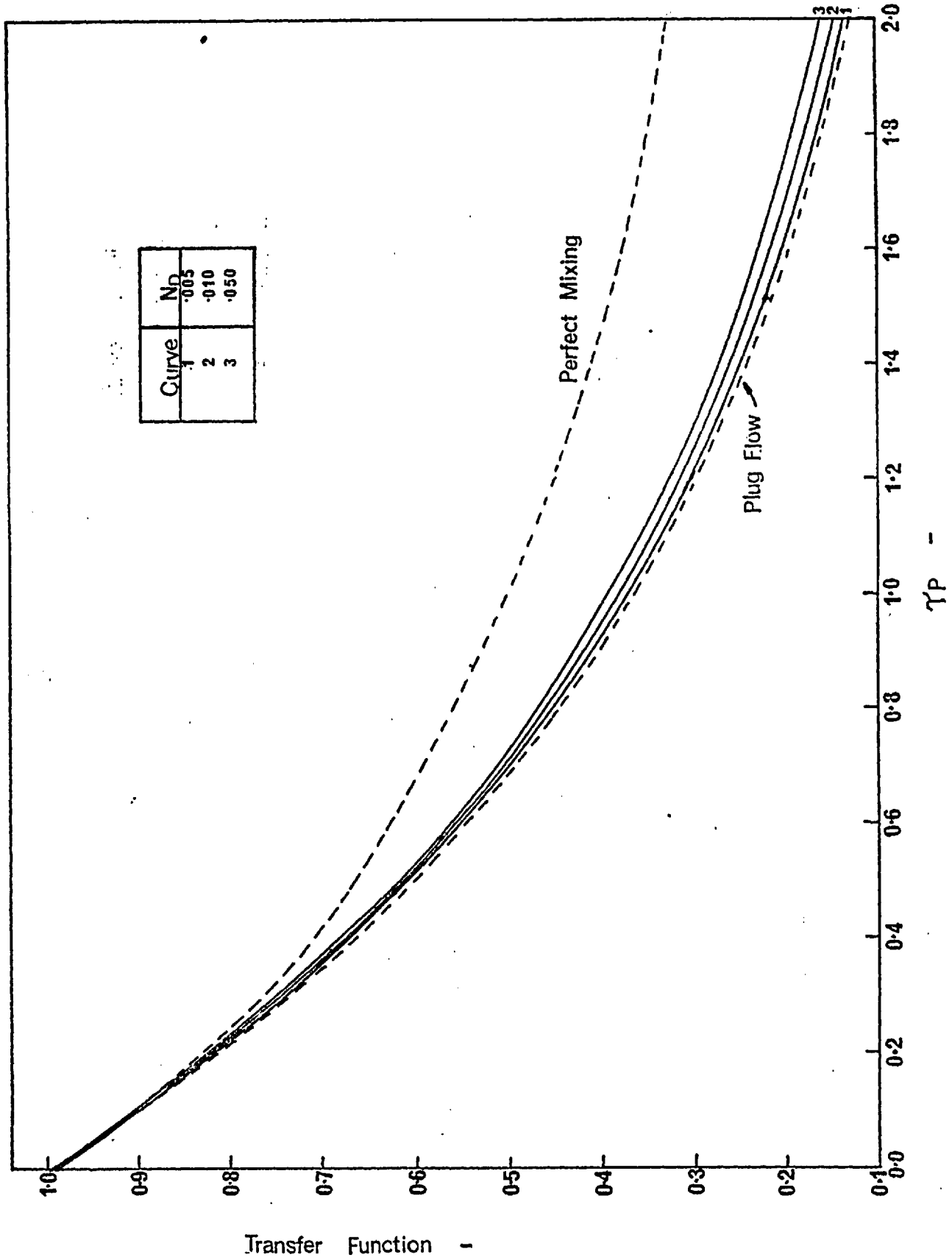

EFFECT OF DISPERSION NUMBER N_D ON SYSTEM TRANSFER FUNCTION FOR AXIALLY DISPERSED PLUG FLOW MODEL

FIG 4.3

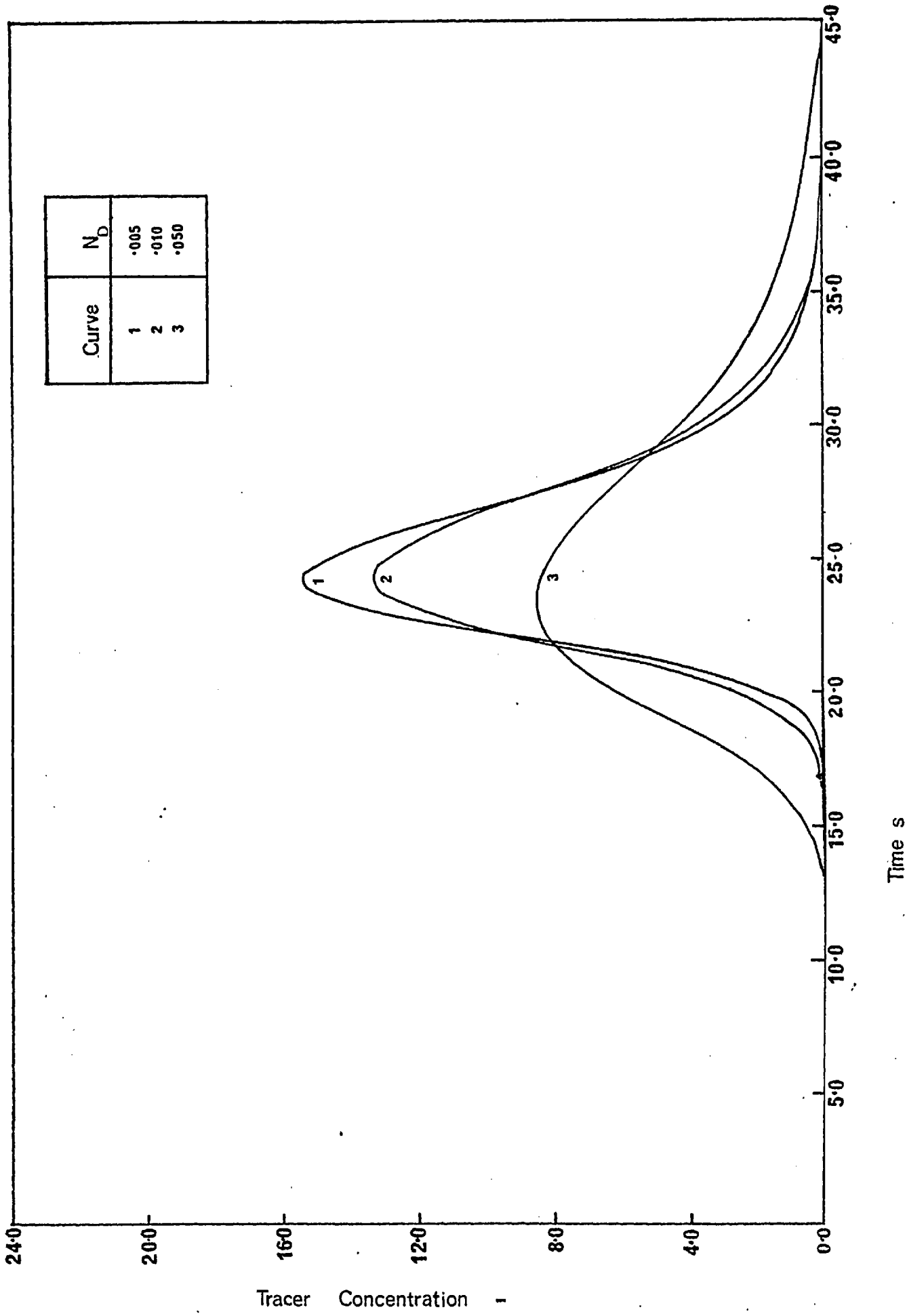

EFFECT OF DISPERSION NUMBER N_D ON SYSTEM RESPONSE FOR AXIALLY DISPERSED PLUG FLOW MODEL

FIG 4.4

illustrated in Fig.4.2 was used as the system forcing function in preference to some imaginary pulse which although mathematically definable, would be unobtainable experimentally.

For the axially dispersed plug flow model, the variation in Transfer Function with τp, given by eq.4.11 is shown in Fig.4.3 with the Dispersion Number as the curve parameter. The equivalent time domain responses are illustrated in Fig.4.4. As the Dispersion Number increases the Transfer Function curves tend towards perfect mixing, whilst in the time domain a greater spread of tracer about the mean occurs.

It is realistic to apply eq.4.11 to a two phase system when the two phases either form an homogeneous pseudo-phase or else when the gas is assumed to be immiscible and limits the liquid flow area, increasing the average interstitial velocity in the direction of macro flow. The numerical value for the Dispersion Number will reflect the degree of gas-liquid interaction.

The liquid holdup ϕ_L i.e. the fraction of the total cross sectional pore flow area available to the liquid, can be simply determined by:

$$\phi_L = \frac{\tau}{\tau^*} \qquad \ldots\ldots\ldots \qquad (4.12)$$

where τ = mean residence time determined from the experimental tracer response measurements

τ^* = mean residence time calculated on the basis of the volumetric liquid flow rate and the volume of bed available for flow.

4.3 A model with regions containing stagnant and flowing liquid

We shall now consider a model in which part of the liquid is considered to be essentially stagnant and some exchange occurs between the flowing and stagnant regions. The stagnant regions will exist in practice at the contact points between particles. The flowing region will be characterised by the axially dispersed plug flow model with an additional term to represent the mass transfer between the two zones. As with the previous model the presence of the gas phase does not enter into the describing equations directly but is reflected in the reduction in pore area available to the flowing liquid and in the values obtained for the liquid Dispersion Number.

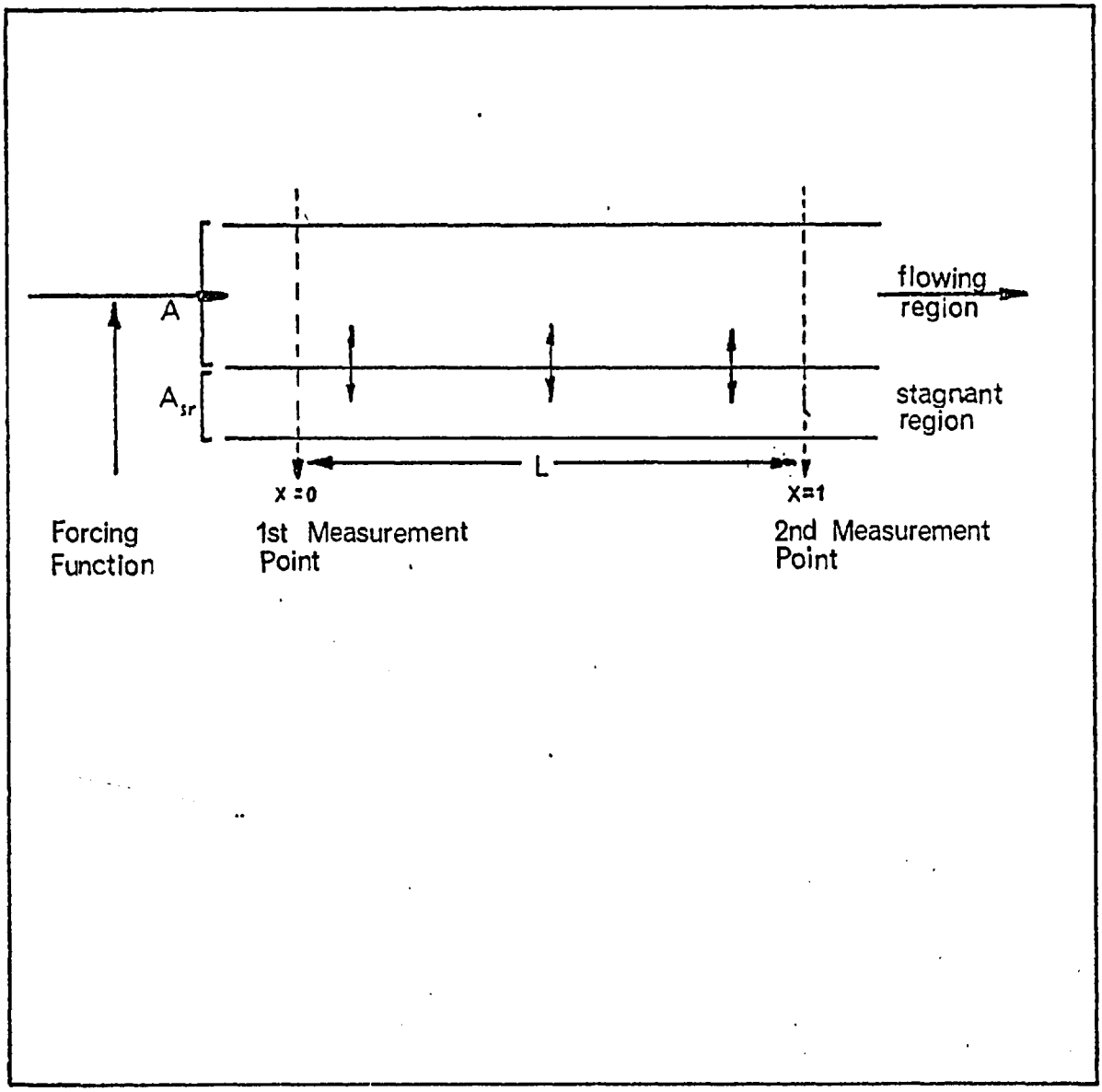

DIAGRAM OF STAGNANCY MODEL WITH INTERACTION BETWEEN FLOWING AND STAGNANT REGIONS

FIG 4.5

This model has been used by VILLERMAUX and VAN SWAAIJ(76) to represent some liquid residence time results obtained in a two phase system by VAN SWAAIJ et al(75). They, however, used moments analysis for a delta function input with a single measurement point to obtain the residence time distribution.

A diagrammatic representation of the model is given in Fig.4.5.

A balance over both flowing and stagnant liquid zones yields the following equations.

For the flowing region we have:

$$u\frac{\partial C}{\partial z} + \frac{k_e A_e}{A}\left[C - C_{sr}\right] + \frac{\partial C}{\partial t} = D_L\frac{\partial^2 C}{\partial z^2} \quad \ldots\ldots\ldots \quad (4.13)$$

and for the stagnant region

$$\frac{k_e A_e}{A_{sr}}\left[C - C_{sr}\right] = \frac{\partial C_{sr}}{\partial t} \quad \ldots\ldots\ldots \quad (4.14)$$

where: the subscript sr signifies conditions in the stagnant region

k_e	is a mass exchange coefficient	LT^{-1}
A_e	is the exchange area/unit bed length	L
A	is the pore area occupied by the flowing liquid	L^2
A_{sr}	is the pore area occupied by stagnant liquid	L^2

Defining γ as the fraction of the pore area available to the liquid which is occupied by flowing liquid we have

$$\gamma = \frac{A}{A+A_{sr}} \quad \ldots\ldots\ldots \quad (4.15)$$

As with the basic axially dispersed plug flow model we set $x = z/L$ and $\tau = L/u$ and after taking Laplace Transforms of eqs.4.13 and 4.14 we obtain:

$$\frac{d\bar{C}}{dx} + \frac{k_e A_e \tau}{A}\left[\bar{C} - \bar{C}_{sr}\right] + \tau p\bar{C} = N_D\frac{d^2\bar{C}}{dx^2} \quad \ldots\ldots\ldots \quad (4.16)$$

and

$$\frac{k_e A_e \tau}{A_{sr}}\left[\bar{C} - \bar{C}_{sr}\right] = \tau p\bar{C}_{sr} \quad \ldots\ldots\ldots \quad (4.17)$$

From eq.4.16 subsituting for A_{sr} in eq. 4.17 we find:

$$\bar{C}_{sr} = \frac{N_T\gamma}{N_T\gamma+\tau p(1-\gamma)}\ \bar{C} \quad \ldots\ldots\ldots \quad (4.18)$$

where $N_T = \frac{k_e A_e \tau}{A}$ is termed the number of Transfer Units (dimensionless)

Substituting for $\bar{C}_{sr}$ into eq. 4.16 we obtain:

$$N_D \frac{d^2\bar{C}}{dx^2} - \frac{d\bar{C}}{dx} - \left[\frac{N_T + \tau p\ (1 - \gamma)}{N_T\ \gamma + \tau p\ (1 - \gamma)}\right]\tau p\ \bar{C} = 0 \quad \ldots\ldots \quad (4.19)$$

For no stagnancy $A_{sr} = 0$ i.e. $\gamma = 1$ and eq. 4.19 reduces to the basic axially dispersed plug flow equation (eq.4.8).

Hence by analogy with eq. 4.11 the Transfer Function for the liquid stagnancy model is given by:

$$F(p) = \exp\left[\frac{1}{2N_D}\left\{1 - (\ + 4\tau pN_D\alpha)^{\frac{1}{2}}\right\}\right] \quad \ldots\ldots\ldots \quad (4.20)$$

where $$\alpha = \frac{N_T + \tau p\ (1 - \gamma)}{N_T\gamma + \tau p(1 - \gamma)} \quad \ldots\ldots\ldots \quad (4.21)$$

Whilst the model is characterised by the three parameters N_D, N_T and γ, it is better to write eq. 4.21 as:

$$\alpha = \frac{k_1 + p\ (1 - \gamma)}{k_1\gamma + p\ (1 - \gamma)} \qquad \text{where } k_1 = \frac{k_e A_e}{A} \quad \ldots \quad (4.22)$$

and to set $\tau = \gamma\phi_L\tau^*$ similar to eq.4.12.

A search is made in the four variables N_D, k_1, γ and ϕ_L.

Details of the effect of the model's parameters on the system's response are presented by VILLERMAUX and VAN SWAAIJ(76). Although these workers gave an expression for the inverse of the Laplace Transformed concentration it is so complicated as to limit its use in parameter estimation methods involving optimisation techniques. It is felt that the Transfer Function representation derived above, though lacking some of the advantages of a time domain solution, is to be preferred for its simplicity and clear resemblance to the form obtained for the axially dispersed plug flow model.

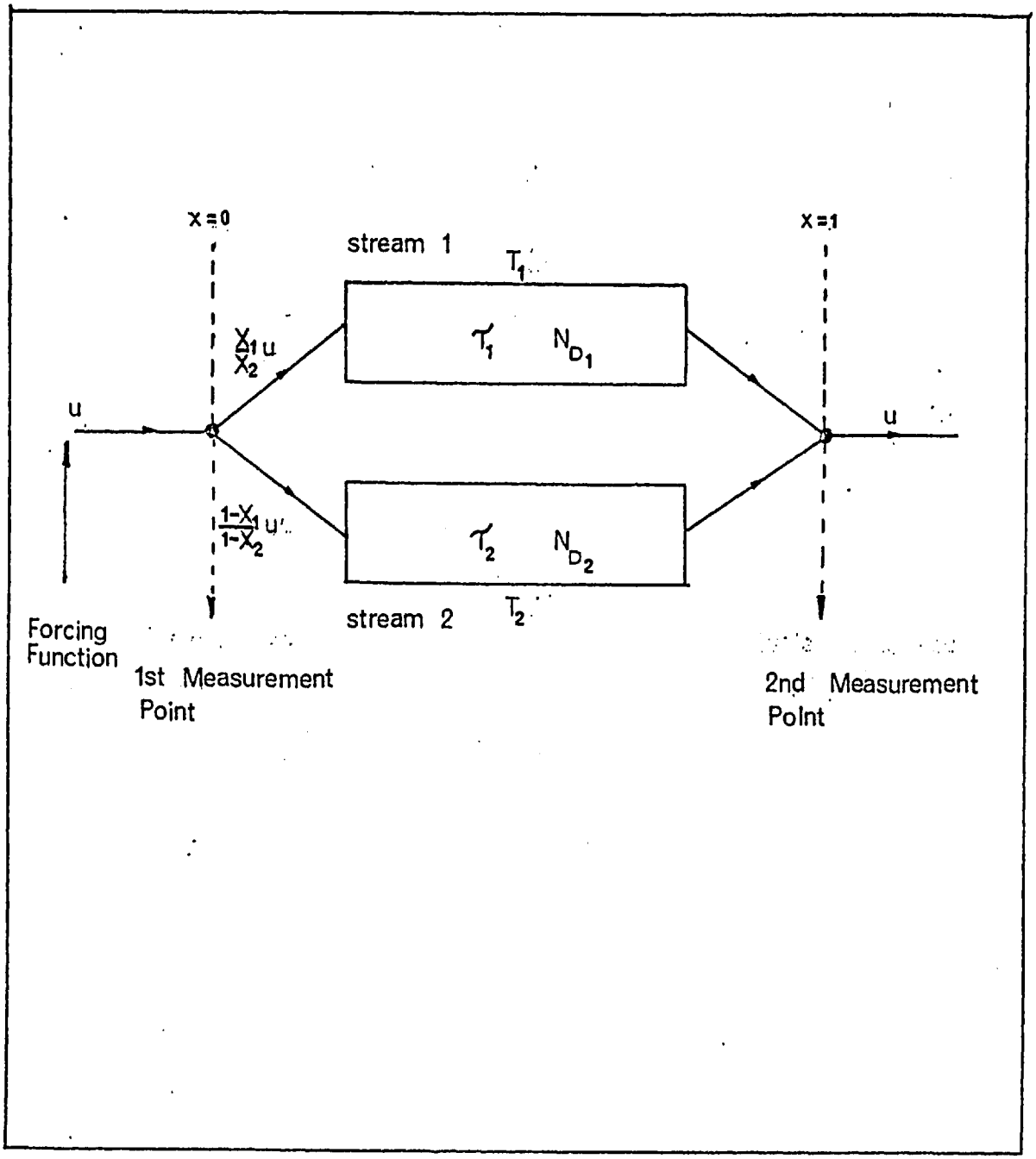

DIAGRAM OF SPLIT FLOW MODEL WITHOUT INTERACTION

FIG 4.6

4.4 A split flow model without stream interaction

In a two phase system the overall liquid hold up ϕ_L may be achieved by an infinite number of gas-liquid configurations. The idealisation of this complex physical situation results in every case in the postulation of two distinct flow areas. One zone will contain liquid whose passage through the packed bed can be considered to be unaffected by the gas. The other region will contain liquid streams which are influenced by the gas. In both zones it will be assumed that the liquid flows in such a manner that the basic axially dispersed plug flow model is applicable. Each region can, therefore, be described by Transfer Functions of the form given by eq.4.11. This two region model encompasses the liquid distribution model of EISENKLAM and FORD (20). If all the liquid passes through the region uninfluenced by gas then the flow regime is single phase pore flow. The other extreme when all the liquid flows with the gas is the two phase pore flow region.

The model is shown diagrammatically in Fig.4.6. The liquid phase is assumed to split on entry to the packed bed into its two idealised flow regions, designated 1 and 2, and recombines at the bed exit.

Each flow region is characterised by a mean interstitial velocity u_i and Dispersion Coefficient D_{Li}. As shown in Fig.4.6, two additional parameters X_1 and X_2 greatly increase the model's flexibility where:

X_1 is the fraction of the total liquid flow going through region 1

X_2 is the fraction of the total pore area available to the liquid which is associated with stream 1.

The liquid velocities in regions 1 and 2 are $\frac{X_1}{X_2}u$ and $\frac{1-X_1}{1-X_2}u$ respectively where u is the average pore velocity prior to flow splitting.

By analogy with eq.4.11 the two subsystem Transfer Functions $T_1(p)$ and $T_2(p)$ are given by:

$$T_1(p) = \exp\left[\frac{1}{2N_{D1}}\left\{1 - (1 + 4\tau_1 pN_{D1})^{\frac{1}{2}}\right\}\right] \quad \ldots\ldots \quad (4.23)$$

$$\text{and } T_2(p) = \exp\left[\frac{1}{2N_{D2}}\left\{1 - (1 + 4\tau_2 pN_{D2})^{\frac{1}{2}}\right\}\right]$$

The subsystem mean residence times τ_1 and τ_2 are related to the overall theoretical mean residence time τ^* by

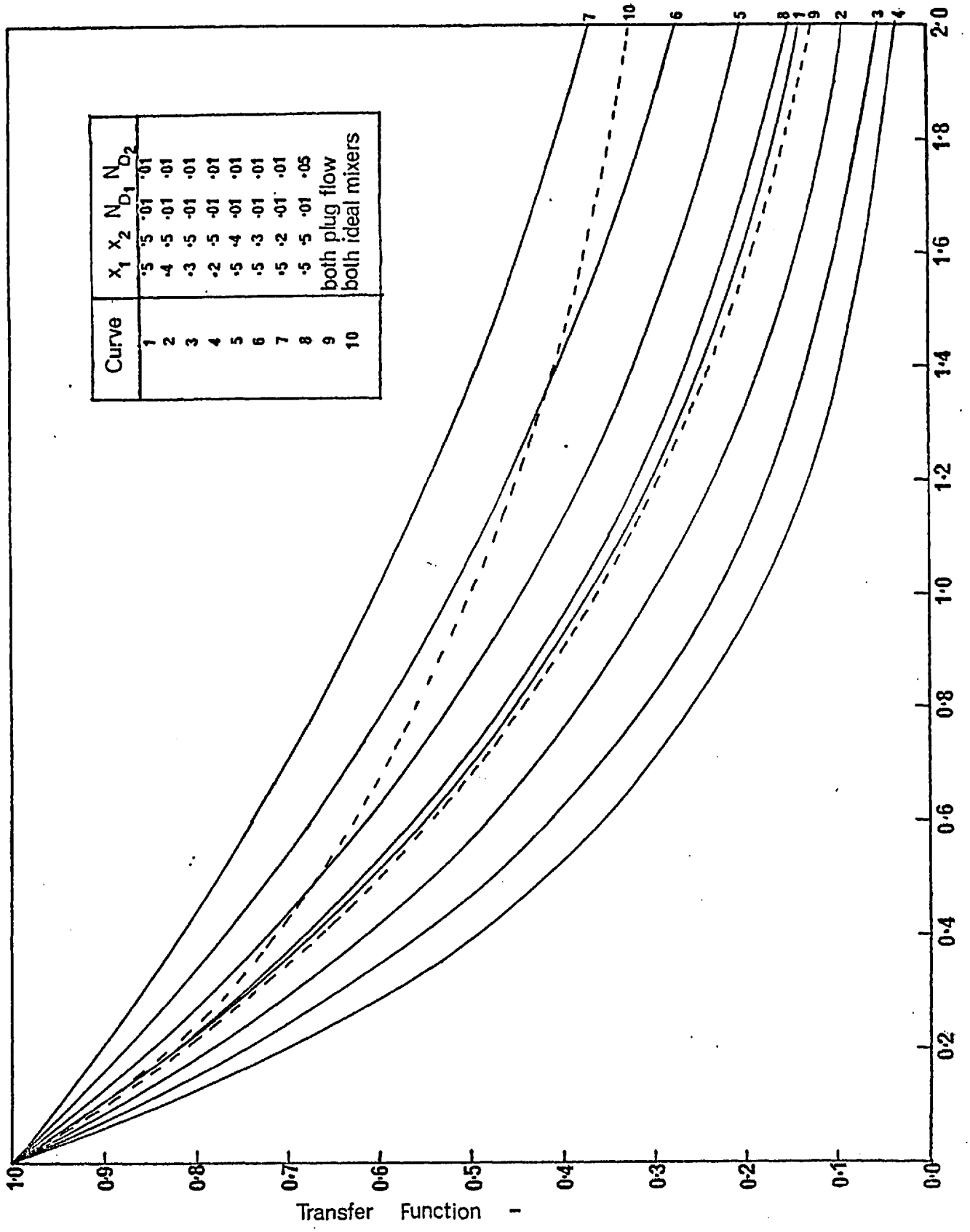

EFFECT OF SPLIT FLOW MODEL PARAMETERS ON SYSTEM TRANSFER FUNCTION

FIG 4.7

$$\tau_1 = \frac{X_2}{X_1}\ \phi_L\ \tau^* \quad \text{and} \quad \tau_2 = \frac{1 - X_2}{1 - X_1}\ \phi_L\ \tau^* \quad \ldots\ldots\ldots \quad (4.24)$$

In theory it is possible to assign either section to the flow region in which the liquid is influenced by the gas. The overall Transfer Function F(p) of the system is obtained simply by mass balance at the exit mixing point where, due to the linearity of Laplace Transforms, we find

$$F(p) = X_1 T_1(p) + (1-X_1) T_2(p) \quad \ldots\ldots\ldots \quad (4.25)$$

The flexibility of this model is shown in Fig.4.7, for the Laplace (p) domain, by the wide range of Transfer Function values possible at any given value of τp. The effects of varying the model's parameters in the time domain are illustrated in Figs. 4.8 to 4.10. For $X_1 = X_2 = 0.5$ and $N_{D1} = N_{D2} = N_D$ the split flow model is identical to the basic axially dispersed plug flow model with a Dispersion Number value of N_D. Thus curve 1 in Fig.4.7 is identical to curve 2 in Fig.4.3.

By adjusting the fractional flow split X_1 in Fig.4.8, from 0.5 to 0.2 it is possible to produce increasingly assymmetric curves. The peak of the curves appears earlier since the higher velocity stream is weighted by the greatest volumetric flow and hence has the greatest effect on the overall Transfer Function as indicated by eq. 4.25. Secondary peaks after the main peak are due to the slower stream. Curves 2, 3 and 4 in Fig.4.8, where the bulk of the liquid is travelling at a velocity greater than the overall mean velocity have Transfer Functions lying below curve 9 of Fig. 4.7 representing plug flow in both regions. It is clear therefore that there are no values for the Dispersion Number in the basic axially dispersed plug flow model which will match curves of the form shown in Fig.4.8. Similar effects are observed in Fig.4.9 where the area ratio is varied but 50% of the total volumetric flow always passes through each region. Again there is a tendency to form two peaks but this time the smaller peaks occur before the main peak. In the Laplace domain of Fig.4.7 the curves 5,6 and 7 move rapidly towards and beyond curve 10 which represents two equal volume perfect mixers in parallel. Thus any system where there are regions of differing velocity will be characterised by large, and often unrealistic values for the Dispersion Number, if only the basic axially dispersed plug flow model is used.

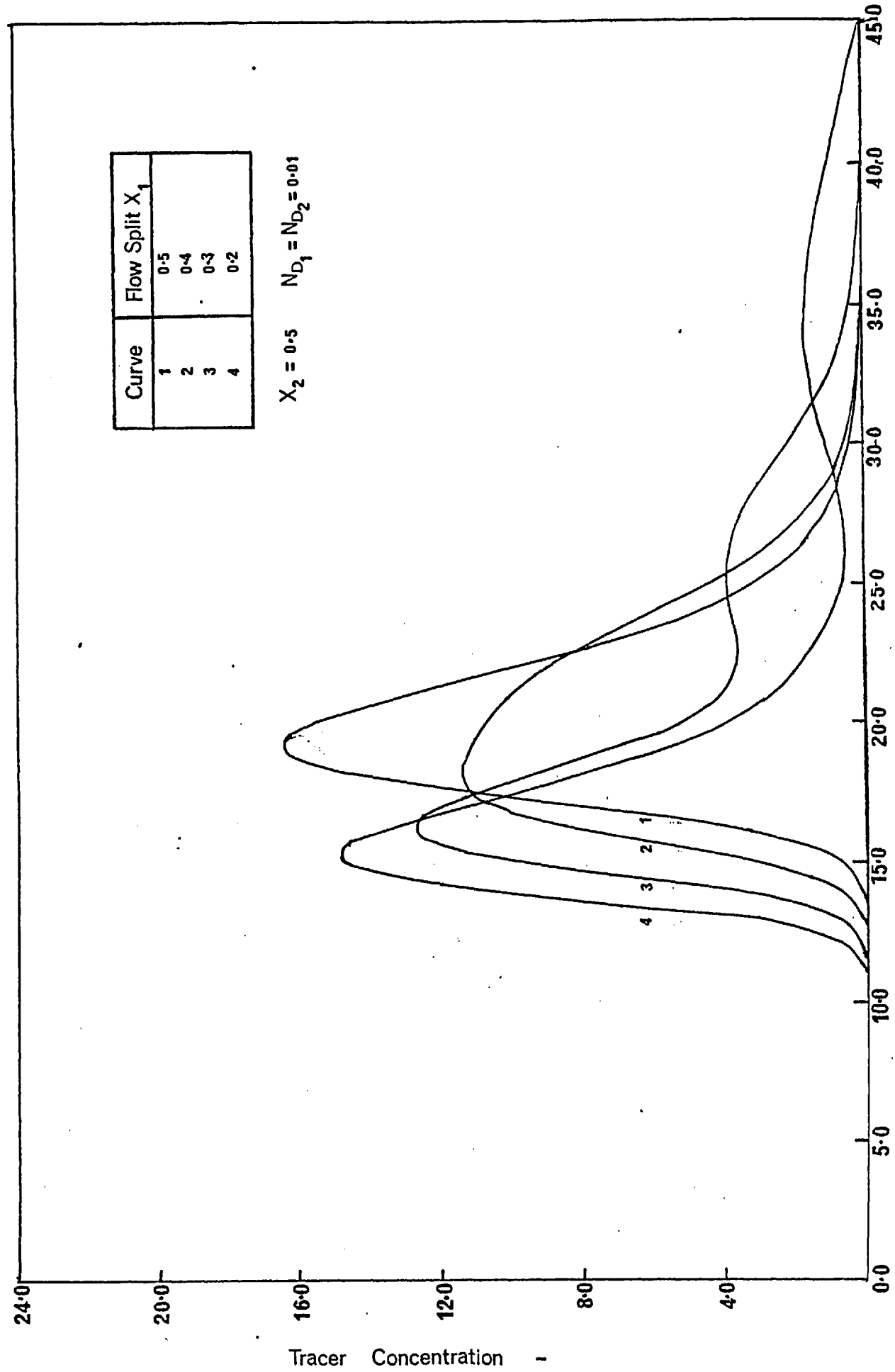

EFFECT OF FLOW SPLIT ON SYSTEM RESPONSE FOR SPLIT FLOW MODEL

FIG 4.8

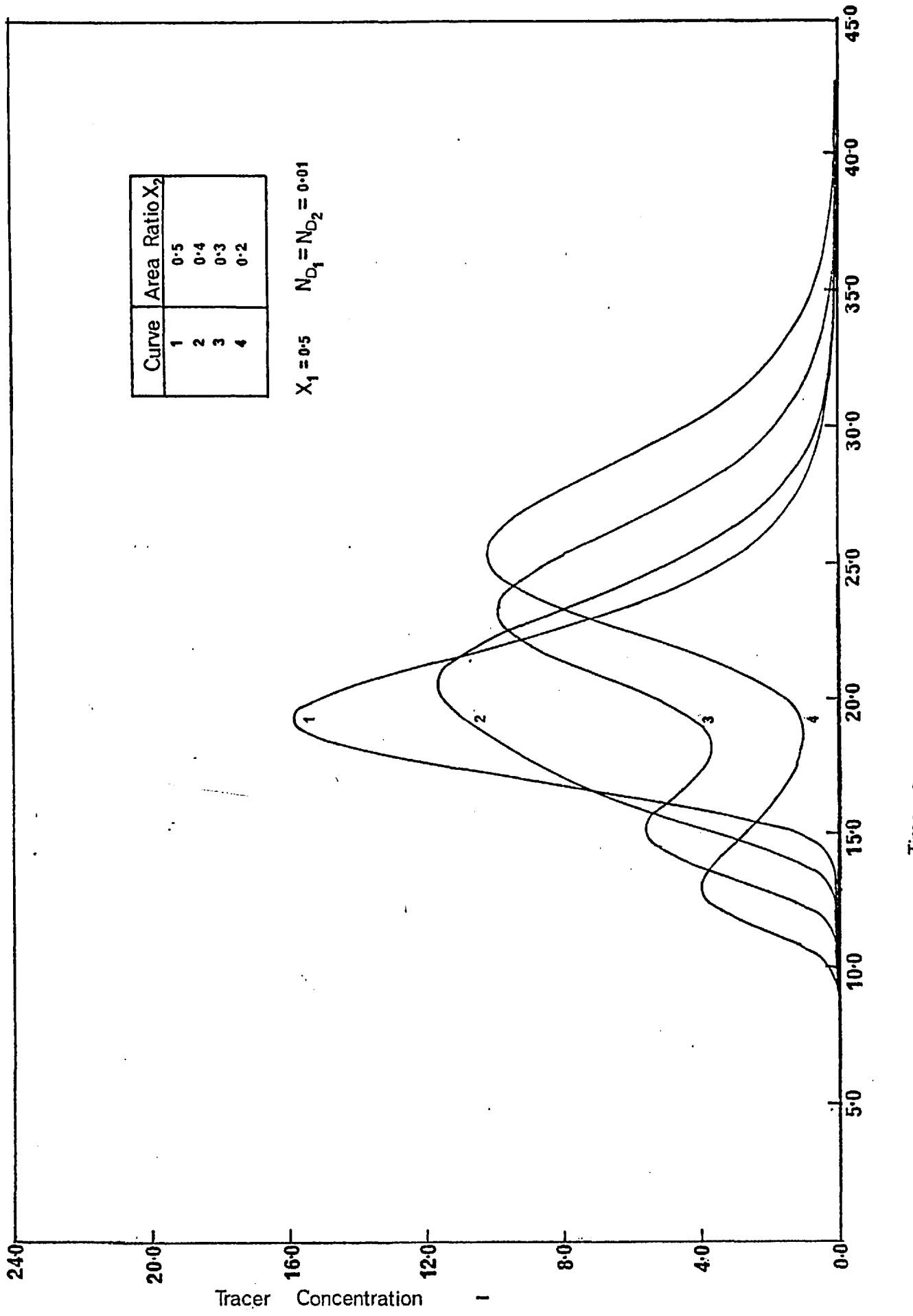

EFFECT OF FLOW AREA RATIO ON SYSTEM RESPONSE FOR SPLIT FLOW MODEL

FIG 4.9

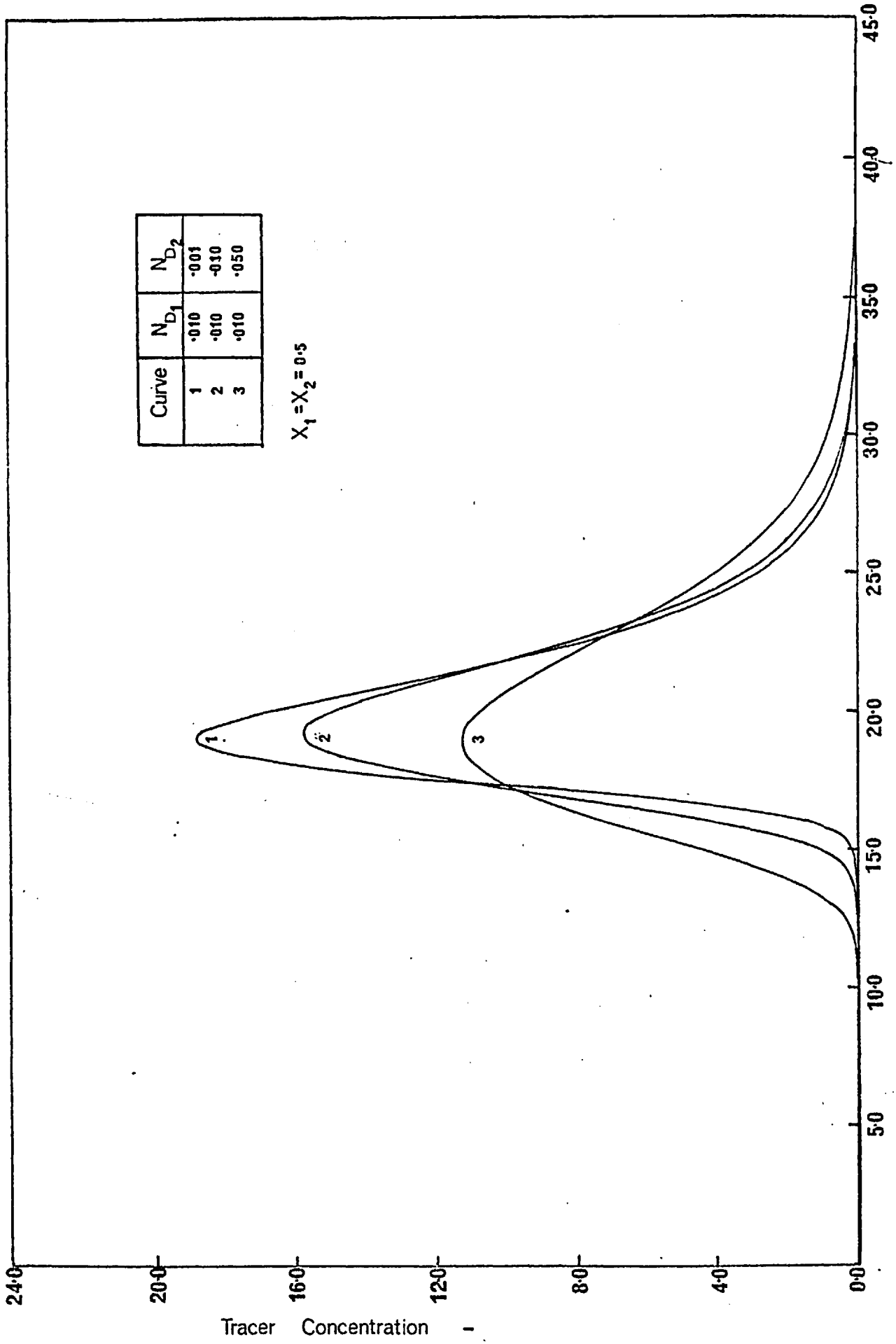

EFFECT OF SUBSYSTEM DISPERSION NUMBERS ON SYSTEM RESPONSE FOR SPLIT FLOW MODEL

FIG 4.10

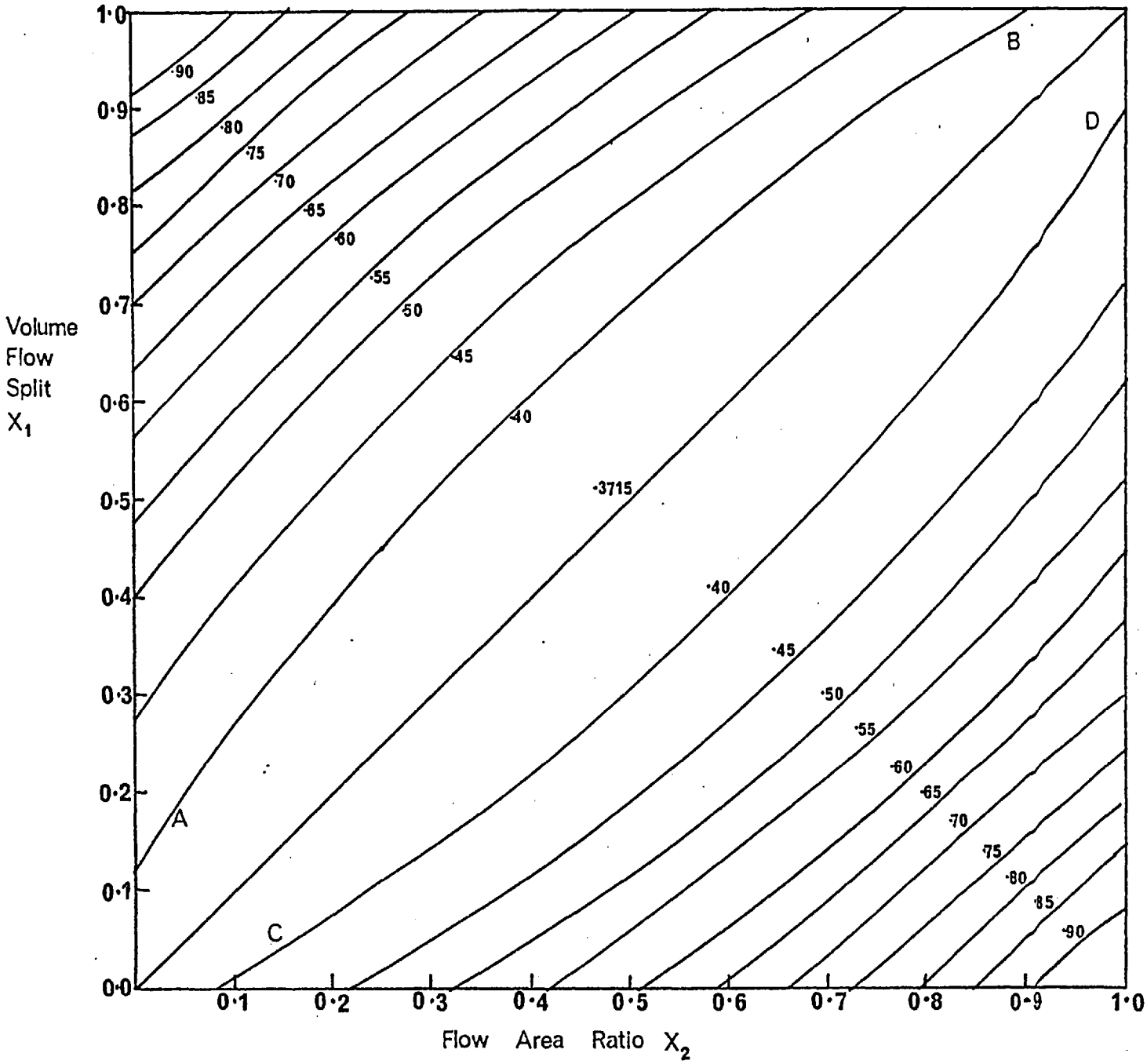

TRANSFER FUNCTION CONTOURS AT $\tau P = 1{\cdot}0$ AND SUBSYSTEM DISPERSION NUMBERS CONSTANT AT 0·01 FOR OVERALL SYSTEM

FIG 4.11

In the split flow model the effect of a subsystem Dispersion Number on the overall response will depend largely on the weighting given to that subsystem by the flow split. In Fig.4.4 curve 3, for the basic axially dispersed plug flow model with a Dispersion Number of 0.05, shows a large spread in the tracer curve. This spread is reduced quite considerably if only 50% of the fluid travels through a subsystem with a Dispersion Number of 0.05 and the remainder through a subsystem for which say $N_D = 0.01$ as shown by curve 2 of Fig.4.10.

It is possible to derive Transfer Function contours at any value of τp as functions of the parameters X_1 and X_2 whilst maintaining, as an example, the subsystem Dispersion Numbers constant. Typical contours are shown in Fig.4.11 for $\tau p = 1.0$ and $N_{D1} = 0.01$. Symmetry about the line $X_1 = X_2$ exists so that points such as A and D in Fig.4.11 are equivalent. A system whose Transfer Function at $\tau p = 1.0$ is 0.4 can be represented by any point on the curves AB or CD. The difficulties introduced by this symmetry when determining the model's parameters are discussed in Chapter 5.

From the above discussion the flexibility of the split flow model is apparent. The features of this model are:

(i) the reduced influence of the subsystem Dispersion Numbers on the overall Transfer Function, with the main deviations from plug flow accounted for by zones of different velocity

(ii) the ability to handle systems where the basic Dispersion model is not applicable.

4.5 A split flow model with stream interaction

It is recognised that the previous flow model is a simplification in that physical interaction between the two zones must result in some form of mass exchange between the streams.

Denoting the two regions by subscripts 1 and 2 we have, by analogy with eq. 4.16 which describes the flowing stream in the liquid

stagnancy model the following two equations:

$$N_{D1}\frac{d^2\bar{C}_1}{dx^2} - \frac{d\bar{C}_1}{dx} - \frac{k_e A_e \tau_1}{A_1}\left[\bar{C}_1 - \bar{C}_2\right] - \tau_1 p\bar{C}_1 = 0 \quad \ldots. \quad (4.26)$$

and $$N_{D2}\frac{d^2\bar{C}_2}{dx^2} - \frac{d\bar{C}_2}{dx} + \frac{k_e A_e \tau_2}{A_2}\left[\bar{C}_1 - \bar{C}_2\right] - \tau_2 p\bar{C}_2 = 0 \ldots. \quad (4.27)$$

where A_1 and A_2 represent the pore flow areas available to zones 1 and 2.

From eq. 4.27 we obtain:

$$\bar{C}_1 = \frac{A_2}{k_e A_e \tau_2}\left[\left\{\tau_2 p + \frac{k_e A_e \tau_2}{A_2}\right\}\bar{C}_2 + \frac{d\bar{C}_2}{dx} - N_{D2}\frac{d^2\bar{C}_2}{dx^2}\right] \quad \ldots. \quad (4.28)$$

Differentiating eq.4.28 twice with respect to x yields the following:

$$\frac{d\bar{C}_1}{dx} = \frac{A_2}{k_e A_e \tau_2}\left[\left\{\tau_2 p + \frac{k_e A_e \tau_2}{A_2}\right\}\frac{d\bar{C}_2}{dx} + \frac{d^2\bar{C}_2}{dx^2} - N_{D2}\frac{d^3\bar{C}_2}{dx^3}\right]$$

$$\frac{d^2\bar{C}_1}{dx^2} = \frac{A_2}{k_e A_e \tau_2}\left[\left\{\tau_2 p + \frac{k_e A_e \tau_2}{A_2}\right\}\frac{d^2\bar{C}_2}{dx^2} + \frac{d^3\bar{C}_2}{dx^3} - N_{D2}\frac{d^4\bar{C}_2}{dx^4}\right]$$

Substituting for $\bar{C}_1$ and its derivatives into eq.4.26 we obtain:

$$m_1\frac{d^4\bar{C}_2}{dx^4} + m_2\frac{d^3\bar{C}_2}{dx^3} + m_3\frac{d^2\bar{C}_2}{dx^2} + m_4\frac{d\bar{C}_2}{dx} + m_5\bar{C}_2 = 0 \quad \ldots. \quad (4.29)$$

where $m_1 = -N_{D1} N_{D2} m6$

$$m_2 = (N_{D1} + N_{D2})\, m_6$$

$$m_3 = \left(p\left[N_{D1}\tau_2 + N_{D2}\tau_1\right] - 1 + \frac{N_{D2}}{m_7}\right) m_6 + N_{D1}$$

$$m_4 = \left[p(\tau_1 - \tau_2) + {}^1/m_7 - {}^1/m_6\right] m_6$$

$$m_5 = {}^1/m_7 - (\tau_2 p + {}^1/m_6)(\tau_1 p + {}^1/m_7)\, m_6$$

$$m_6 = \frac{A_2}{k_e A_e \tau_2}$$

$$m_7 = \frac{A_1}{k_e A_e \tau_1}$$

The two liquid flow areas A_1 and A_2 and the two mean residence times can be related using the split flow model parameters X_1 and X_2.

By definition $X_2 = \frac{A_1}{A_1 + A_2}$

and $\tau_1 = \frac{X_2}{X_1} \phi_L \tau^*$, $\tau_2 = \frac{1 - X_2}{1 - X_1} \phi_L \tau^*$

The auxiliary equation of the 4^{th} order differential equation represented by eq. 4.29 will be a quartic, whose coefficients are functions of the model's parameters and whose roots are say Δ_i, i=1,4.

The solution to eq. 4.29 is therefore:

$$\bar{C}_2 (x,p) = \sum_{i=1}^{i=4} a_i \exp\left[\cdot \Delta_i x\right] \qquad \ldots\ldots\ldots \qquad (4.30)$$

where the constants a_i must be determined from the appropriate boundary conditions. MITAUCHI and VERMEULEN(51) have considered a steady state analysis for the above model and obtained an equation similar to eq. 4.29 except that since in the original equation $\frac{\partial C}{\partial t} = 0$, one root can be taken as $\Delta = 0$, reducing the problem to solving a cubic auxiliary equation. An extremely complex solution in terms of the coefficients m_i was obtained for each root Δ_i and using four boundary conditions the coefficients a_i were evaluated as functions of the model's parameters.

The solution to this unsteady state problem is extremely difficult by the conventional approach but these difficulties may be overcome by postulating a series solution to eq. 4.29 of the form:

$$\bar{C}_2 (x,p) = \sum_{k=0}^{k=\infty} a_k x^k \qquad \ldots\ldots\ldots \qquad (4.31)$$

where in general $\frac{d^r \bar{C}_2}{dx^r} = \sum_{k=r}^{k=\infty} k(k-1)(k-2)\ldots(k-r+1) a_k x^{k-r}$

$\ldots\ldots$ (4.32)

By definition $T_2(p) = \frac{\bar{C}_2(1,p)}{\bar{C}_2(0,p)}$ as in eq. 4.3.

$$\text{Thus } T_2(p) = \frac{1}{a_o} \sum_{k=0}^{k=\infty} a_k \qquad \ldots\ldots \qquad (4.33)$$

$$\text{or } T_2(p) = 1 + \sum_{k=1}^{k=\infty} b_k \text{ where } b_i = \frac{a_i}{a_o} \qquad \ldots\ldots \qquad (4.34)$$

The Transfer Function of both subsystems can be obtained in this manner.

The solution to this model will not be derived since the use of a model with this number of parameters is not justified unless some of the parameters can be determined by means other than tracer studies. However to illustrate this technique, a detailed solution to the problem of estimating the dispersion for isothermal compressible gas flow through a packed bed is given in Appendix A. To the author's knowledge the use of equations 4.31 to 4.34 in obtaining the system Transfer Function and the solution to the isothermal compressible flow problem have not been reported prior to this work. It is felt that this approach will extend the range of systems whose Transfer Functions are desired but are difficult to obtain by the usual techniques.

CHAPTER 5 PARAMETER ESTIMATION FROM EXPERIMENTAL DATA

5.1 Summary

We are concerned in this Chapter with particular methods for estimating the parameters of the three specific models developed in Chapter 4. For the basic axially dispersed plug flow model, four methods presented by MICHELSEN and OSTERGAARD(50) are considered. These methods enable the Dispersion Number to be determined directly from the system Transfer Function and its derivatives with respect to the Laplace Transform variable p. The problems associated with determining the optimum range of values for p are covered in detail. The two other models described in Chapter 4 must be analysed by parameter fitting through optimisation techniques due to the number of parameters involved. Finally, brief details are given of the computer programs used to interpret the experimental data and estimate the model's parameters by each method.

5.2 Analysis of the Axially Dispersed Plug Flow Model

Four methods have been derived by MICHELSEN and OSTERGAARD(50) for estimating the Dispersion Number from the system Transfer Function and its derivatives with respect to p.

5.2.1 Methods requiring one value of the Laplace Transform variable p

The Transfer Function for the axially dispersed plug flow model is given by eq. 4.11 as:

$$F(p) = e^{J} \quad \ldots\ldots\ldots \quad (5.1)$$

where $J = J(p)$ such that $J = \frac{1}{2N_D}(1 - k)$ .... (5.2)

and $k^2 = 1 + 4\tau p N_D$ ..... (5.3)

Differentiating eq. 5.1 we obtain:

$$\frac{dF(p)}{dp} = F(p)\frac{dJ}{dp} \quad \text{i.e.} \quad -\frac{dJ}{dp} = -\frac{dF(p)}{dp}/F(p)$$

From eq. 5.2 we find $\frac{-dJ}{dp} = \frac{\tau}{k} = Q$ say .... (5.4)

Combining eqs. 5.2 and 5.4 we can derive the following expressions for τ and N_D :

$$\tau = \frac{-JQ}{2Qp+J} \qquad \ldots\ldots\ldots \qquad (5.5)$$

$$N_D = \frac{J+Qp}{J(J+2Qp)} \qquad \ldots\ldots\ldots \qquad (5.6)$$

We now require to express J and Q in terms of the weighted moments $\bar{M}_i^r$. As defined by eq. 3.16 and eq. 3.18 we have

$$\bar{M}_i^r = \int_o^\infty t^r C_i(t) e^{-pt}\, dt = (-1)^r \frac{d^r \bar{C}_i}{dp^r}$$

In the subsequent derivations the subscripts i = o and i = 1 refer to the first and second measurement points respectively.

From eq. 5.1 $J = \log_e \left[F(p)\right]$

and by definition $F(p) = \dfrac{\int_o^\infty C_1(t)e^{-pt}\,dt}{\int_o^\infty C_o(t)e^{-pt}\,dt} = \dfrac{\bar{M}_1^o}{\bar{M}_o^o} \quad \ldots \qquad (5.7)$

Hence $J = \log_e \left[\dfrac{\bar{M}_1^o}{\bar{M}_o^o}\right] \qquad \ldots\ldots\ldots \qquad (5.8)$

From eq. 5.4 $Q = -\dfrac{dF(p)}{dp} / F(p)$

and from eq. 5.7 $F(p) = \dfrac{\bar{C}_1}{\bar{C}_o}$

$$\therefore \quad \frac{dF(p)}{dp} = \frac{\bar{C}_1'}{\bar{C}_o} - \frac{\bar{C}_1 \bar{C}_o'}{\bar{C}_o^2} \qquad \ldots\ldots\ldots \qquad (5.9)$$

where $\bar{C}_i' \equiv \dfrac{d\bar{C}_i}{dp} = -\bar{M}_i'$

$$\therefore \quad Q = -\frac{\bar{C}_1'}{\bar{C}_1} + \frac{\bar{C}_o'}{\bar{C}_o}$$

$$Q = \frac{\bar{M}_1^1}{\bar{M}_1^o} - \frac{\bar{M}_o^1}{\bar{M}_o^o} \qquad \ldots\ldots\ldots \qquad (5.10)$$

From the experimental tracer concentration measurements the weighted moments $\bar{M}_i^r$ can be calculated and hence J and Q from

eqs. 5.8 and 5.10. The parameters τ and N_D are then determined from eqs. 5.5 and 5.6 using the values of J and Q. These equations constitute the 1st method.

For the 2nd method we require $\frac{d}{dp}\left\{\frac{dF(p)}{dp}/F(p)\right\} = H$ say ... (5.11)

Thus from eq. 5.4 $H = -\frac{d}{dp}\left\{\frac{dJ}{dp}\right\} = -\frac{d}{dp}\left\{\frac{\tau}{k}\right\}$

$\therefore$ using eq. 5.3 $H = \frac{2\tau^2 N_D}{k^3}$ ..... (5.12)

Combining eq. 5.12 and 5.4 we obtain:

$$\tau = Q\left(1 - \frac{2pH}{Q}\right)^{-\frac{1}{2}} \quad \text{.....} \quad (5.13)$$

and $$N_D = \frac{H}{2Q^2}\left(1 - \frac{2pH}{Q}\right)^{-\frac{1}{2}} \quad \text{.....} \quad (5.14)$$

To evaluate eqs. 5.13 and 5.14 we require H in terms of the weighted moments $\bar{M}_i^r$.

Using eq.5.9 we have:

$$\frac{dF(p)}{dp}/F(p) = \frac{\bar{C}_1'}{\bar{C}_1} - \frac{\bar{C}_o'}{\bar{C}_o}$$

$$\therefore H = \frac{d}{dp}\left\{\frac{dF(p)}{dp}/F(p)\right\} = \frac{\bar{C}_1''}{\bar{C}_1} - \left\{\frac{\bar{C}_1'}{\bar{C}_1}\right\}^2 - \frac{\bar{C}_o''}{\bar{C}_o} + \left\{\frac{\bar{C}_o'}{\bar{C}_o}\right\}^2 \quad \text{...} \quad (5.15)$$

where $\bar{C}_i'' \equiv \frac{d^2\bar{C}_i}{dp^2} = \bar{M}_i^2$

Thus $$H = \frac{\bar{M}_1^2}{\bar{M}_1^o} - \left\{\frac{\bar{M}_1^1}{\bar{M}_1^o}\right\}^2 - \frac{\bar{M}_o^2}{\bar{M}_o^o} + \left\{\frac{\bar{M}_o^1}{\bar{M}_o^o}\right\}^2 \quad \text{.....} \quad (5.16)$$

The 2nd method involves evaluating the experimental weighted moments $\bar{M}_i^r$ for r = 0,1,2 at the two measurement points and hence determining H and Q from eqs. 5.16 and 5.10 respectively. Finally the parameters τ and N_D are calculated from eqs. 5.13 and 5.14.

The problem of determining the optimum value for p in methods 1 & 2 is analysed in section 5.3.

5.2.2 Methods requiring several values of the Laplace Transform variable p

From eq. 5.2 and 5.3 we can obtain:

$$-\frac{1}{J} = -N_D + \frac{\tau p}{J^2} \qquad \ldots\ldots \qquad (5.17)$$

Hence a plot of $-\frac{1}{J}$ vs $^{P}/J^2$ should yield a straight line of slope τ and intercept $-N_D$. This constitutes the third method.

From eqs. 5.3 and 5.4 we may also obtain:

$$\frac{1}{Q^2} = \frac{1}{\tau^2} + \frac{4N_D p}{\tau} \qquad \ldots\ldots\ldots \qquad (5.18)$$

A plot of $^{1}/Q^2$ vs p should give a straight line of slope $\frac{4N_D}{\tau}$ and and intercept $^{1}/\tau^2$. This linearisation constitutes the fourth method.

5.3 Determination of suitable p values for the four direct methods

All of the methods given in section 5.2 utilise certain of the weighted moments $\bar{M}_i^r$ of the response curves. The value of any moment for either response curve will depend on the value used for p. In an early paper on this problem by the author et al(35), a general indication of the effect of the weighting function e^{-pt} on the response curves was given for method 3 using the zeroth moments. To minimise errors in both the front and rear portions of the response curve, there must be an upper and lower limit for the range of p values used. From an analysis of some of EDWARDS(19) experimental results for single phase gas flow through a packed bed a range of values for p such that $2 < \tau p < 5$ was suggested.

The more detailed analysis which follows indicates that the following factors also influence the choice of p.

(i) The shape of the system forcing function
(ii) The distance between injection and measurement points
(iii) The dispersion prevailing throughout the system.

These factors must be considered since they affect the measured tracer response curve.

There will also be some experimental error or noise associated with the measurement of $C_i(t)$ at any time t. Thus:

$$ {}_eC_i(t) = {}_tC_i(t) + \bar{v}(t) \text{ for } 0 \leq t \leq T \quad \ldots\ldots \quad (5.19) $$

where: v(t) is the noise component of the measured response

T is the upper time limit beyond which tracer is not detectable.

The pre-subscripts t and e denote the true and error tracer concentrations respectively.

Since the contribution of the noise to $\bar{M}^r$ will be $\int_o^T v(t) t^r e^{-pt} dt$ both the type and magnitude of the noise, as well as the time at which the noise occurs is important. The noise will in general be of two forms:

(i) A constant error, independent of ${}_tC_i(t)$ for all t

(ii) A variable error depending on the magnitude of ${}_tC_i(t)$.

Whether either or both of these two noise forms are present will depend to a large extent on the type of tracer used. Radioactive tracers will exhibit both forms, whilst the dye-photomultiplier arrangement used in this work is characterised by some constant error due to fluctuations about the mean recorded value. The direct methods utilise moments of different orders and it is to be expected that the optimum value(s) of p will vary with each method. The correct choice of p can be determined from a set of noise weighting functions E(t), which relate the error in any response curve to the error it produces in the calculated Dispersion Number N_D.

5.3.1 Evaluation of Noise Weighting Functions

This analysis is directed towards finding a value of p at which the error in the calculated Dispersion Number is a minimum.

Let ΔN_D be the relative error in the Dispersion Number such that:

$$ \Delta N_D = \frac{{}_eN_D - {}_tN_D}{{}_tN_D} \quad \ldots\ldots \quad (5.20) $$

where the true Dispersion Number ${}_tN_D$ would be obtained from noise free curves and the error Dispersion Number ${}_eN_D$ results from noise v(t) at any time t.

If we consider noise at some time t*, lasting for a time interval δt^*, then this will be operated on by some weighting function $E(t^*)$ to give an error δN_D such that:

$$\delta N_D = v(t^*)\, E(t^*)\delta t^* \qquad \ldots\ldots\ldots \qquad (5.21)$$

Assuming the total error in N_D is the sum of individual errors over infinitessimal time intervals we have, for noise at measurement point i only:

$$\Delta N_D = \int_o^\infty v_i(t)E_i(t)dt \qquad \ldots\ldots\ldots \qquad (5.22)$$

For convenience we define an error integral ${}_eI_i$ for noise occurring on the response measured at position i as:

$${}_eI_i = \int_o^\infty v_i(t)E_i(t)dt \qquad \ldots\ldots\ldots \qquad (5.23)$$

As there will be simultaneous noise on the responses at both measurement points it will be assumed, following MICHELSEN and OSTERGAARD(50) that the total error in the Dispersion Number is proportional to the sum of the absolute errors on each individual response

$$\text{Hence} \quad \Delta N_D \propto \left\{ {}_eI_o^{\,2} + {}_eI_1^{\,2} \right\}^{\frac{1}{2}} \qquad \ldots\ldots\ldots \qquad (5.24)$$

The desired value of p is therefore that at which $\left\{ {}_eI_o^{\,2} + {}_eI_1^{\,2} \right\}^{\frac{1}{2}}$ is a minimum. To evaluate the error integrals defined in eq. 5.23 some estimate for $v_i(t)$ must be made. When using a dye-photomultiplier tracer detector, the main error will be in the estimation of the base-line voltage and thus it is reasonable to assume $v_i(t)$ is constant. In this case the mean value of the noise weighting function may be used:

$$\text{Hence} \quad {}_eI_i = \frac{1}{T}\int_o^T E_i(t)dt \qquad \ldots\ldots\ldots \qquad (5.25)$$

where T is the upper time limit beyond which the tracer concentration is not measurable.

Details of the determination of the noise weighting functions E(t), for methods 1 and 2 requiring a single value of p, have been given by MICHELSEN and OSTERGAARD(50). Their results were, however, presented in a form unsuitable for direct use in the present studies for the following reasons:

(a) The system mean residence time τ and Peclet Number Pe (where Pe = $^{1}/N_D$) must be known to evaluate E(t).

(b) The error free weighted moments are required.

Since τ and N_D are to be determined from experimental results, and are therefore unknown (a) makes the following iterative procedure necessary to obtain τ and N_D.

(i) Estimate values for τ and N_D and find minimum value of noise weighting functions to obtain optimum value of p.

(ii) Determine values for τ and N_D from one of the direct methods at this value of p.

If there is any discrepancy between the two sets of estimates the procedure must be repeated.

In the present work, the weighted moments available to calculate the noise weighting functions are those derived from the experimental response curves and hence not error free.

An analysis was undertaken to express the noise weighting functions solely in terms of the modified moments derived from the experimental response curves at the two measurement points.

Details of the analysis are given in Appendix B and the following points should be noted:

(a) The noise weighting function for the Dispersion Number is of the opposite sign to the noise weighting function on the Peclet Number.

(b) In the expressions given by MICHELSEN and OSTERGAARD(50) the error free weighted moments $_t\bar{M}_i^r$ can be replaced by the experimentally measured moments $_e\bar{M}_i^r$.

(c) There are discrepancies between the two analyses, in particular a term $_e\bar{M}_i^o$ is missing from eq.49 in Appendix B of the MICHELSEN and OSTERGAARD(50) study.

Typical noise weighting functions $E_i(t)$ are shown in Fig.5.1 for methods 1 and 2 (section 5.2.1). The curves illustrated are those obtained from experiment 11 for gas and liquid Reynolds Numbers of 59.7 and 48.7 respectively. The curves relating to the 2nd measurement point have large positive noise weighting functions for noise shortly after injection for both methods. Larger errors would be expected with method 2. Due to the exponential damping, noise occurring at times greater than the mean residence time is less important than noise in the early portions of the response. Experimental curves should be filtered to ensure that all base line fluctuations, prior to the time at which a definite curve rise appears, are removed. This filtering is done automatically by eye when using results stored on graph recorders but must be accomplished

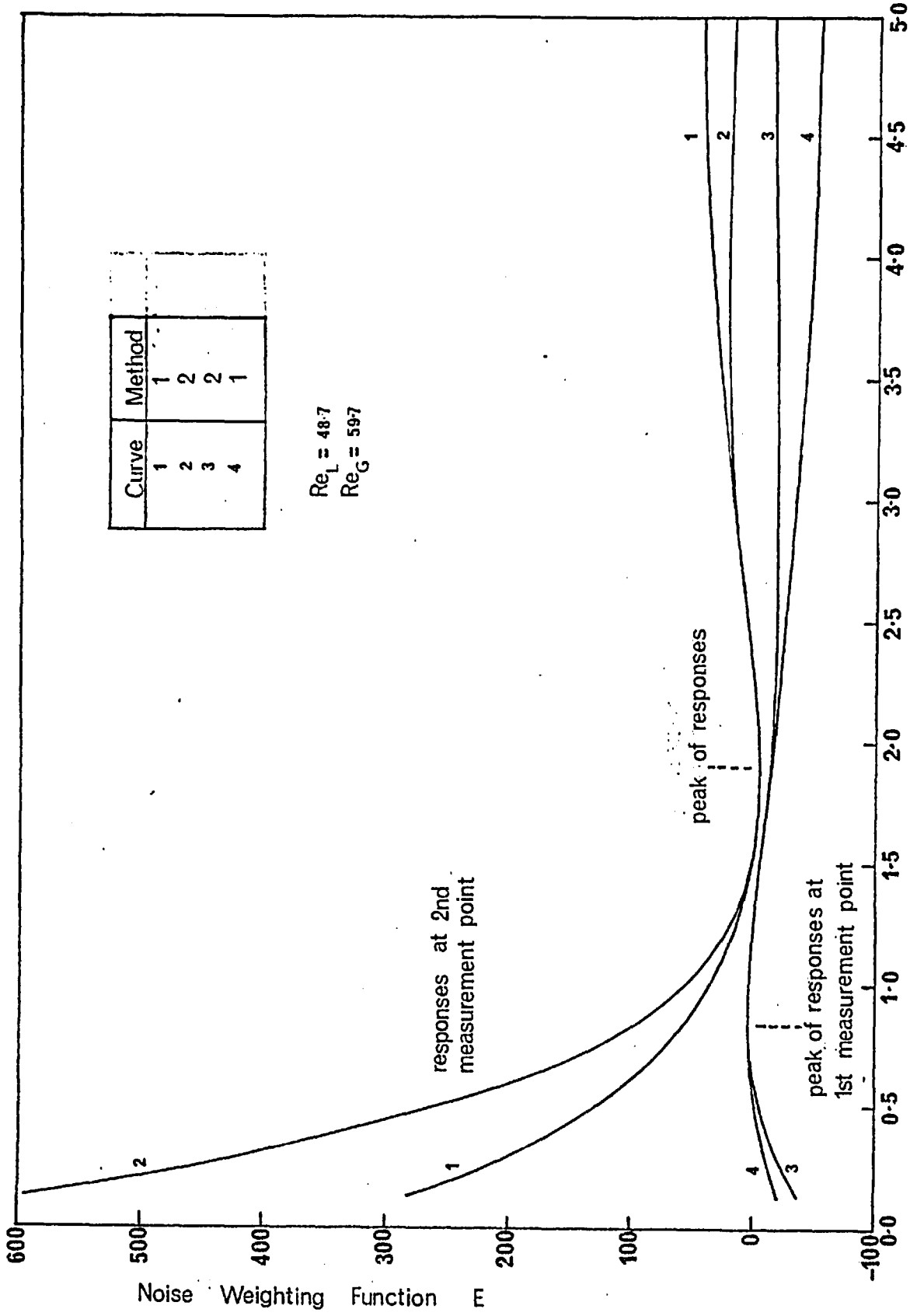

NOISE SENSITIVITY OF SYSTEM RESPONSES WITH METHODS 1 & 2 FOR BASIC DISPERSION MODEL

FIG 5.1

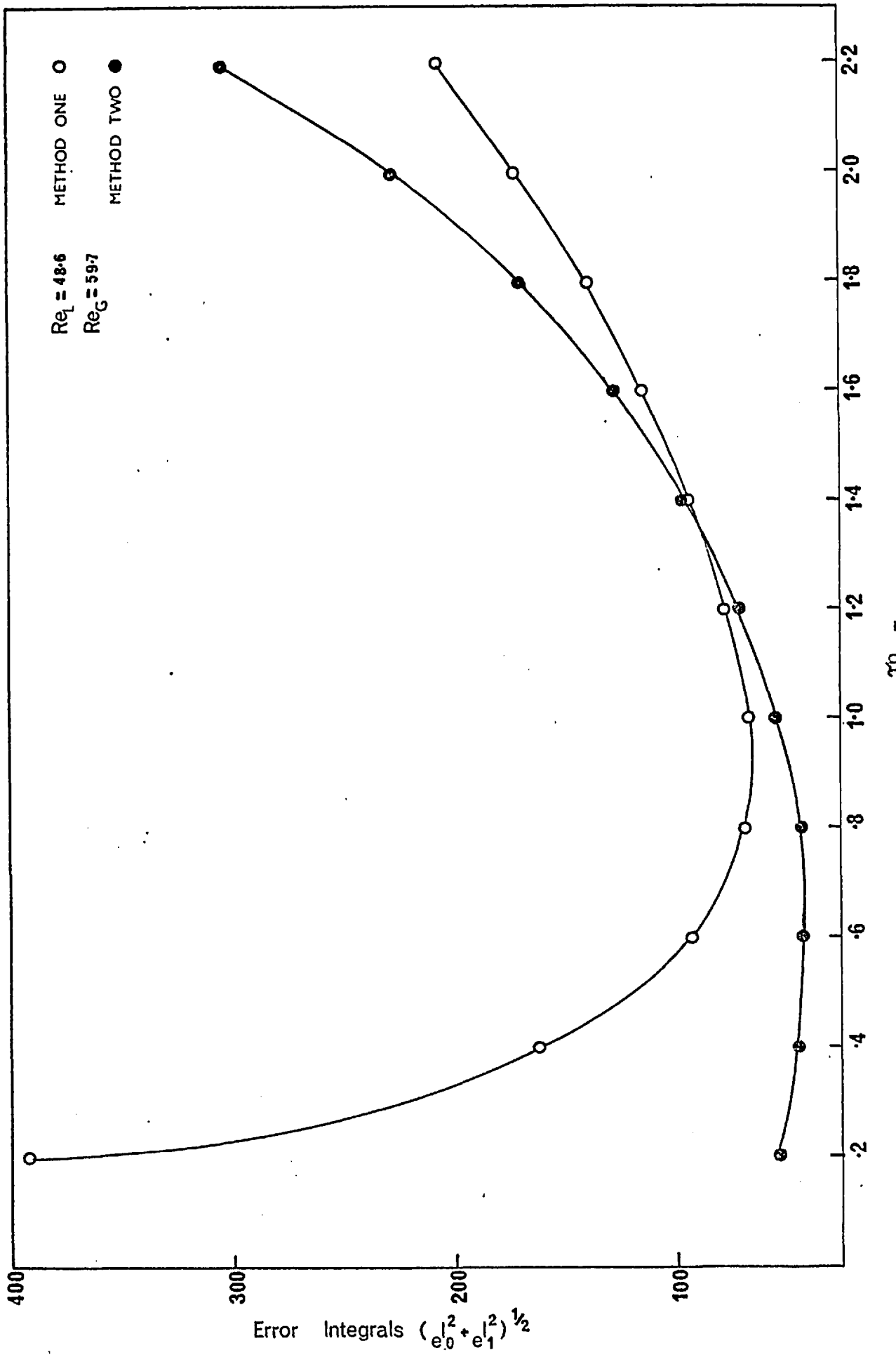

ERROR IN EVALUATION OF DISPERSION NUMBER BY METHODS 1 & 2

FIG 5.2

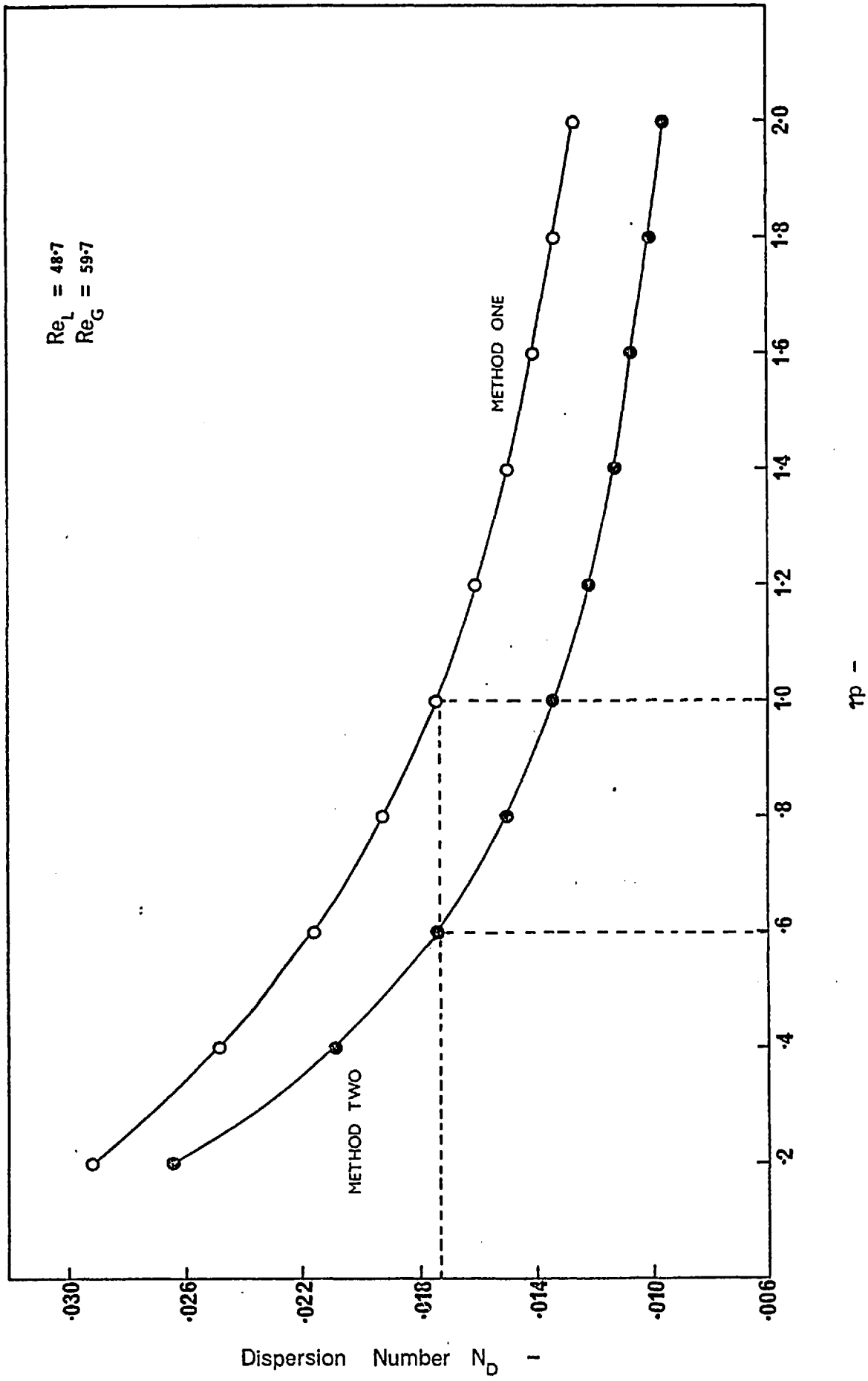

VARIATION IN DISPERSION NUMBER WITH τ_P FOR BASIC DISPERSION MODEL

FIG 5.3

numerically when analysing results stored on magnetic tape as described in Chapter 6.As a qualitative assessment would predict, noise near the mean of either response curve has little effect on the Dispersion Number. The form of the noise weighting functions is shown to be correct by the qualitative discussion given in Appendix C.

The error integral curves for the noise functions shown in Fig.5.1 are illustrated in Fig.5.2. The minima occur at different values of τp for both methods due to the different weighted moments used in each case. Fig.5.3 shows the effect of varying the Laplace Transform variable p, expressed as τp, on the evaluated Dispersion Number. However methods 1 and 2 both give the same value for the Dispersion Number if the value of p used in each method, is taken as that giving the minimum in the appropriate error integral curve of Fig.5.2.

MICHELSEN and OSTERGAARD(5) showed that similar values for τ and N_D were obtained from methods 1 and 3 if the arithmetic mean of the several p values used in method 3 was the same as the single value used in method 1. A similar correspondence was found between methods 2 and 4. Since the noise weighting functions for methods 3 and 4 require an estimate of the Dispersion Number before they can be evaluated, an iterative process is required to determine the minimum in the error integral curves. To avoid this, the findings of MICHELSEN and OSTERGAARD(50) were accepted and two τp values either side of the value used in methods 1 and 2 were used in methods 3 and 4 respectively. The general level of consistency between the values obtained by the four methods, as shown in Appendix E justifies this approach.

5.4 Parameter Estimation for the split flow model without interaction and stagnancy model with interaction

In contrast to the axially dispersed plug flow model it was not possible to obtain explicit relationships for the parameters of these two models due to the larger number of parameters involved. Recourse to some indirect optimisation technique was therefore necessary.

5.4.1 Split flow model without interaction

The Transfer Functions for each region and the overall system Transfer Function for this model were given in Chapter 4 eqs. 4.23 and 4.25 respectively. In order to reduce the number of parameters, one region was assumed gas free. It is reasonable therefore to assume that the Dispersion Number in this region, where liquid would be flowing at a particular Reynolds Number, Re_L, could be taken as that which would occur in a

packed bed in which liquid alone was flowing at that same Reynolds Number. The reported data for liquid dispersion, as summarised by GUNN(28) can be reasonably approximated by:

$$N_D = 0.027\ Re_L^{-0.27} \qquad \ldots\ldots\ldots \qquad (5.26)$$

Since it will be shown later that the importance of the subsystem Dispersion Number is drastically reduced in a split flow model, high accuracy is not demanded from eq. 5.26. The Dispersion Number in the second zone will depend on both the Dispersion coefficient D_{L2} and the liquid velocity in that zone. Since the liquid velocity and hence the mean residence time in both zones can be expressed as functions of X_1 and X_2 and ϕ_L, the system is characterised by the four parameters D_{L2}, X_1, X_2 and ϕ_L.

These parameters can be determined by minimising the difference between some property of the theoretical model and its experimental equivalent.

Two of a number of possibilities are:

(i) At a particular value of p match the Transfer Function, first and higher derivatives with respect to p

(ii) For a range of p values match only the experimental and theoretical Transfer Functions.

The latter approach is better in that a least squares solution can be obtained. In this work, the parameters were estimated by minimising the square error between the experimental Transfer Function G(p) and theoretical Transfer Function F(p) for 20 values of p chosen such that τp lay in the range $0.2 \leq \tau p \leq 3.0$. This range on τp was chosen to cover the region of maximum variation of F(p) with τp. Transfer Function fitting was used in preference to the derivatives due to the increase in experimental errors associated with the latter, since they contain higher weighted moments of the response curves. The derivatives may however be used as checks on the parameter estimates obtained from Transfer Function fitting. WILLIAMS et al(81) found Transfer Function fitting over a range of p values from 1 to 10 quite acceptable in their fitting of a 2 parameter model for gas mixing in a fluidised bed.

The theoretical 1st and 2nd derivatives with respect to p are obtained from eqs. 4.23 and 4.25 for the split flow model:

$$\frac{dF(p)}{dp} = -\left\{\frac{X_1\tau_1 T_1(p)}{(1+4\tau_1 pN_{D1})^{\frac{1}{2}}} + \frac{(1-X_1)\tau_2 T_2(p)}{(1+4\tau_2 pN_{D2})^{\frac{1}{2}}}\right\} \quad \ldots\ldots \quad (5.27)$$

and $$\frac{d^2F(p)}{dp^2} = \frac{X_1\tau_1^2 T_1(p)}{1+4\tau_1 pN_{D_1}}\left\{1 + \frac{2N_{D1}}{(1+4\tau_1 pN_{D_1})^{\frac{1}{2}}}\right\}$$

$$+ \frac{(1-X_1)\tau_2^2 T_2(p)}{1+4\tau_2 p\, N_{D2}}\left\{1 + \frac{2N_{D2}}{(1+4\tau_2 pN_{D2})^{\frac{1}{2}}}\right\} \ldots \quad (5.28)$$

The experimental 1st and 2nd derivatives with respect to p are obtained from eq. 5.7 i.e.

$$G(p) = \frac{\bar{M}_1^o}{\bar{M}_o^o}$$

we find $$\frac{dG(p)}{dp} = \frac{\bar{M}_1^o}{\bar{M}_o^o}\left\{\frac{\bar{M}_o^1}{\bar{M}_o^o} - \frac{\bar{M}_1^1}{\bar{M}_1^o}\right\} \quad \ldots\ldots \quad (5.29)$$

and $$\frac{d^2G(p)}{dp^2} = \frac{\bar{M}_1^o}{\bar{M}_o^o}\left\{\frac{\bar{M}_1^2}{\bar{M}_1^o} - \frac{\bar{M}_o^2}{\bar{M}_o^o}\right\} + 2\,\frac{\bar{M}_o^1}{\bar{M}_o^o}\left\{\frac{\bar{M}_1^o}{\bar{M}_o^o}\left[\frac{\bar{M}_o^1}{\bar{M}_o^o} - \frac{\bar{M}_1^1}{\bar{M}_1^o}\right]\right\} \ldots \quad (5.30)$$

We can therefore define the problem as one of seeking values for the model parameters such that S is minimised where:

$$S = \sum_{i=1}^{i=20}\left[1 - \frac{F_i(p)}{G_i(p)}\right]^2 \quad \ldots\ldots \quad (5.31)$$

The fractional errors at each p value prevent the solution being dominated by the numerically largest values occurring at low values of τp.

Fig.5.4 illustrates a typical response surface, during Transfer Function minimisation, as a function of the variables X_1 and X_2 when, for example, $N_{D1} = N_{D2} = 0.01$. The similarity between this surface and the Transfer Function contours given in Fig.4.11 is clear, with the symmetry about $X_1 = X_2$. In Fig.5.4, for which the solution lies at $X_1 = 0.6$, $X_2 = 0.4$, two curved valleys appear, separated by a ridge. Since there is also a solution at $X_1 = 0.4$, $X_2 = 0.6$, then if the same solution is to be found from different initial points, these starting points must be on the same side of the ridge. All the contours in Fig.5.4 are open-ended. However, the expanded view around the solution point, indicated by the box

Contours of $\sum_{i=1}^{i=20} \left[1 - \frac{F_i}{G_i}\right]^2$ = constant

● solution points

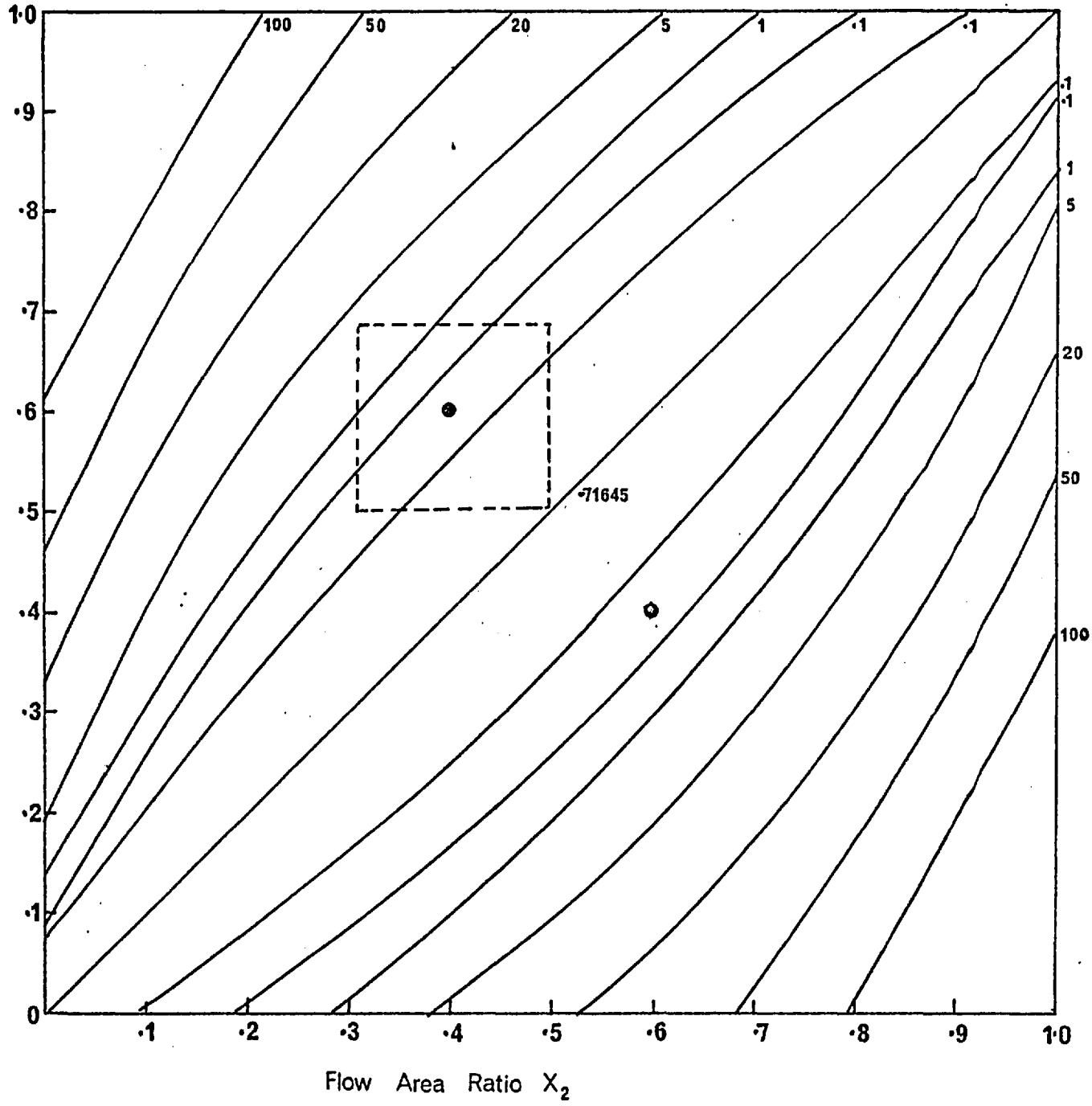

RESPONSE SURFACE FOR TRANSFER FUNCTION FITTING OF SPLIT FLOW MODEL

FIG 5.4

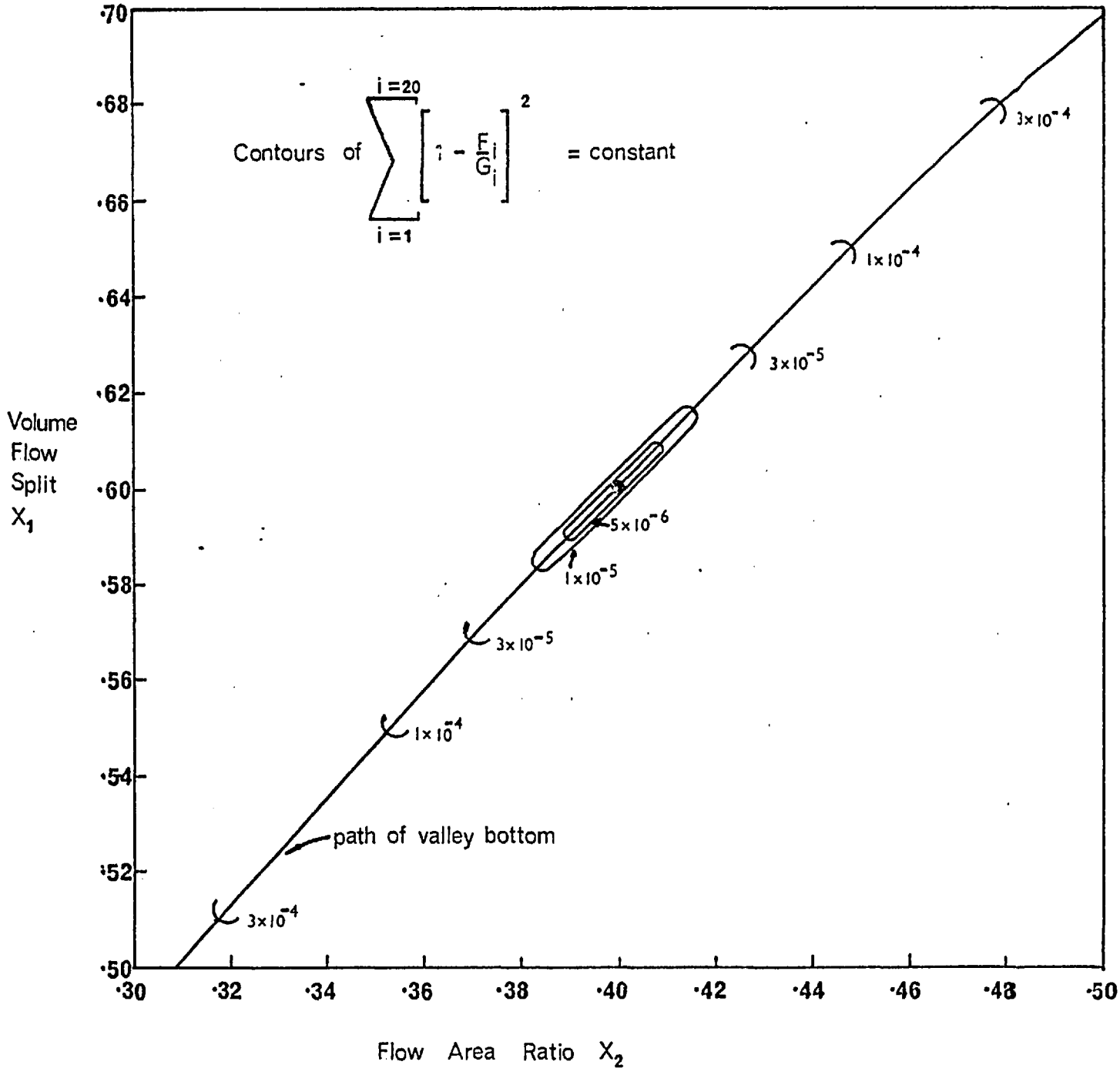

LOCALISED RESPONSE SURFACE FOR TRANSFER FUNCTION FITTING OF SPLIT FLOW MODEL

FIG 5.5

in Fig.5.4, shows that contours representing a sum of squares less than 3×10^{-4} are closed by the parameter values $0.5 \leq X_1 \leq 0.7$ and $0.3 \leq X_2 \leq 0.5$. This is shown in Fig.5.5.

The curve representing the path of the valley bottom, as determined by a Fibonacci search, is shown and a number of contour values marked on it. For the parameter values shown this curve is approximately represented by the line $X_1 = X_2$. The contours are elongated parallel to the valley bottom, yet very narrow normal to the valley. Thus to remain within a given contour for a given value of X_2 say, only small changes can be made in X_1. However the ratio X_1/X_2 may vary considerably and still remain within the same sum of squares contour. A response surface very similar to that shown in Fig.5.4 would be obtained if any of the derivatives of the Transfer Function were used in the minimisation.

5.4.2 Liquid stagnancy model with interaction

The following four parameters were estimated for the liquid stagnancy model by Transfer Function minimisation using eq.4.20.

(i) The system Dispersion Number N_D

(ii) The number of Transfer units N_T, representing the interchange between the flowing and stagnant liquid zones.

(iii) The fraction of the pore area available to the liquid which is occupied by flowing liquid, γ.

(iv) The overall liquid holdup ϕ_L.

5.5 Optimisation Algorithms used in parameter estimation studies

Of the three minimisation algorithms tried, that developed by POWELL(55) proved to be the most successful.

Initially a general method suggested by ROSENBROCK and STOREY(59) was tested, in which successive function evaluations were compared, and a set of rules defined the action to be taken according to the outcome of the comparison. If $S(\underline{x}_1)$ and $S(\underline{x}_2)$ where $S(\underline{x}_2) = S(\underline{x}_1 + \underline{\Delta})$ were two such evaluations the problem reduced to finding the length and direction of $\underline{\Delta}$ such that the step made was an improvement. A set of n orthogonal unit vectors $\underline{V}_i$ and an associated set of step lengths e_i were stored such that successive steps in $\underline{x}$ were

$e_{1-1}V_1$, $e_{2-2}V_2$....$e_{n-n}V_n$... The step lengths were either trebled or halved depending on whether the last step was successful or not. The procedure was rejected due to the large number of function evaluations required and the problems encountered in escaping from the constraint boundaries on the parameter values, especially with the split flow model where both X_1 and X_2 are bounded by $0 \leq X_1 \leq 1$ and $0 \leq X_2 \leq 1$.

The second method by MURTAGH and SARGENT(52), whilst in principle the most powerful, sometimes proved unreliable and unable to obtain the best solution. The method was based on assuming a local quadratic approximation to the function and constructing successive approximations to the inverse of the Hessian matrix $\underline{\underline{H}}^{-1}$. This is then used to estimate the position of the minimum at each step.

Thus if $\underline{g}_{k-1}$ is the gradient at the point $\underline{x}_{k-1}$, then the change is given by:

$$\underline{g}_k - \underline{g}_{k-1} = \underline{\underline{H}} (\underline{x}_k - \underline{x}_{k-1}) \quad \ldots\ldots \quad (5.32)$$

Hence if $\underline{x}_k^*$ is the solution then $\underline{g}_k^* = 0$ and providing $\underline{\underline{H}}$ is non-singular

$$\underline{x}_k^* = \underline{x}_{k-1} - \underline{\underline{H}}^{-1} \underline{g}_{k-1} \quad \ldots\ldots \quad (5.33)$$

A method such as this should have been the most reliable especially as the gradient of the objective function was available analytically.

The method finally adopted was that due to POWELL(55), which did not require derivatives. Starting from the best known approximation to the overall minimum a search is made down the n linearly independent directions, so that the function is minimised in each direction. On each iteration a new direction is defined such that if a quadratic were being minimised the minimum would be found after n iterations.

5.6 Analysis of Experimental Data to obtain the weighted moments

The experimentally recorded tracer measurements were stored directly onto a magnetic tape by a data logging system as described in detail in Chapter 6. The response curve, at each measurement point, was described by 829 data points, each point being represented by the photomultiplier voltage. The first 50 data points were averaged to obtain a value for the base voltage and any reading greater than

this value, was set equal to the base voltage. This avoided negative estimates of the tracer concentration when using the logarithmic transformation on the photomultiplier voltages as described in Chapter 6.

From an estimate of the mean residence time, 20 values of the Laplace parameter p were chosen so that $0.2 \leq \tau p \leq 3.0$. For each of these p values, the zeroth, 1st and 2nd weighted moments were calculated together with the error integrals.

As a check on how rapidly the Dispersion Number was changing with p three values of p, around the p value giving the minimum in the error integrals, were used in the direct methods 1 and 2, eqs. 5.6 and 5.14, to determine the Dispersion Number and mean residence time. Five p values around the minimum error integral value of p were used in methods 3 and 4 which required several p values for the straight line relationships given in eqs. 5.17 and 5.18. Finally the experimental Transfer Function and its 1st and 2nd derivatives were calculated for use in the later optimisation studies for estimating the parameters in the two more complex models.

CHAPTER 6 EXPERIMENTAL EQUIPMENT AND MEASUREMENT TECHNIQUES

6.1 Summary

The experimental equipment and techniques used to obtain the dynamic response of a packed bed system containing two phases in upward cocurrent flow are described in this Chapter. The underlying reasons behind the choice of tracer and its effect on the experimental arrangement are discussed. The systems for injecting, detecting and recording the tracer pulses are examined in detail.

6.2 Choice of Tracer and Experimental Technique

The choice of tracer depends primarily on the environment to be studied. The mathematical techniques, described in section 3.4, for estimating the model's parameters from the experimental results, are to some extent of secondary importance. There are two possible ways to measure the system response at two bed positions:

either (i) the detector can be situated within the packed bed itself in such a manner as to minimise any disturbance of the fluid flow patterns

or (ii) the tracer must be capable of detection by equipment external to the packing.

A summary of the tracers used in single phase liquid dispersion studies is given by CHUNG and WEN(12). Tracers utilising the conductive properties of certain solutions have been used extensively with the small conductivity cell conveniently incorporated within the bed packing material. As with photoelectric techniques, the use of such systems is severely limited in two phase work due to the high level of noise induced by the presence of the gas phase.

Radioactive tracers, on the other hand, seem ideally suited since measurements can be made external to the packed bed and recordings are unaffected by the presence of either a second phase or any packing material. SATER and LEVENSPIEL(63) used I^{131}, a high toxicity nuclide, the radiation from which was detected by a scintillation counter. The pulses were amplified and sent via a rate meter to a pen recorder. The rate meter converted pulses received over a finite time interval into an instantaneous rate. The combination of resistances and capacitances effectively averages out these pulses over a time interval equal to twice the instrument's time constant

which is usually in the region of about 0.2 seconds at its lowest value. In this time interval a tracer particle can move 40mm along the column axis at the highest velocities encountered in the present study, resulting in completely erroneous pulse rates.

Even if a sufficiently fast rate meter, or some alternative device, were available to overcome this problem, a second difficulty inherent in the use of radiation would still exist. Since radioactive disintegration is random, sufficient pulses must be counted, over the time interval in question, to reduce the error in the count estimate to an acceptable level. Since the distribution is Gaussian, a 1% standard deviation would require 10,000 counts or a count rate of about 2.5×10^4 counts/sec for the time constant given above. For the high energy gamma emitters in the MeV range scintillation counter efficiency is around 20%. Since the pulse rate is taken to represent the average tracer concentration at a particular axial position, the solid angle viewed by the detector should be small. After allowing for all these factors, count rates in the region of 3×10^7 counts/sec are necessary. This corresponds to a radioactive solution strength of approximately 1 millicurie which is greater than that acceptable in normal laboratories if I^{131} is used. Due to its moderate toxicity it would however be possible to use Na^{24}, in the form of sodium chloride solution, at these concentrations if the necessary precautions were taken.

EDWARDS(19), in recognising this problem, has suggested an alternative theoretical and experimental technique. In view of this development it is felt that the practical difficulties associated with radioactive tracers outweigh their advantages. EDWARDS(19) approximation to the original two point measurement technique requires measurements of the tracer concentration at the bed exit. If phase separation can be achieved, without obliterating the tracer response, then either conductivity or photoelectric methods may be utilised. Due to its simplicity and rapid response to changes in tracer concentration, a photomultiplier-dye arrangement was chosen. Full details of the equipment are given in section 6.6.

For the following reasons tracer injection in the gas phase was not considered:

(i) Gas phase detectors such as beta ionisation and hot wire are sensitive to both water vapour and water droplets.

(ii) The response times of such detectors are usually slow.

(iii) The gas velocities encountered in this study are much greater than the liquid velocities, increasing the detection difficulties.

(iv) There are difficulties associated with the analysis of a compressible gaseous phase as illustrated in Appendix A.

(v) There are no indications that tracing the gas phase will yield more information on the flow regimes than can be deduced from studying the liquid phase.

6.3 The Overall Experimental System

The approximation to the two point technique allows separate measurements to be made outside of two packed bed sections of different lengths, as shown in Fig.3.2, providing conditions at both extremes of either packed bed remain the same and the tracer pulse is reproducible. A diagrammatic representation of the experimental apparatus used to obtain the system responses at two different bed lengths is shown in Fig.6.1. The positions of the bed inlet relative to the injection system G and the bed exit relative to the detector J must remain unchanged when using beds of different lengths. To accommodate the change in bed length, the injection system, in preference to the detection system, was moved in a vertical plane as the performance of the latter was easily upset by any movement. The necessary air and water supplies could be provided at the two elevations approximately 0.835 m apart by simply rerouting the streams via the thre-way valves, as indicated in Fig.6.1.

A line diagram of the experimental system is given in Fig.6.3. Air from a two stage compressor A at a discharge pressure of 3×10^6 Nm^{-2} was stored in a series of large reservoirs prior to use within the system. This allowed some separation of entrained water and oil droplets and also avoided the pulsations in the air supply which were present when the compressor was running. A suitable working pressure range was obtained by a dome-type reducing valve V_1 with the safety valve V_2 set at the desired upper limit of 6.9×10^5 Nm^{-2}. The charcoal separator B removed any remaining oil droplets.

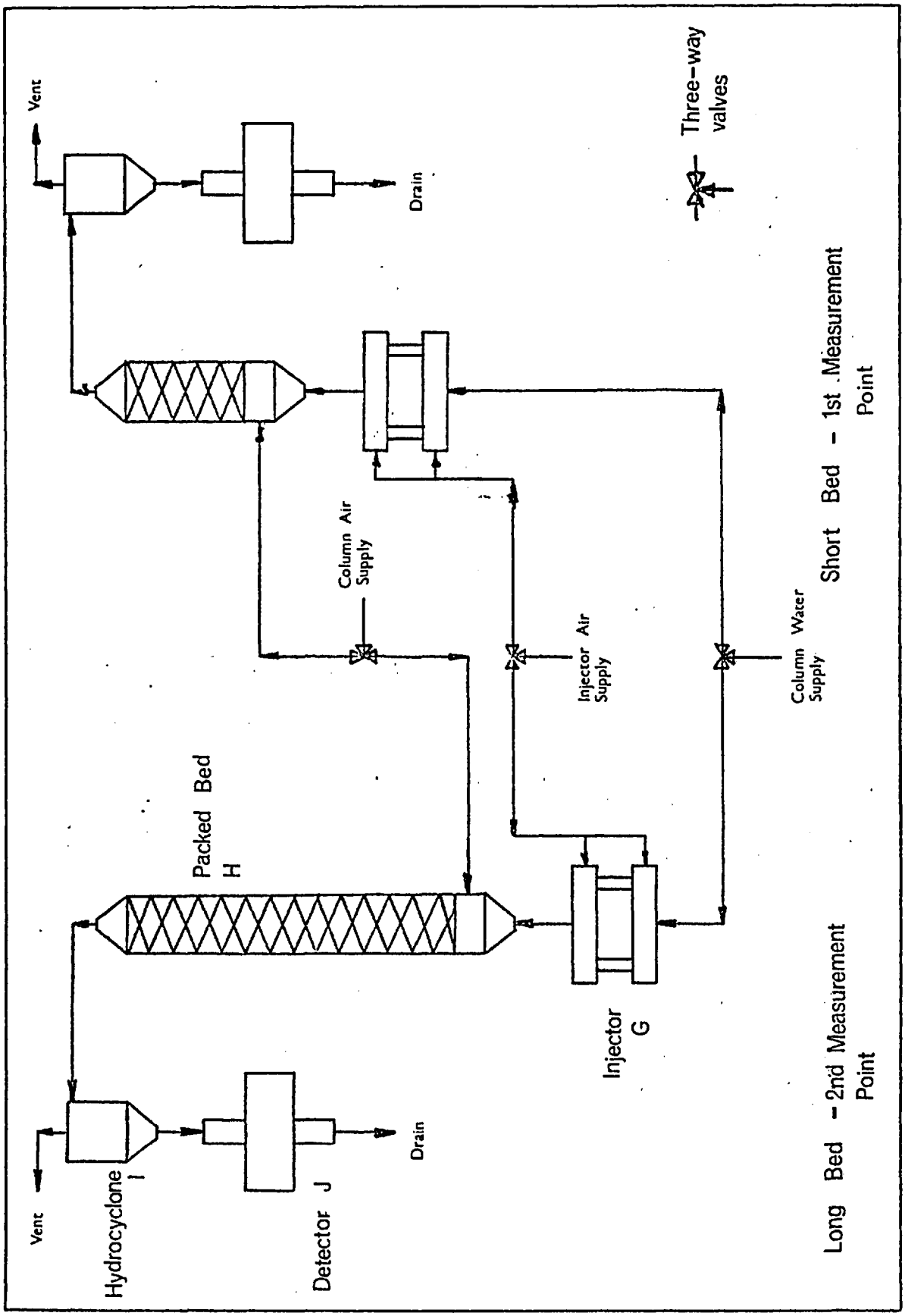

EXPERIMENTAL SYSTEMS FOR TWO-POINT MEASUREMENT TECHNIQUE

FIG 6.1

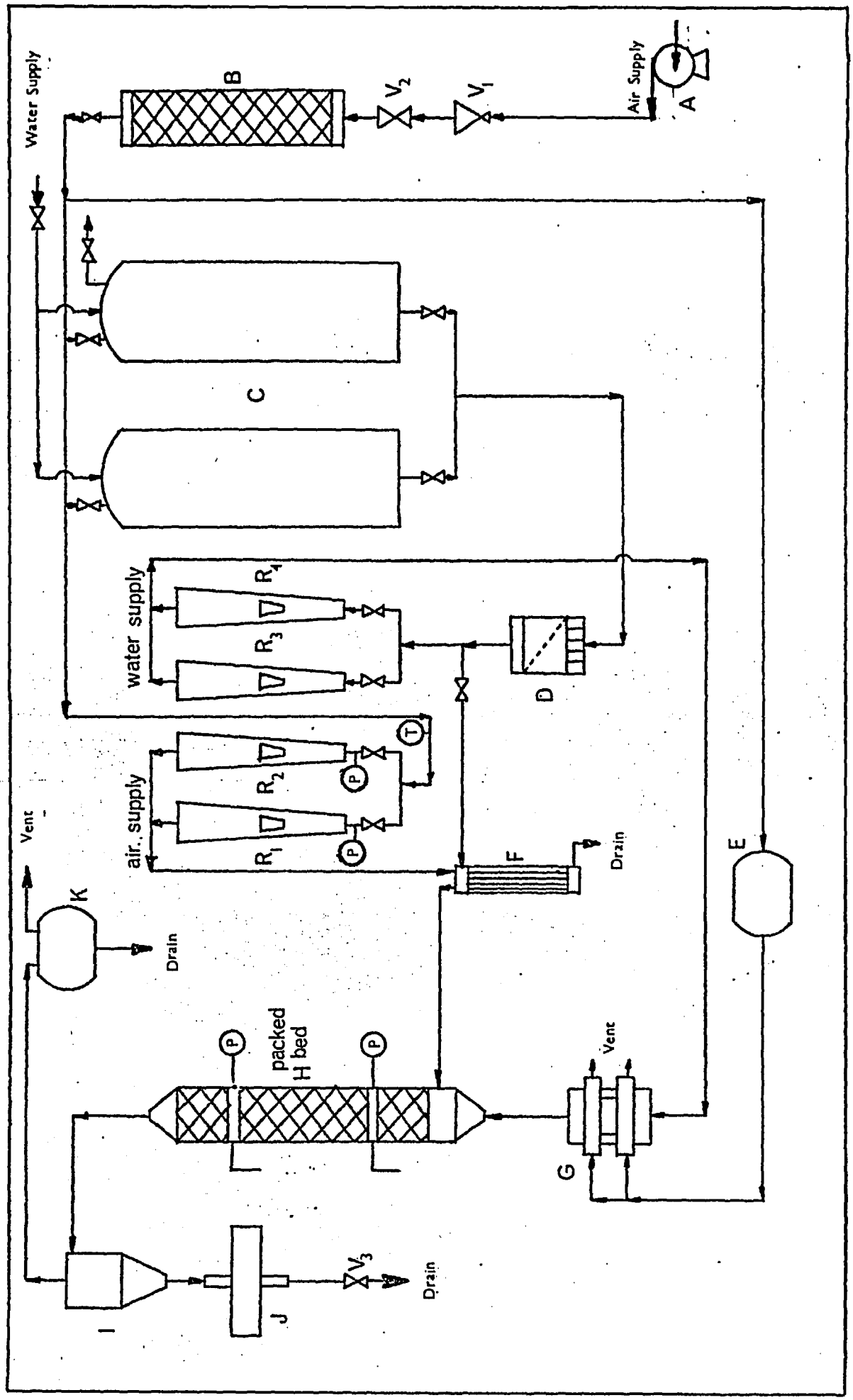

FLOW DIAGRAM OF EXPERIMENTAL SYSTEM

FIG 6.2

The air supply had to fulfil three functions:

(i) provide metered air for the packed bed system
(ii) provide a high pressure water flow by displacement
(iii) operate the tracer injection system.

Two rotameters R_1 ($4\text{-}18\times10^{-4}$ m^3s^{-1}) and R_2 ($17\text{-}75\times10^{-4}$ m^3s^{-1}) fitted with pressure gauges and a thermometer metered the air flow through the system. Liquid displacement, by the high pressure air, from the storage tanks C gave a steady high pressure water supply to the packed bed. This was a superior arrangement to the alternative of a reciprocating pump with its inherent flow fluctuations. Prior to metering in rotameters R_3 (.02-.12 kgs^{-1}) and R_4 (.12-.42 kgs^{-1}), a filter D packed with 4 mm ballotini removed any suspended solids. A small bleed after the filter provided sufficient water for the heat exchanger F which maintained the air and water streams to the packed bed at a similar temperature. Both the air and the water entered the base of the packed bed column H at either of the elevations by using the three-way valve arrangements with the water passing through the tracer injection system G en route. On leaving the packed bed system the air and water were separated in a hydrocyclone I. The gas-free liquid underflow from the hydrocyclone was analysed by the tracer detection system J before passing to the drain. The gas overflow with a small amount of entrained water was vented to atmosphere after passing through the final separation tank K.

The relative positions of the various items of equipment when using the long packed bed are shown in the photograph of Fig.6.3.

The tracer injection system, G, required air at a pressure of 5.5×10^5 Nm^{-2} to operate its two parallel solenoid valves. This requirement was met from a storage drum E periodically charged to this pressure.

6.4 Details of the Packed Bed

It was intended to use the same column and packing as that employed previously in the study by SAADA(60). A larger, longer column and consequently a larger packing size were chosen finally, for the following reasons:

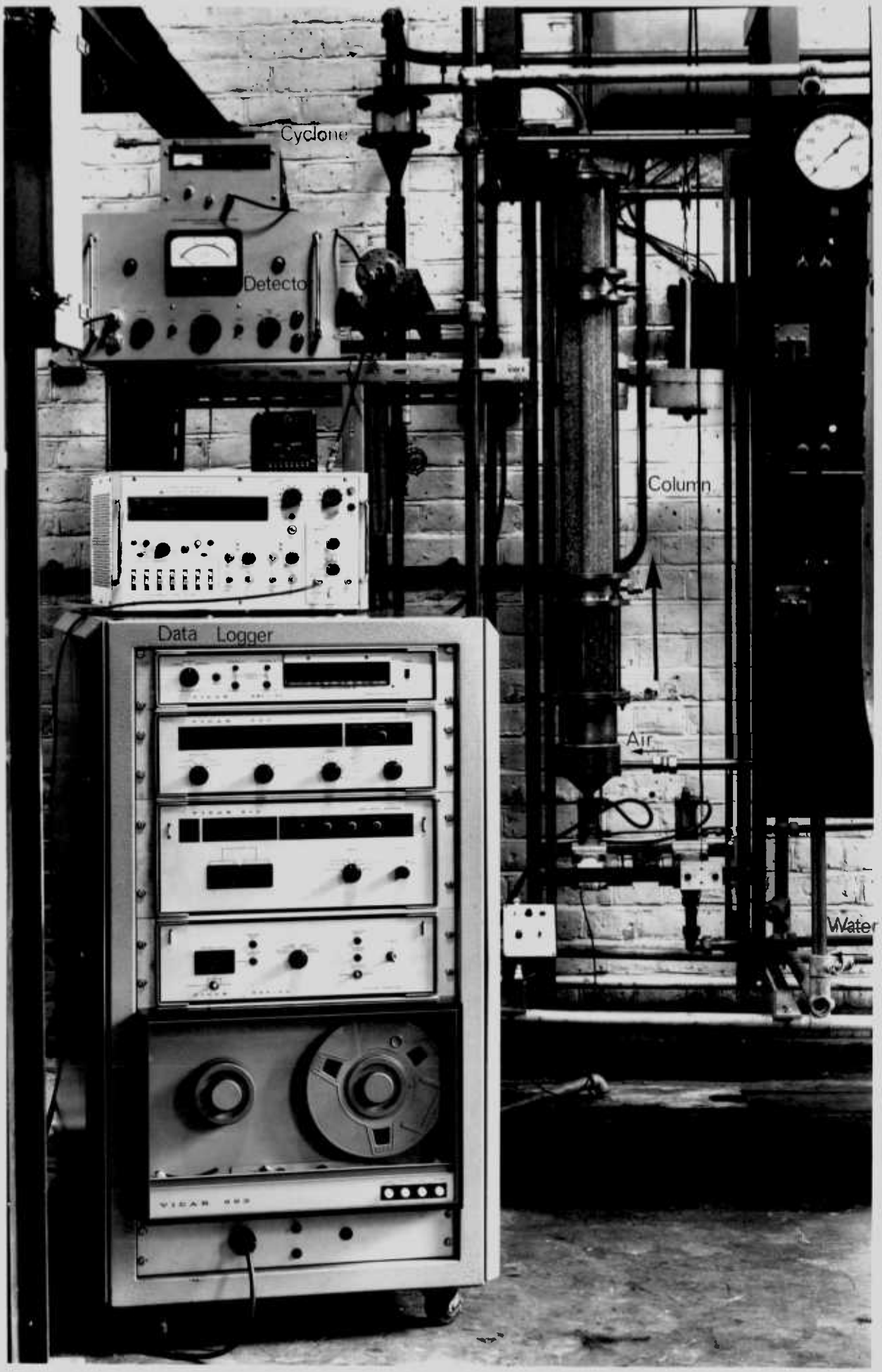

GENERAL ARRANGEMENT OF EXPERIMENTAL EQUIPMENT

FIG 6.3

(i) Increasing the packing size greatly reduced the pressure drop in the column preventing compressibility effects.

(ii) The increase in bed length made possible by the reduction in pressure drop enabled more accurate mean residence time measurements to be made.

(iii) The required ranges of gas and liquid Reynolds Numbers could be covered at lower fluid velocities reducing the difficulties in recording the tracer.

(iv) The injection of tracer was made substantially easier using a low pressure liquid stream.

The two column sections used for the short and long packed beds were constructed from 101.6mm I/D Perspex tube with a wall thickness of 6.35mm. Negligible wall effects were present by keeping the ratio of column diameter to particle diameter above 20, enabling glass ballotini of 5 mm nominal size to be used. Wire gauzes attached to brass flanges at both ends of each column section enabled the sections to be removed without disturbing the packing. These gauzes also prevented the ballotini fluidising at high fluid velocities. Leakage past the flanges, which occurred at moderate column pressures when Perspex flanges were used, was overcome by connecting the flanges with tie rods as shown in Fig.6.3.

The gas and liquid streams entered the packed bed through a distributor, based on a design used by SAADA(60). The original work on this distributor by HELSBY(32) indicated that if a perforated plate was used of thickness greater than 4d, with holes greater than 4d apart; d being the hole diameter, then the gas streams emerge separately from the holes and do not intermix. Immediately above the distributor a calming section 0.2m in length and identical in construction to the test sections was sufficient to establish the fluid flow patterns.

6.5 Details of the Gas-Liquid Hydrocyclone

One of the most difficult problems in tracing part of a two phase system, by other than radioactive means is the prevention of fluctuations in the detector signal caused by the presence of a second phase. This is particularly true when the estimate of the tracer concentration depends on the variation in light intensity received by the detector. The apparatus chosen to give complete separation of the phases prior to the detection equipment must

fulfil two conditions:

(i) The equipment must have a linear response i.e. its output signal is linearly related to its input signal.

(ii) The mean residence time of the separation equipment should be small in comparison with that of the packed bed system.

When the pseudo two point measurement technique is used the input function to the separation equipment will obviously be different for the two bed lengths used. Since the Transfer Functions for all subsystems but that representing the test section, must be identical when different test bed sections are inserted then clearly (i) is a necessary condition. With regard to the second condition De WAAL and VAN MAMEREN(77) found that a mixer, of up to 10% of the bed volume in size, situated at the bed exit, had little effect on their results. However as OTTO and GESTRICH(54) pointed out when using an ideal mixer at the exit of their test section, this condition is relaxed if the response of the subsystem is known or can be eliminated.

BRADLEY(6) has suggested that separation of a gas-liquid stream can be done quite easily using a hydrocyclone, although there seems to be no criteria by which the hydrocyclone diameter can be gauged. In their normal form of operation this diameter is governed by the particle size to be separated but in this application the bubble size is unknown. A review of commercial hydrocyclones by the author suggested that a 76 mm diameter cyclone might prove adequate for the range of gas and liquid flow rates under consideration. The remaining hydrocyclone parameters could then be estimated from relationships given by BRADLEY(6).

A view of the hydrocyclone showing constructional details, together with the principle dimensions is given in Fig.6.4. A valve in the underflow, and the vortex breaker in the cone apex ensured that no air bubbles left with the liquid stream. The overflow could be moved vertically within the cyclone body and locked in a position which minimised the liquid carryover with the gas overflow. A skirt around the overflow greatly reduced the losses due to short circuit flow of liquid across the hydrocyclone roof. In the majority of experimental runs there was negligible liquid carryover but at the highest liquid and gas flow rates, the liquid loss in the overflow

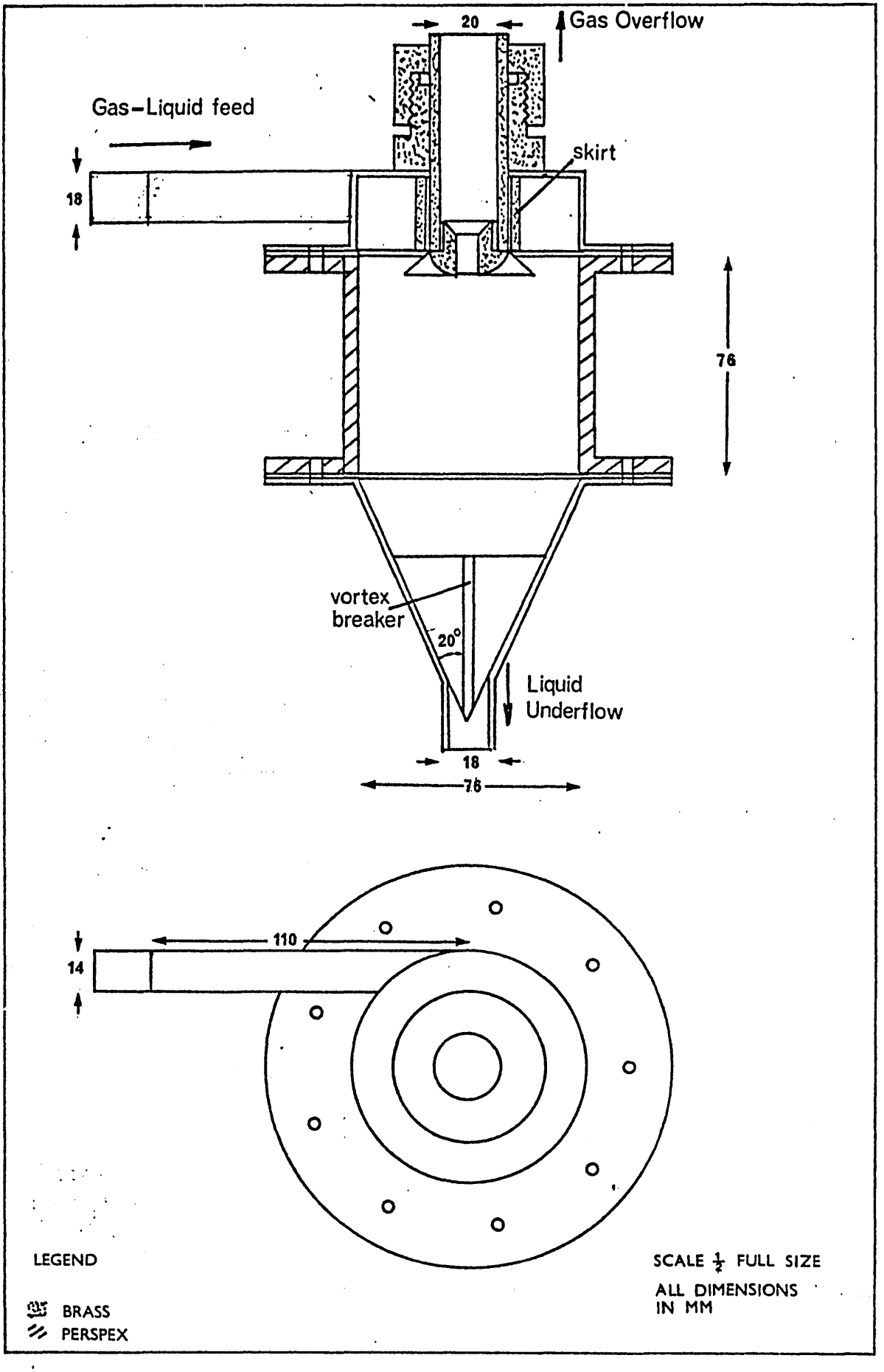

DETAILS OF GAS–LIQUID HYDROCYCLONE

FIG 6.4

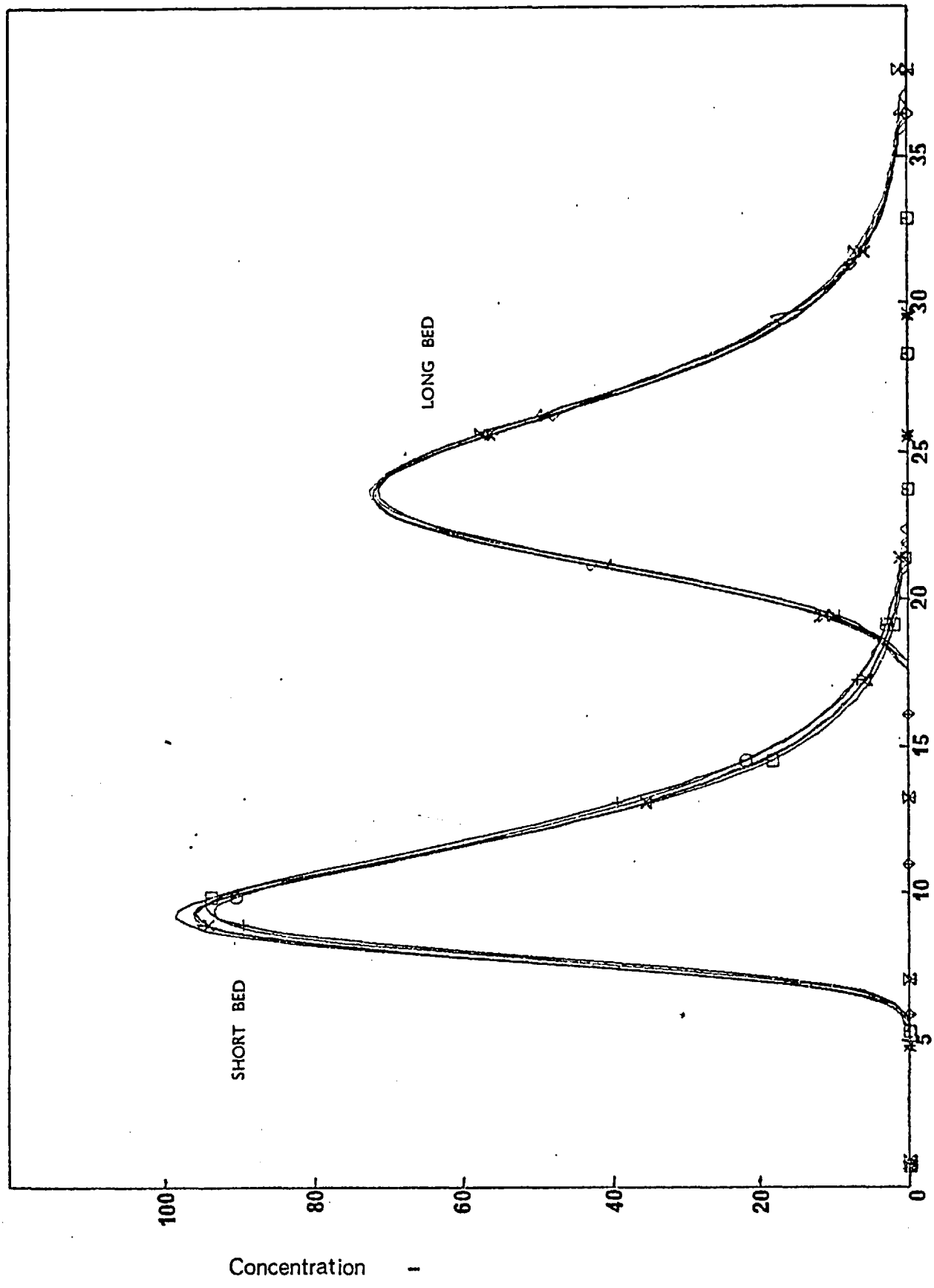

REPRODUCIBILITY OF LIQUID TRACER RESPONSE CURVES

FIG 6.5

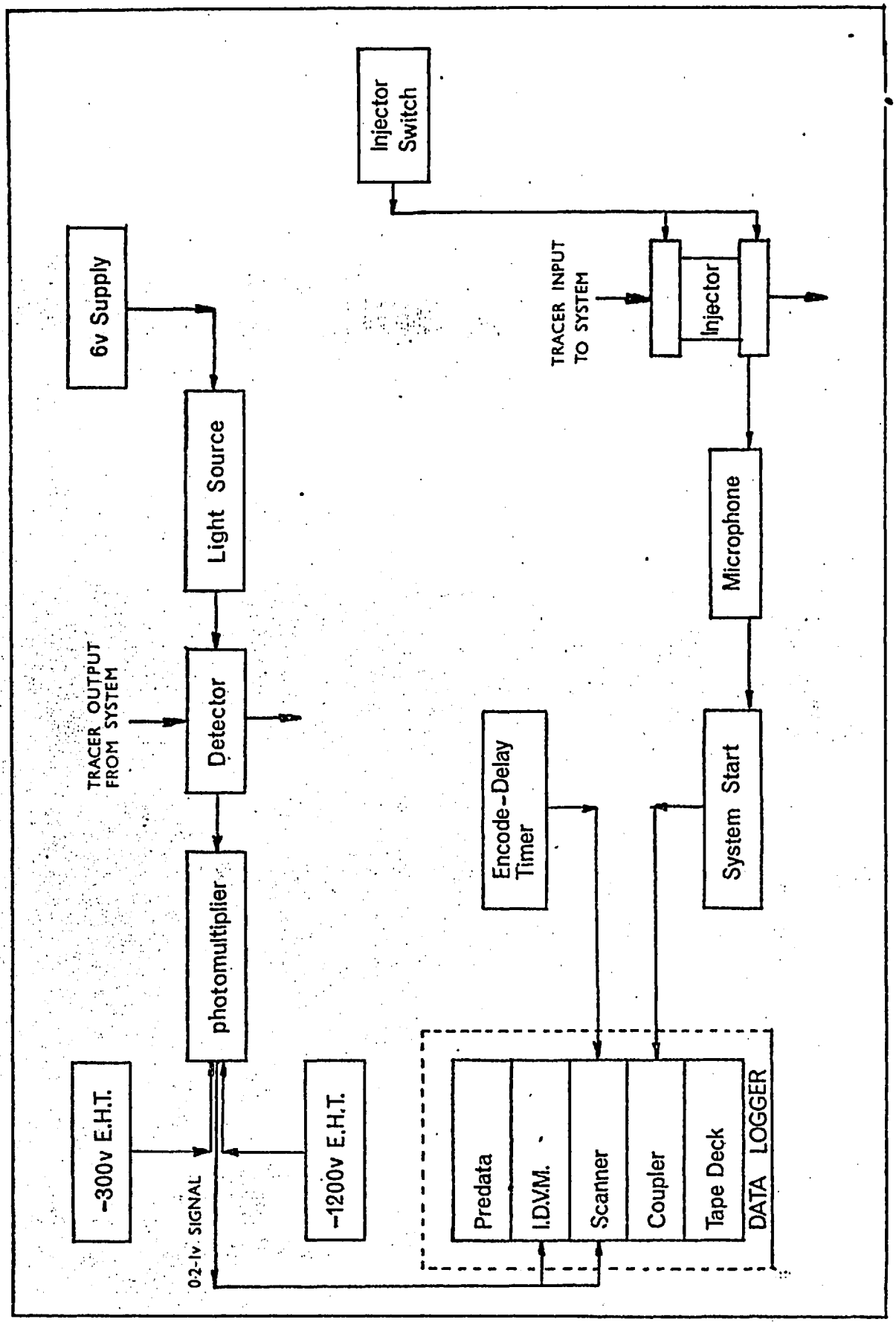

TRACER DETECTION AND RECORDING SYSTEM

FIG 6.6

was up to 7%. These losses had little effect on the tracer curves since the quantities of liquid in the overflow were very similar for both bed lengths and the tracer response curves were normalised prior to model parameter estimation.

By manufacturing the cyclone body in Perspex, the base of the vortex could be seen easily during the experimental runs and maintained at a convenient fixed position by adjusting the valve in the underflow. Although the hydrocyclone frequently required slight adjustments to counter a very slow cyclical variation in vortex height, the reproducibility exhibited by the tracer curves shown in Fig.6.5 indicates the accuracy possible with careful control. These normalised response curves were obtained with different initial tracer concentrations and therefore also illustrate the hydrocyclone's linearity. A valuable insight into the separation efficiency to be expected from this hydrocyclone was obtained from the short study by LUCAS(48).

6.6 The Tracer Analysis System

The equipment required to obtain the dynamic response of the packed bed system, for a pulse of tracer injected into the liquid phase, is shown diagrammatically in Fig.6.6. The overall system can be conveniently subdivided into the injection, detection and recording subsystems.

6.6.1 The Tracer Injection System

The theoretical analysis required a reproducible tracer pulse to be injected near to the column inlet. With the two point technique the source term does not enter into the equations describing the system and hence the pulse need not be represented mathematically. It is sufficient that the forcing function varies from zero for a finite time in such a manner that the system dynamics are excited.

The methods available for creating a pulse depend mainly on the nature of the fluid to be traced. In gaseous systems direct injection is possible, using a solenoid valve arrangement of the tracer line. One advantage of this method is the ease with which the pulse length may be changed simply by varying the time the solenoid valve is open. Care must be taken however over the tracer expansion on entry into the gas feed due to the reduction in pressure. With liquid systems a large force would be required to inject sufficient liquid in a short time and also a pressure wave would be set up since the

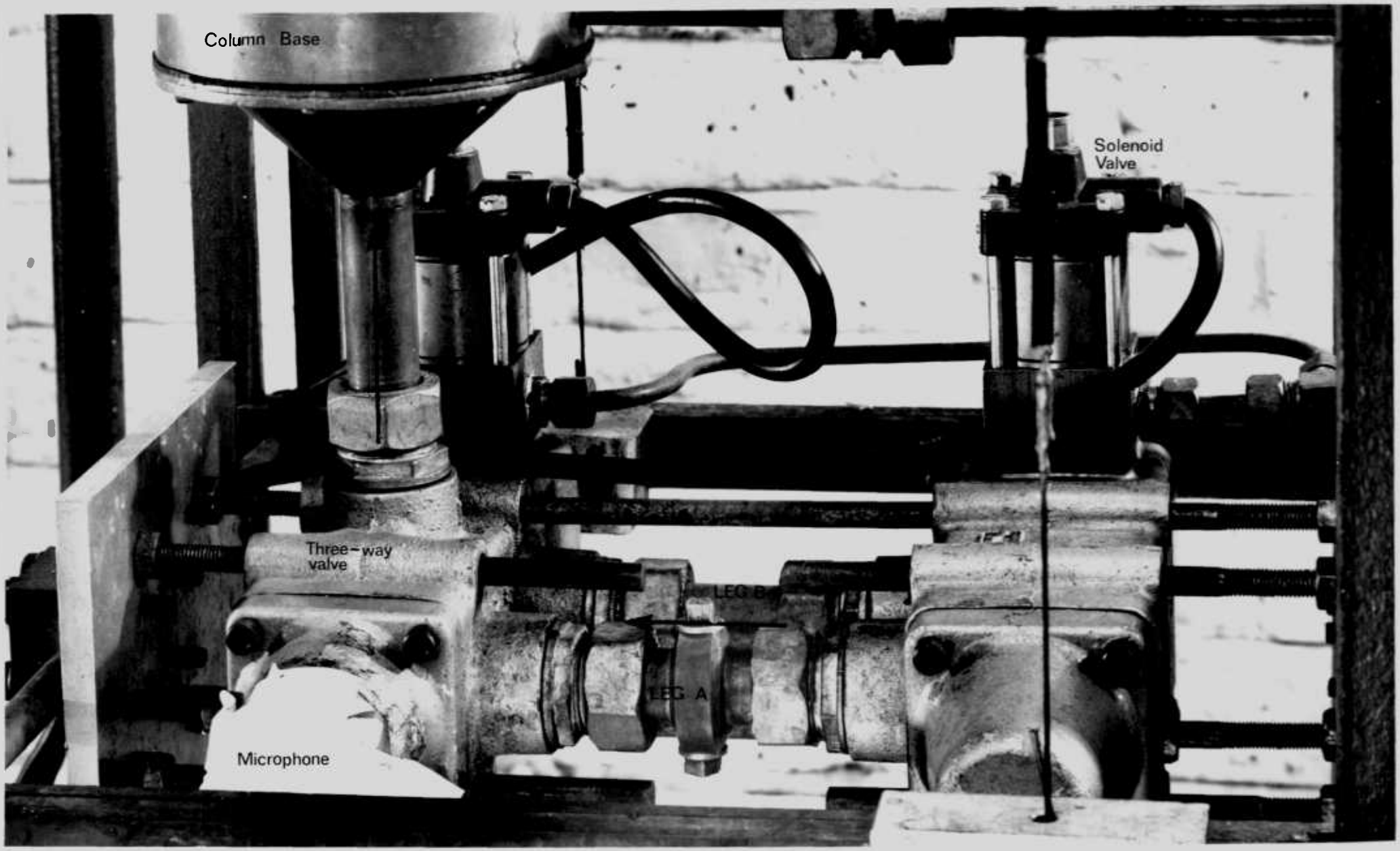
Column Base
Solenoid Valve
Three-way valve
LEG B
LEG A
Microphone

liquid in the feed to the column would have to be accelerated to accommodate the volume of tracer introduced. This may destroy the fluid flow patterns within the packed bed system.

The approach developed in this study and shown in Fig.6.7 was found to work well. Two three way valves were coupled by two equal lengths A and B of 19 mm diameter copper tube. A cylindrical brass section containing two removable 6.3mm screw plugs was inserted in leg A to allow the contents of leg A to be charged or discharged. Approximately 100 ml of tracer were placed in leg A whilst the column was operating on liquid passing through leg B. The two three-way valves were switched over simultaneously by high pressure air, controlled by two solenoid valves. This pushed the tracer out of leg A to replace the same volume of liquid trapped in leg B. The valves were quick acting because of their operation by high pressure air and produced negligible disturbance to the column's liquid supply by virtue of their sliding piston arrangement for diverting the fluid streams. A microphone attached to the end of one valve picked up the impact of the piston within the valve hitting its end stop. This signal was taken to indicate tracer injection and via a transistor circuit the recording system was shorted to earth and automatic data logging initiated. The reproducibility of this form of injection system is shown in Fig.6.5.

6.6.2 The Tracer Detection System

The tracer detection system illustrated in Fig.6.6 consisted of a light source and a photomultiplier situated either side of a perspex tube through which the underflow from the hydrocyclone passed. A line filament bulb powered by a 6V stabilised supply illuminated the perspex tube. Two ground glass diffuser plates were inserted between the light source and the narrow viewing slot to provide even illumination. This prevented variations in the photomultiplier output voltage due to any bulb vibration when the system was operating. To obtain good output voltage stability at fast recording rates -300V was applied to the first stage of the photomultiplier. A separate E.H.T source of -1200V powered the remaining stages. The output signal from the photomultiplier which varied from 1V to 300mV was connected to one input of the multichannel data logger.

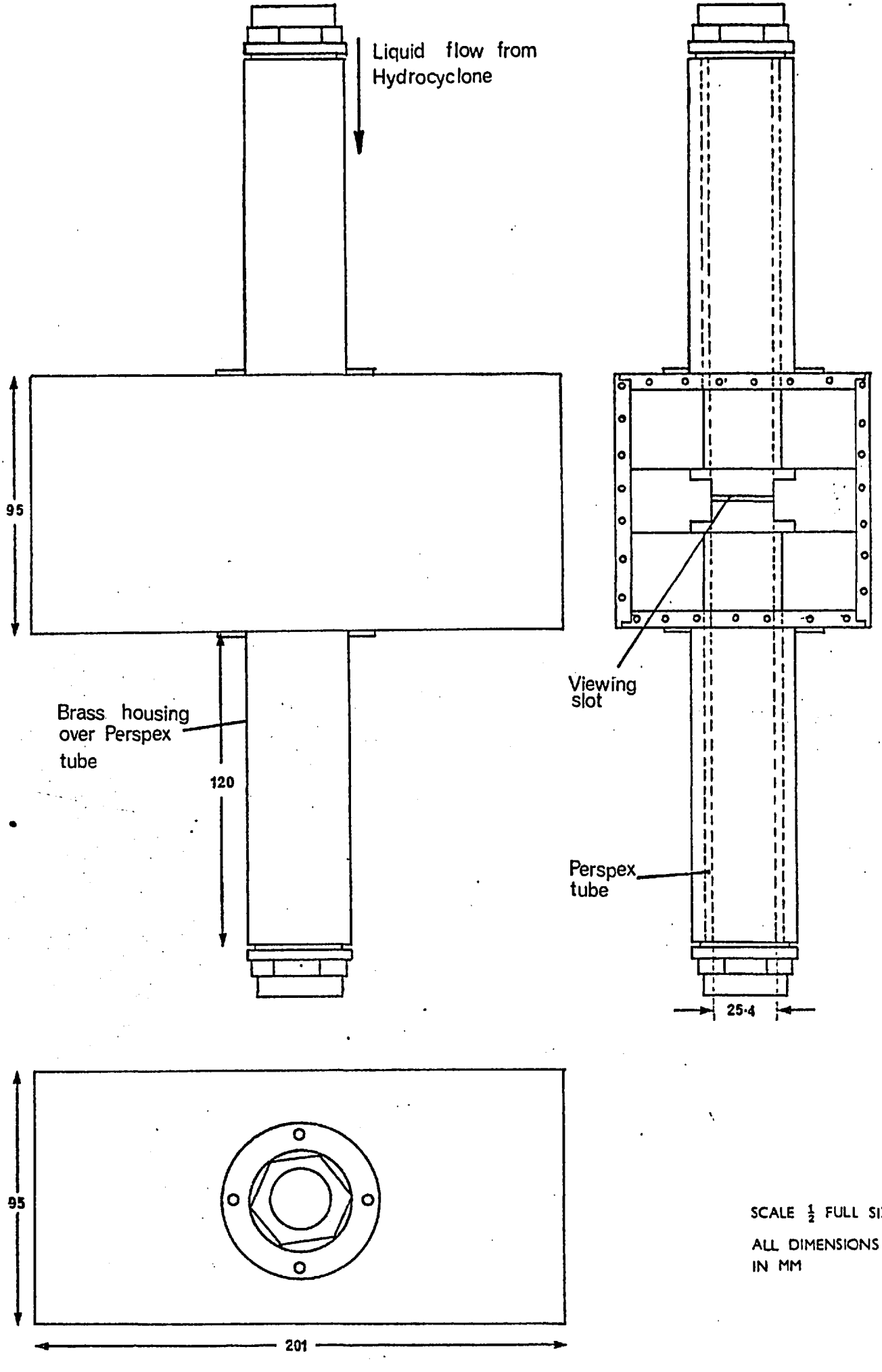

DETAILS OF TRACER DETECTOR

FIG 6.8

Constructional details of the detector itself are given in Fig.6.8 together with the principal dimensions. The detector consisted of a 30 mm O/D perspex tube surrounded by a light-tight aluminium box. A rectangular section containing a 25.4 mm x 2.54 mm slot was held perpendicular to the perspex tube such that at any instant the photomultiplier measured only the light passing through this cross-sectional area. A light-tight brass housing connected the photomultiplier to the detector end plate.

Lamberts Exponential Law for the absorption of monochromatic light in an homogeneous medium states that the light intensity I, is reduced by a constant factor k per unit depth of penetration such that:

$$I_t = I_o \exp^{-kx}$$

where I_o = initial light intensity
x = penetration depth

This equation can be modified to determine the concentration of the medium by defining a molar absorption coefficient $k' = k/C$ leading to the relationship often termed the Lambert-Beer Law:

$$\ell n\, I_t = \ell n\, I_o - k'xC \qquad \ldots\ldots \qquad (6.1)$$

The photomultiplier output voltage, V_t, is directly proportional to the incident light intensity I_t and hence a plot of $\ell n\, V_t$ vs C should be linear. For the photomultiplier used it was necessary to limit the detector output voltage to a maximum of 1V to avoid any nonlinearities. This voltage will occur when the detector contains only water and can be achieved at numerous settings of the E.H.T. and low voltage supplies. By trial and error the best stability was obtained with the main E.H.T. at -1200V and the light source supply at 4.5V. The light intensity incident on the Perspex tube was reduced to the desired level by inserting two exposed photographic plates in the cylindrical tube housing the light supply.

The region over which the Lambert-Beer Law applied in this detector is shown in Fig.6.9. The maximum concentration that could be used was 24×10^{-3} kg.m^{-3} corresponding to a detector output voltage of approximately 240mV.

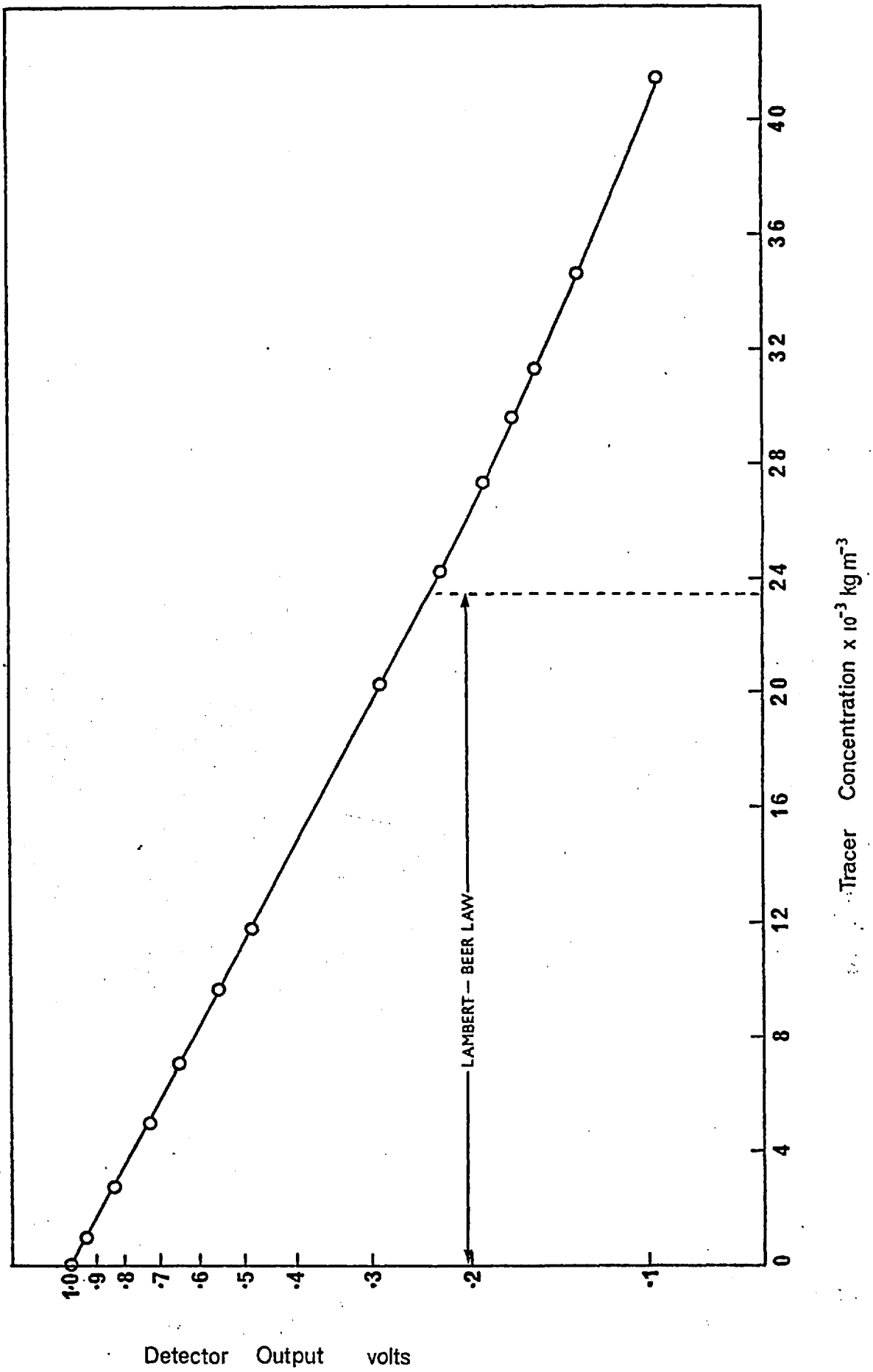

TRACER DETECTOR CALIBRATION CURVE

FIG 6.9

Rearranging eq. 6.1 we have:

$$C = k \ln \left\{ \frac{V_o}{V_{t'}} \right\} \qquad \ldots\ldots\ldots \qquad (6.2)$$

where V_o = base voltage i.e. water only passing through the detector

$V_{t'}$ = voltage at any time t.

Since the methods used in this study for estimating the models' parameters in effect only involve ratios of Laplace Transformed concentrations, the k values for the responses at both measurement points cancel out. Hence the ratio $\ln\left(\frac{V_o}{V_{t'}}\right)$ is sufficient to represent the tracer concentration.

6.6.3 The Tracer Recording System

The output signal from the photomultiplier was connected to one channel of a multichannel Vidar magnetic tape Data Logger. Unfortunately towards the latter part of the experimental program, faults developed in the Data Logger and nearly 25% of the experimental runs recorded had to be discarded since they were impossible to read off the magnetic tape.

The photomultiplier signal was periodically sampled at preset time intervals by an integrating digital voltmeter and the resultant voltage encoded into Binary Coded Decimal format and transferred to the tape. The sampling rate could be varied continuously between the limits of one reading every 5 secs and 25 readings per second. This sampling rate was adjusted to suit the particular conditions of each experimental run and enabled the whole response curve to be recorded within 830 voltage-time measurements. Since each voltage was represented by a 12 character word, 9960 characters were recorded per run. An end-of-record gap was automatically inserted after the 9960 characters had been recorded. Due to the high recording speed it was impossible to stop recording immediately after the 9960 characters had been coded onto the magnetic tape. Every experimental record was, therefore, followed by an unknown number of unwanted characters, until recording was stopped. The digital voltmeter integration period could be set to one of $1^2/3$, $16^2/3$ or $166^2/3$ milliseconds. For each experimental run, the integration period was chosen so any fluid entering the 2.54 mm wide viewing

slot the instant the integration period started, remained within the slot for the whole of the integration period. Any fluid dispersion occurring within the viewing slot whilst the readings were taken was neglected.

After several experimental runs were recorded a special record was inserted manually onto the tape to signify the end of the experimental data. This special record, consisting of 4 words with each word containing the characters 999999999999, was entered via the predata panel of the Data Logger shown in Fig.6.3.

6.7 Experimental Procedure to obtain the system response

The procedure was the same for either length of bed.

Once the desired packed bed section had been secured in its correct position between the tracer injection system and the tracer detection systems, and the gas and liquid streams correctly routed via the three-way valves, a slight gas flow was started. Water was then introduced slowly and then both fluid flows adjusted to their desired levels. The valve in the pipe leaving the tracer detector was continually adjusted such that the back pressure created was sufficient to ensure the liquid stream from the hydrocyclone passing to the detector was gas free. When the flow patterns had stablised, the liquid stream was diverted by the solenoid valves through the limb of the injection system containing the dye tracer. From this instant the recording of the tracer curve by the detector and its storage on magnetic tape for subsequent analysis were fully automated.

CHAPTER 7 ANALYSIS AND DISCUSSION OF THE EXPERIMENTAL RESULTS

7.1 Summary

The experimental results from the dynamic response of the packed bed system are analysed through Transfer Functions for the Basic Axially Dispersed Plug Flow Model, the Liquid Stagnancy Model and the Split Flow Model. The Dispersion Number results from the simple Axially Dispersed Plug Flow Model are interpreted in the context of the liquid distribution model described by SAADA(60) and EISENKLAM and FORD(20).

7.2 Liquid Only Experiments Analysed by Axially Dispersed Plug Flow Model

A number of runs were made with only the liquid phase present. This enabled the reproducibility of the injection/detection equipment to be checked, in particular the linearity of the hydrocyclone system. Details of the results are tabulated in Appendix E and shown in Fig.7.1. Given in this figure for comparison are the correlations derived by the author from the data summarised by GUNN(28) and the correlation of CHUNG and WEN(12) namely:

$$e\,Pe = 0.2 + 0.011\,Re_L^{0.48} \quad \ldots\ldots \quad (7.1)$$

where Pe = The system Peclet Number $\frac{U\,d_p}{D_L}$

e = bed voidage.

In terms of the Dispersion Number, bed voidage and particle diameter used in this work eq.7.1 becomes:

$$N_D^{-1} = 93.82 + 5.16\,Re_L^{0.48} \quad \ldots\ldots \quad (7.2)$$

The standard deviation of the CHUNG and WEN(12) correlation was $\pm$46% based on 482 data points. The present liquid phase results are therefore well within the limits of this correlation. The reproducibility of the results has already been discussed in Section 6.5. The response curves for both bed lengths are shown in Fig.6.5 for the 5 repeat runs at Re_L = 108.5. For all the single phase liquid results the theoretical and experimental mean residence times agreed to within 3%.

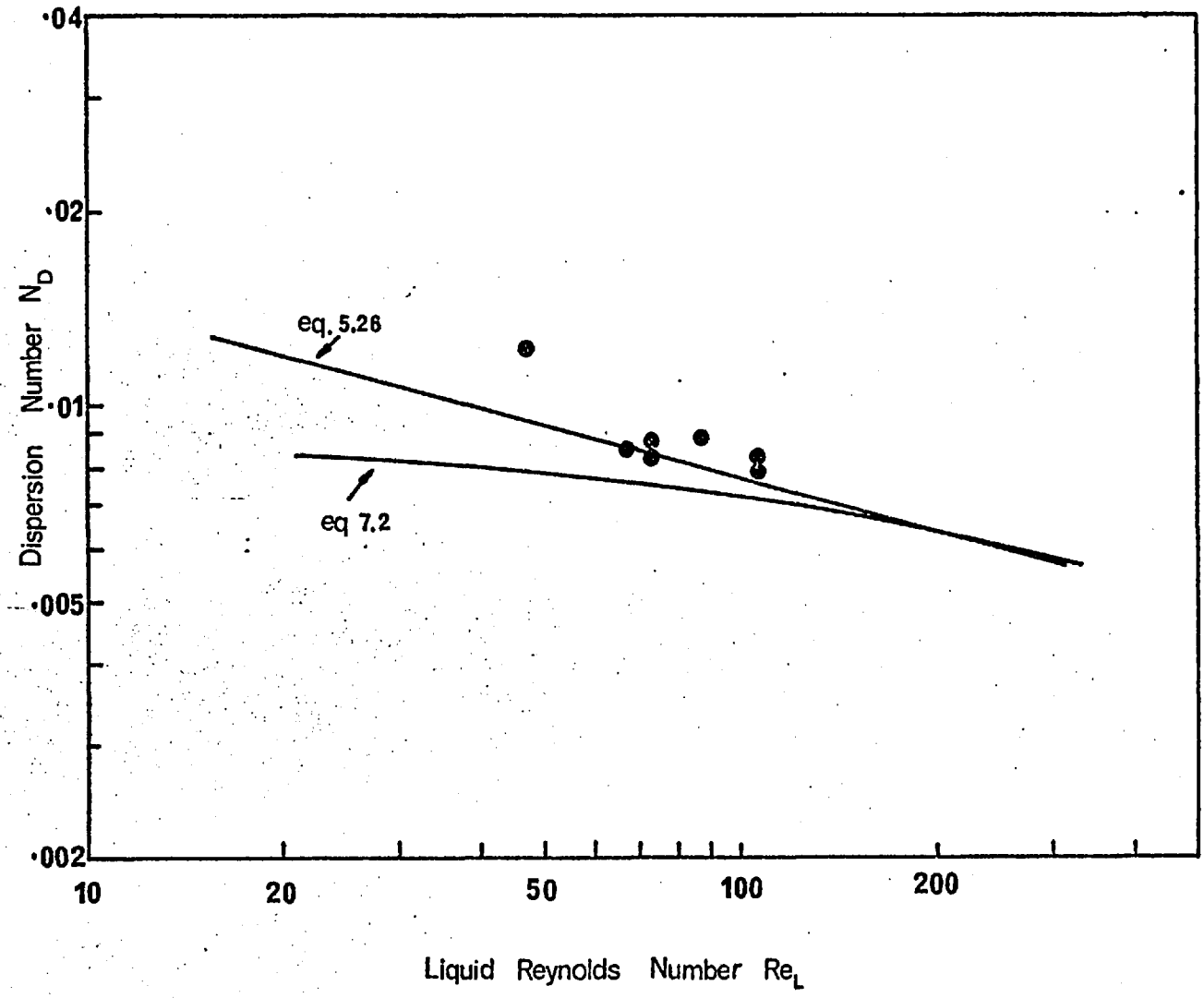

DISPERSION RESULTS FOR SINGLE PHASE LIQUID FLOW FROM BASIC MODEL

FIG 7.1

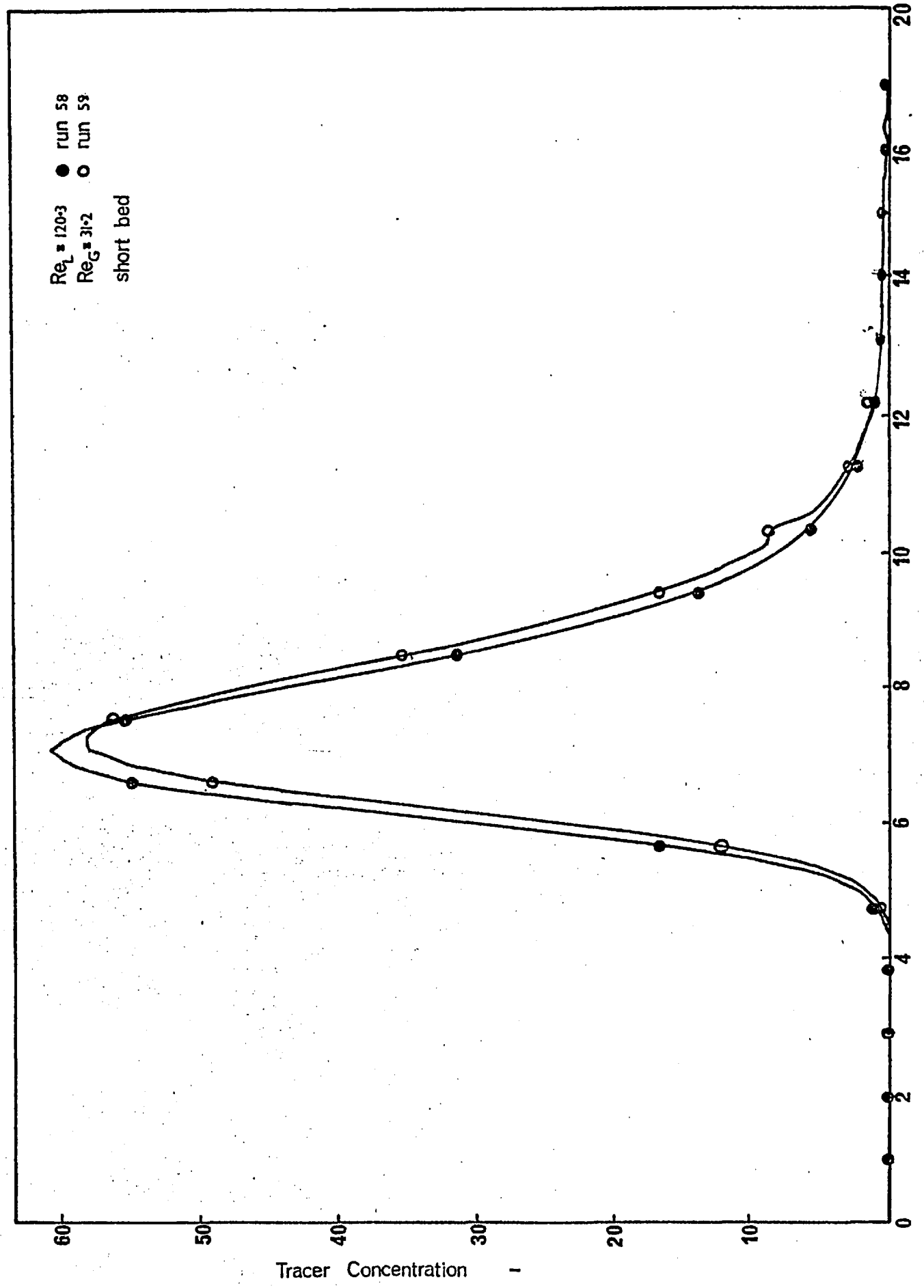

REPRODUCIBILITY OF LIQUID RESPONSE DURING TWO PHASE FLOW

FIG 7.2

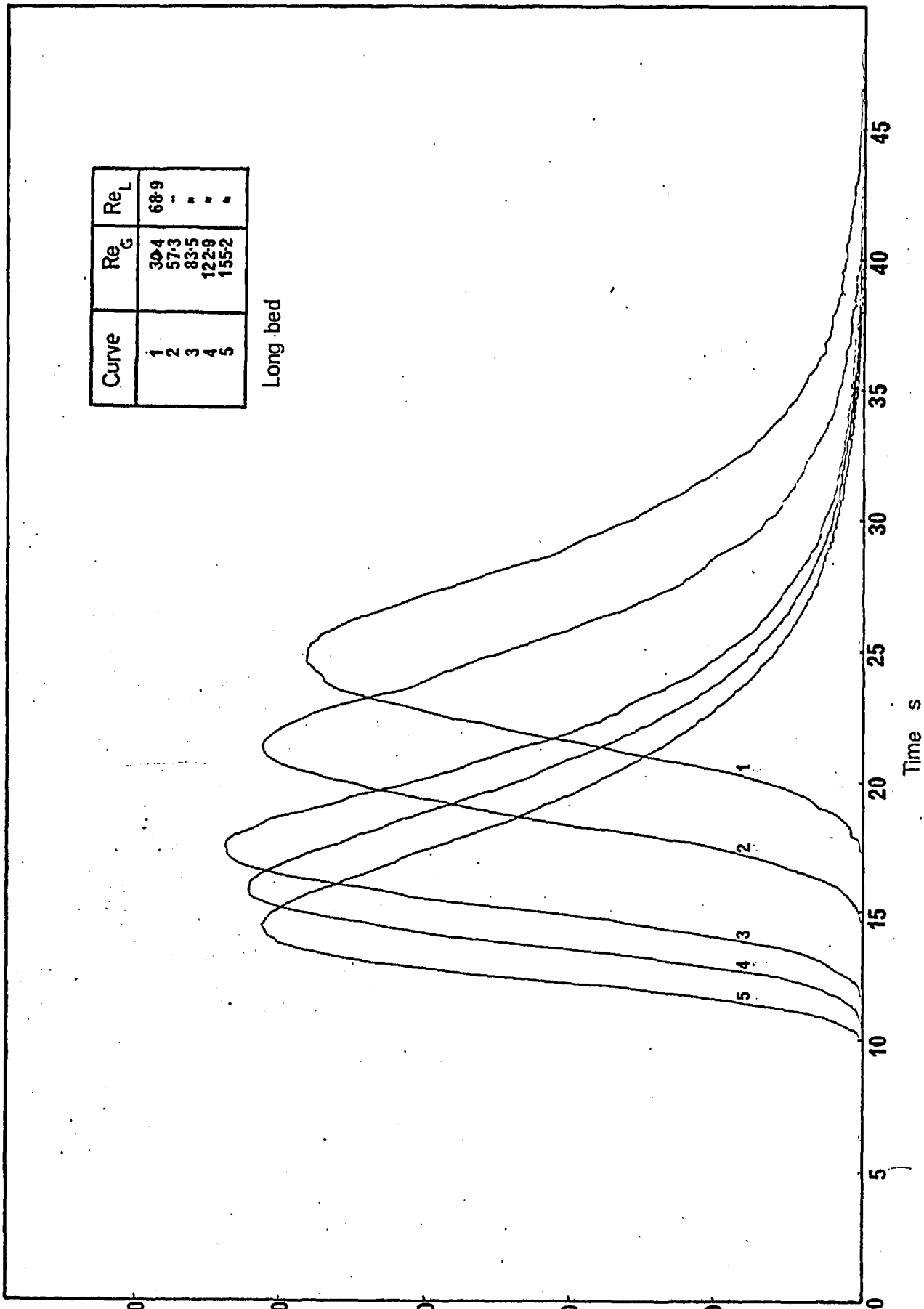

VARIATION IN SYSTEM RESPONSE WITH GAS FLOW RATE

FIG 7.3

7.3 Variation in Liquid Phase Response with Gas Rate

The reproducibility of the system response when there are two phases present is illustrated in Fig.7.2 for liquid and gas Reynolds Numbers of 120.3 and 31.2 respectively. Comparison with Fig.6.5 for the liquid only responses shows a slight decrease in reproducibility when the second phase is present although the Dispersion Number for both runs as given in Appendix F is approximately the same at 0.015. The effect on the system response, at a constant liquid Reynolds Number of 68.9, due to varying the gas Reynolds Number from 30.4 to 155.2 is shown in Fig.7.3. The change in the liquid holdup, reflected in the reduction in the overall mean residence time, can be seen clearly. Little however can be inferred, from a visual inspection of the spread of each response curve, concerning the effect on the system Dispersion Number of varying the gas rate.

7.4 Analysis by the Basic Axially Dispersed Plug Flow Model

The Dispersion Number and liquid holdup results from the analysis of the system responses by the Basic Axially Dispersed Plug Flow Model are given in Appendix F. The Dispersion Number is evaluated by the four methods developed in Chapter 5.2. In almost every run the liquid holdup was the same from all four methods and only the average value is listed. The Dispersion Number results are shown in Fig.7.4 for all experimental runs.

7.4.1 Dispersion Numbers from the Basic Model

At low liquid flow rates high Dispersion Numbers are encountered particularly for high gas Reynolds Numbers. For liquid Reynolds Numbers below 61.4 the gas flow rate has a significant effect on the Dispersion Number. As the liquid rate increases the Dispersion Numbers tend towards the values shown in Fig.7.1 and those reported by CHUNG and WEN(12) for single phase liquid flow. The effect of gas rate diminishes as the liquid Reynolds Number increases. At any given gas Reynolds Number there is a tendency for the Dispersion Number to decrease with increasing liquid Reynolds Number. Again this effect is most apparent at the lowest liquid flowrates. In common with most other studies of phenomena in two phase flow in packed beds the Dispersion results were correlated against the system variables of gas and liquid Reynolds Numbers assuming a functional relationship of the form:

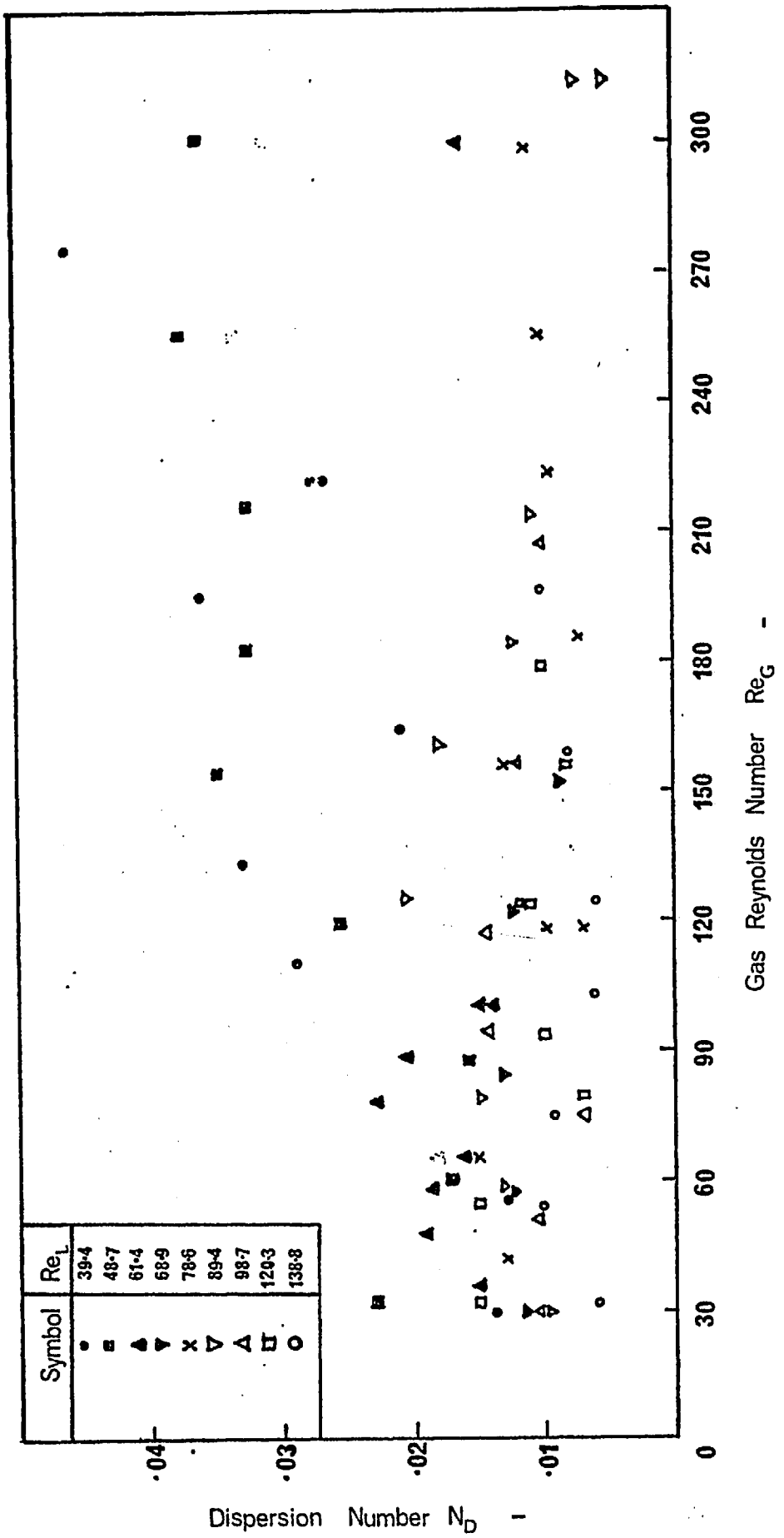

VARIATION IN DISPERSION NUMBER WITH GAS & LIQUID REYNOLDS NUMBERS FROM BASIC MODEL

FIG 7.4

$$N_D = a\, Re_L^{\,b}\, Re_G^{\,c} \qquad \ldots\ldots \qquad (7.3)$$

The regression program used to correlate the data rejected any variable which was not significant at the 5% level. Since the liquid and gas velocities within the packed bed itself have a direct influence on the fluid intermixing, the results were fitted using interstitial Reynolds Numbers as well as the more usual superficial Reynolds Numbers.

The interstitial Reynolds Numbers are defined in terms of the superficial Reynolds Numbers by:

$$I^{Re}_L = \frac{Re_L}{e\phi_L} \quad \text{and} \quad I^{Re}_G = \frac{Re_G}{e(1-\phi_L)}$$

where e = bed voidage and ϕ_L is the average liquid holdup.

The coefficients obtained from fitting eq. 7.3 to all the experimental results are given in Table 7.1 below.

Reynolds Numbers	a	b	c	d/F	95% Confidence limits		% Fit
					b	c	
Superficial	0.874	-0.957	rejected	72	±0.202	-	55.7
Interstitial	0.407	-1.1	0.504	72	±0.21	±0.17	61.9

Table 7.1 Regression of all Dispersion Number Results

For the correlation based on superficial Reynolds Numbers the gas rate has no significant effect and is rejected. A better fit is obtained with the interstitial Reynolds Numbers and the dependence on gas rate is retained. The % fit stated in Table 7.1 is the ratio of the reduction due to regression to the total variance. The interstitial correlation is shown in Fig.7.5 and the main area where the fit is relatively poor is for the lower liquid Reynolds Number.

The scatter in the Dispersion Number shown in Fig.7.4 is replaced by a distinct grouping of the results if the points are distinguished on the basis of the liquid distribution model developed by

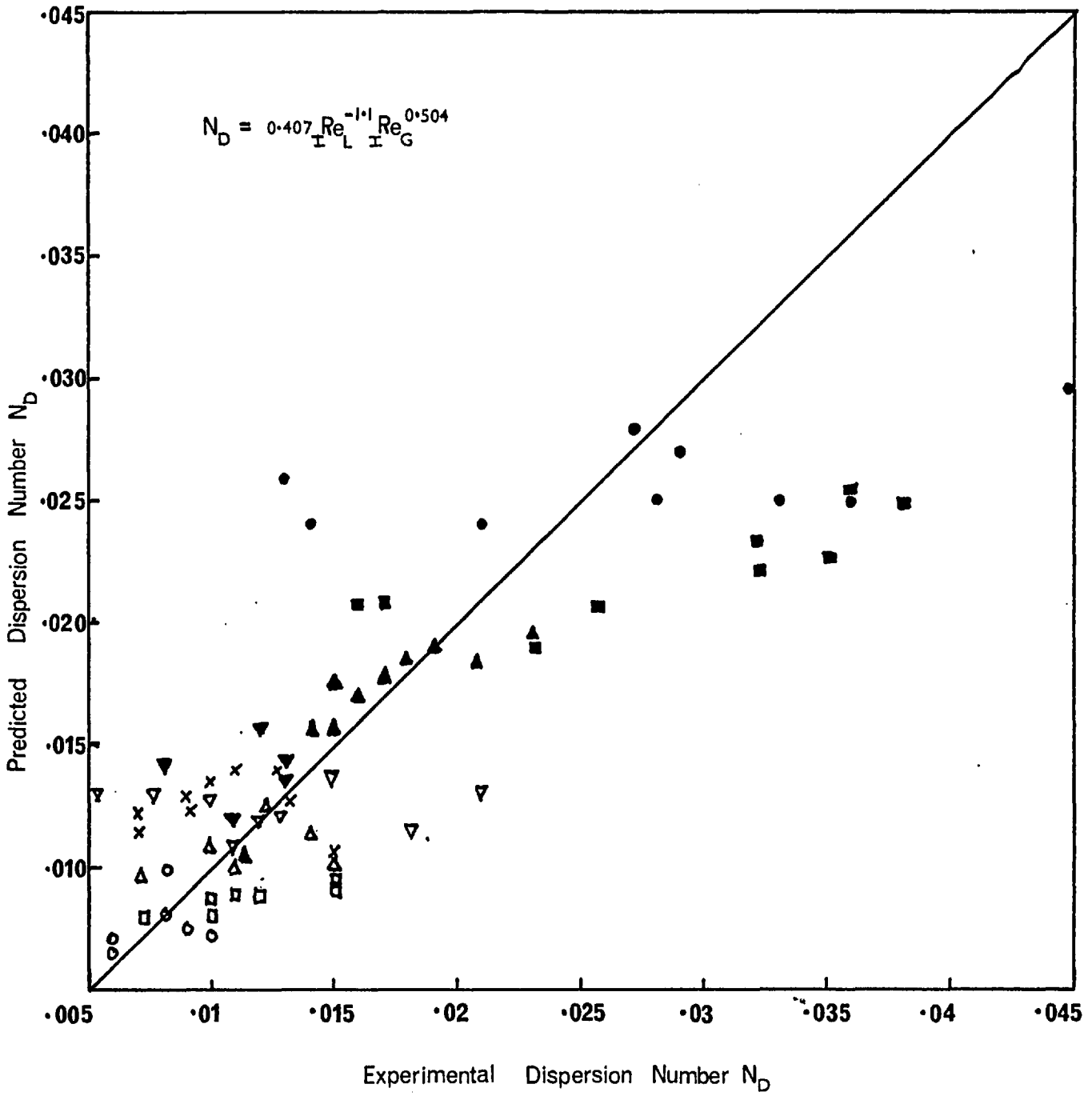

CORRELATION FOR ALL DISPERSION NUMBER RESULTS BASED ON INTERSTITIAL REYNOLDS NUMBERS

FIG 7.5

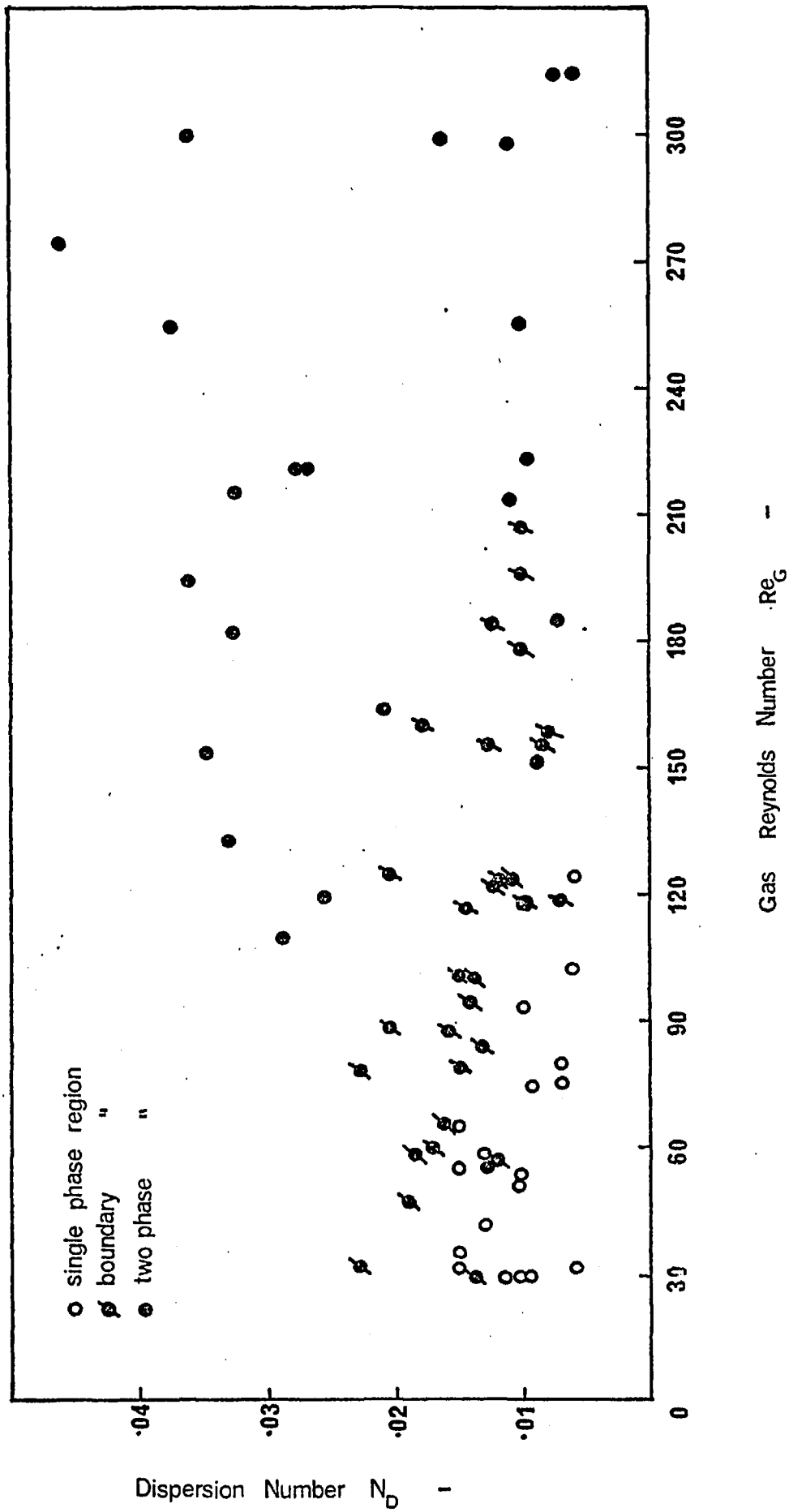

DISPERSION RESULTS FROM BASIC MODEL GROUPED INTO FLOW REGIMES

EISENKLAM and FORD(20) and SAADA(60). Fig.7.6 shows the single phase pore flow results separated from the two phase pore flow points by a band of values termed the boundary region. In the single phase pore flow region the predominant flow regime is one in which the gas and liquid flow through separate pores. The gas phase should therefore have little influence on the passage of liquid through the packed bed. At the other extreme of well established two phase pore flow, the gas and liquid flow through the same pores. In this region the gas phase will affect the liquid dispersion. Between these limits there will be a transition region in which the predominant mode of flow changes. The boundary curve between the two regions identified by SAADA(60) was extended in section 2.2.3 into a boundary region as shown in Fig.2.6. Separation of the Dispersion results into the three regions shown in Fig.7.6 was on the basis of the broad boundary region.

From Fig.7.6 it is seen that the Dispersion Numbers in the single phase pore flow region are lower than those in the other regions and very similar to the values obtained during the single phase liquid studies. These results are in agreement with a model in which the liquid is unaffected by the presence of a gas phase. The highest Dispersion Numbers are in the two phase pore flow region where the presence of a gas phase can have a significant effect on the liquid phase. This is particularly true at low liquid rates and high gas rates when the difference in velocities between the two phases is largest. Even in two phase pore flow however the Dispersion Numbers tend towards the liquid only values at the highest liquid Reynolds Numbers. The values of the Dispersion Number in the boundary region are consistent with a transition from one mode of flow to the other.

Correlations of the same functional form as before were fitted to the results in the three regions based on interstitial Reynolds Numbers. Details of the coefficients are given in Table 7.2 below.

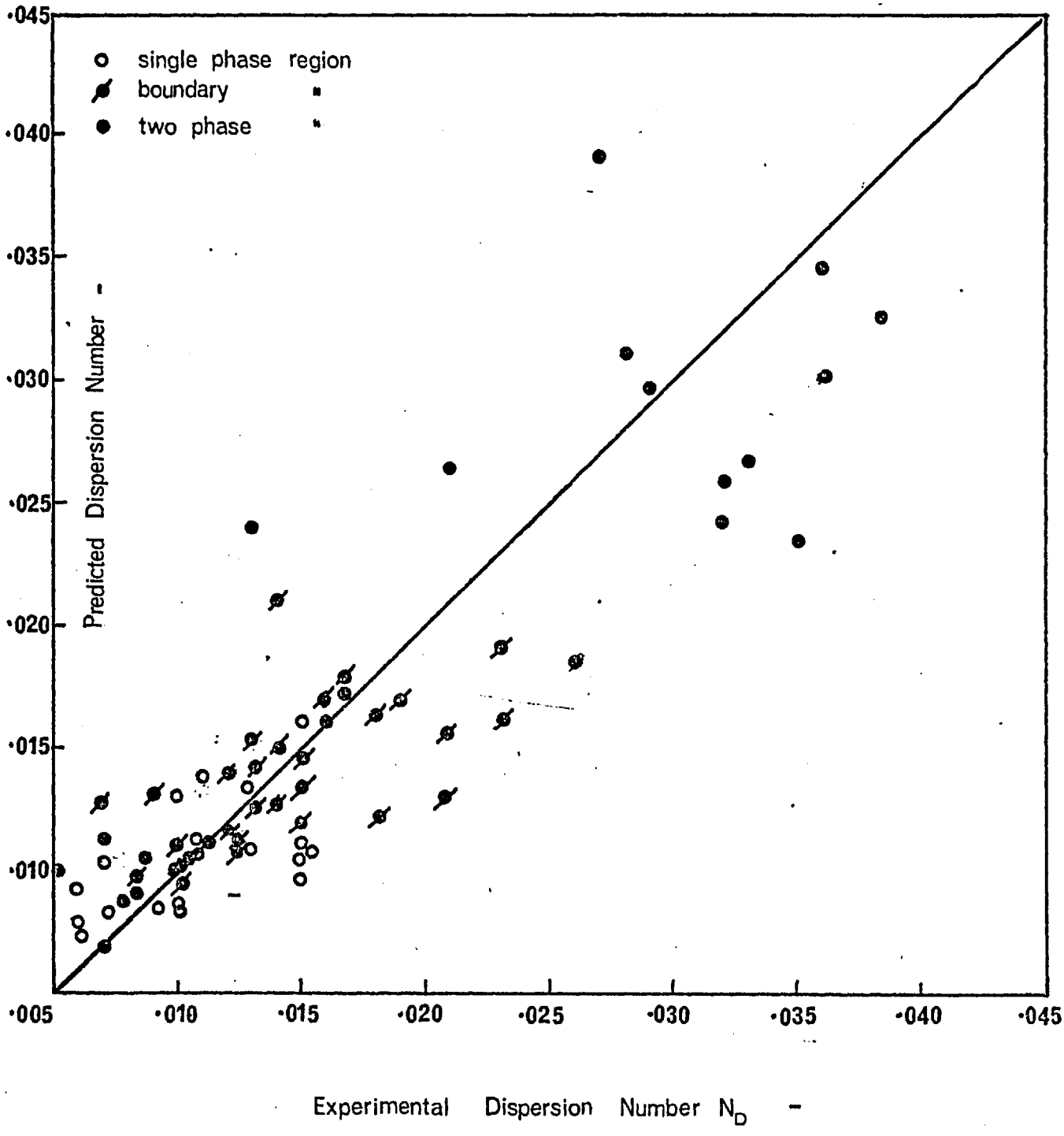

SEPARATE CORRELATIONS FOR DISPERSION NUMBER IN EACH REGION

FIG 7.7

Reynolds Numbers	a	b	c	d/F	95% Confidence Limits		% Fit
					a	b	
Single phase region	.645	-.675	rejected	18	±0.419	-	40.2
Boundary region	.246	-.482	rejected	30	±0.211		42.9
Two phase region	.571	-2.17	1.36	22	±0.486	±0.554	81.4

Table 7.2. Separate Correlations for Dispersion Number in each Region

Table 7.2 shows that only in the two phase pore flow region is any dependency retained on the gas Reynolds Numbers.

For the 95% confidence limits given in Table 7.2 there is a significant difference between the coefficients for the two phase region and those in the other two regions. To test whether three correlations rather than a single correlation should be fitted to the data, the sum of squares due to regression for these two situations were compared as shown in Table 7.3.

		D/F	MS	F
SS due (3 regressions)	1347.076	9		
SS due (1 regression)	1344.6258	3		
Difference	2.4502	6	.4084	5.65
Error	4.6242	64	.0722	
Total	1351.7016	73		

Table 7.3 Comparison of separate regressions for each region vs single regression

Since the F ratio is significant at the 1% level it is concluded that three regressions should be used instead of one.

A plot of experimental vs predicted Dispersion numbers using separate correlations for each region is given in Fig.7.7.

7.4.2 Liquid Holdup from the Basic Model

The liquid holdup results are shown in Fig.7.8 for all experimental runs. There is a strong decrease in liquid holdup with increasing gas Reynolds Numbers at any given liquid Reynolds Number. However at high gas rates there is a tendency for the liquid holdup to reach a constant value of about 0.4 irrespective of the liquid Reynolds Number. At any given gas Reynolds Number the liquid holdup increases with liquid Reynolds Number. The results were fitted to the same form of functional relationship as used for the Dispersion Number:

$$\phi_L = a\, Re_L^{\,b}\, Re_G^{\,c} \qquad \ldots\ldots\ldots \qquad (7.4)$$

The coefficients for eq.7.4 are tabulated in Table 7.4 and the correlation plotted in Fig.7.9.

a	b	c	d/F	95% confidence limits		% Fit
				b	c	
1.33	0.0752	-0.272	72	±.0252	±.0145	95.6

Table 7.4 Coefficients for all liquid holdup results

Figure 7.10 shows the same correlation for liquid holdup as Fig.7.9 except that the results are now distinguished on the basis of the prevailing flow regime. As in the case of the Dispersion Numbers the liquid holdup results separate out into groups. This effect is particularly apparent in the two phase flow regime which is characterised by low liquid holdups in the range 0.37 to approximately 0.49. The flow regimes pass from predominantly single phase pore flow through the boundary region towards two phase pore flow as the liquid holdup decreases from unity.

A comparison of three separate regressions with a single regression was made on the liquid holdup results similar to the Dispersion Number analysis. In this instance however the F ratio was not significant and only the single correlation for all data points has been retained.

A functional form similar to that used by SAADA(60) namely

$$\phi_L = a\,(Re_L/Re_G)^b$$

was tried but rejected due to the poor fit obtained.

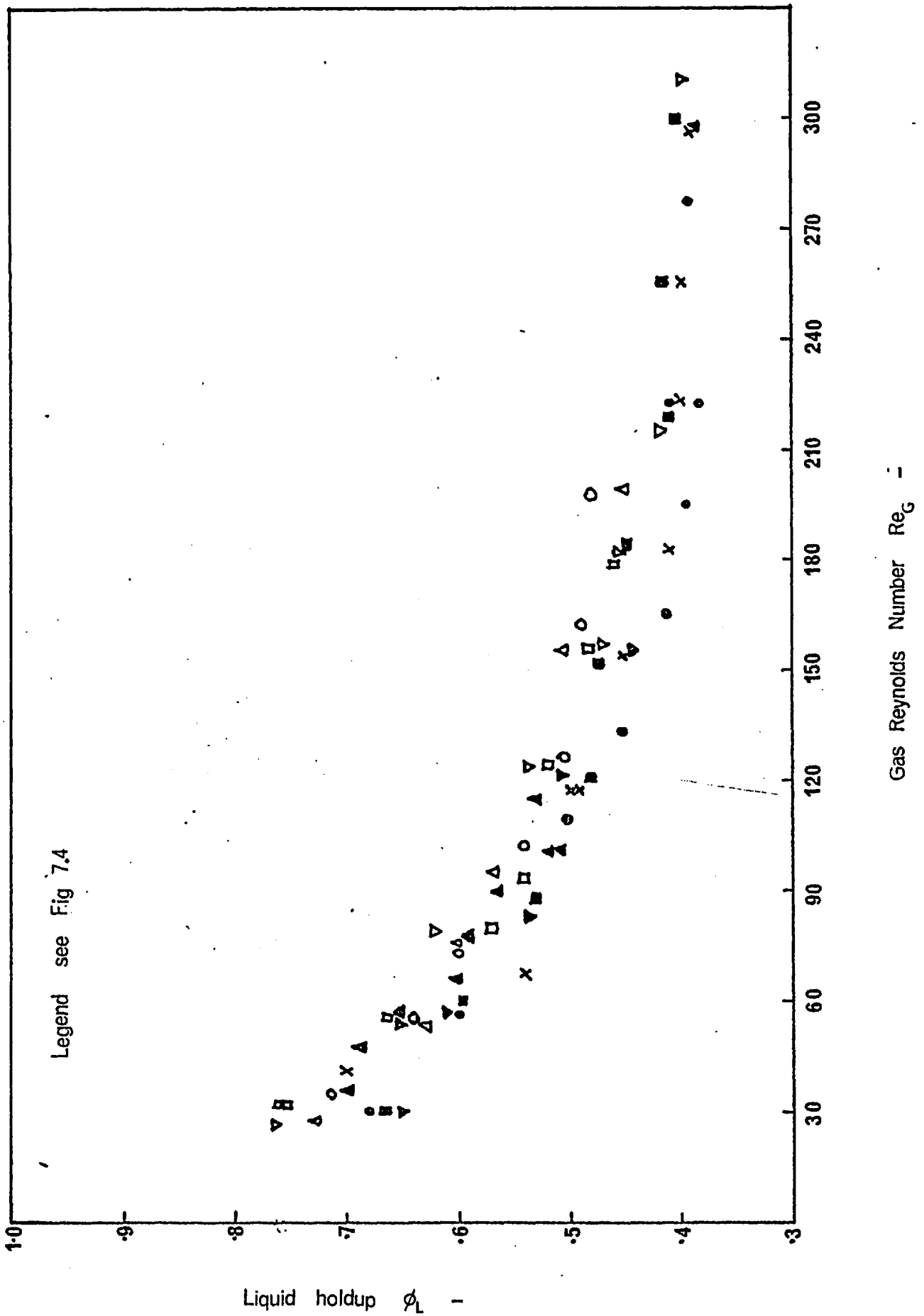

LIQUID HOLDUP AS A FUNCTION OF GAS AND LIQUID REYNOLDS NUMBERS

FIG 7.8

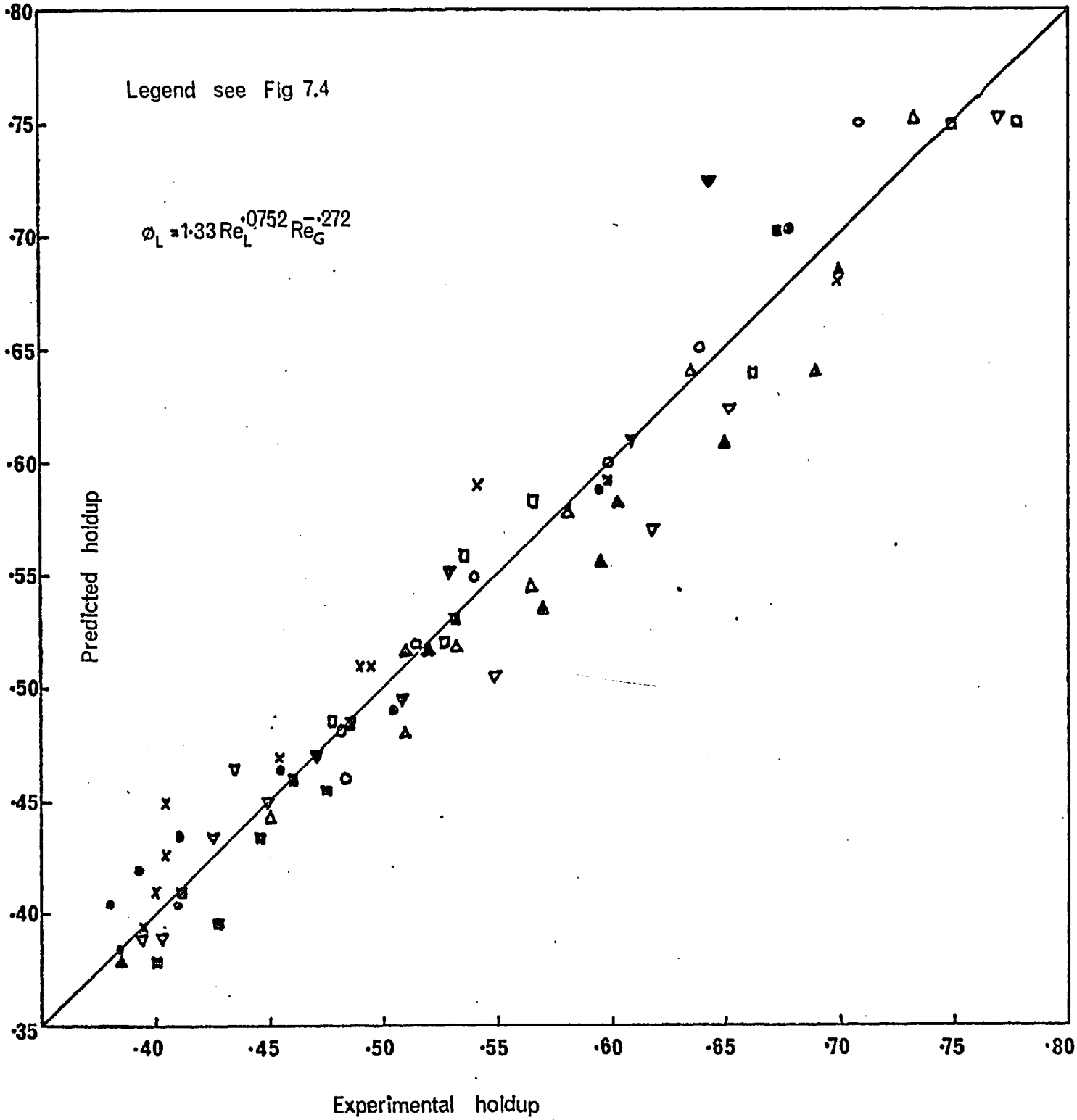

CORRELATION OF ALL LIQUID HOLDUP RESULTS

FIG 7.9

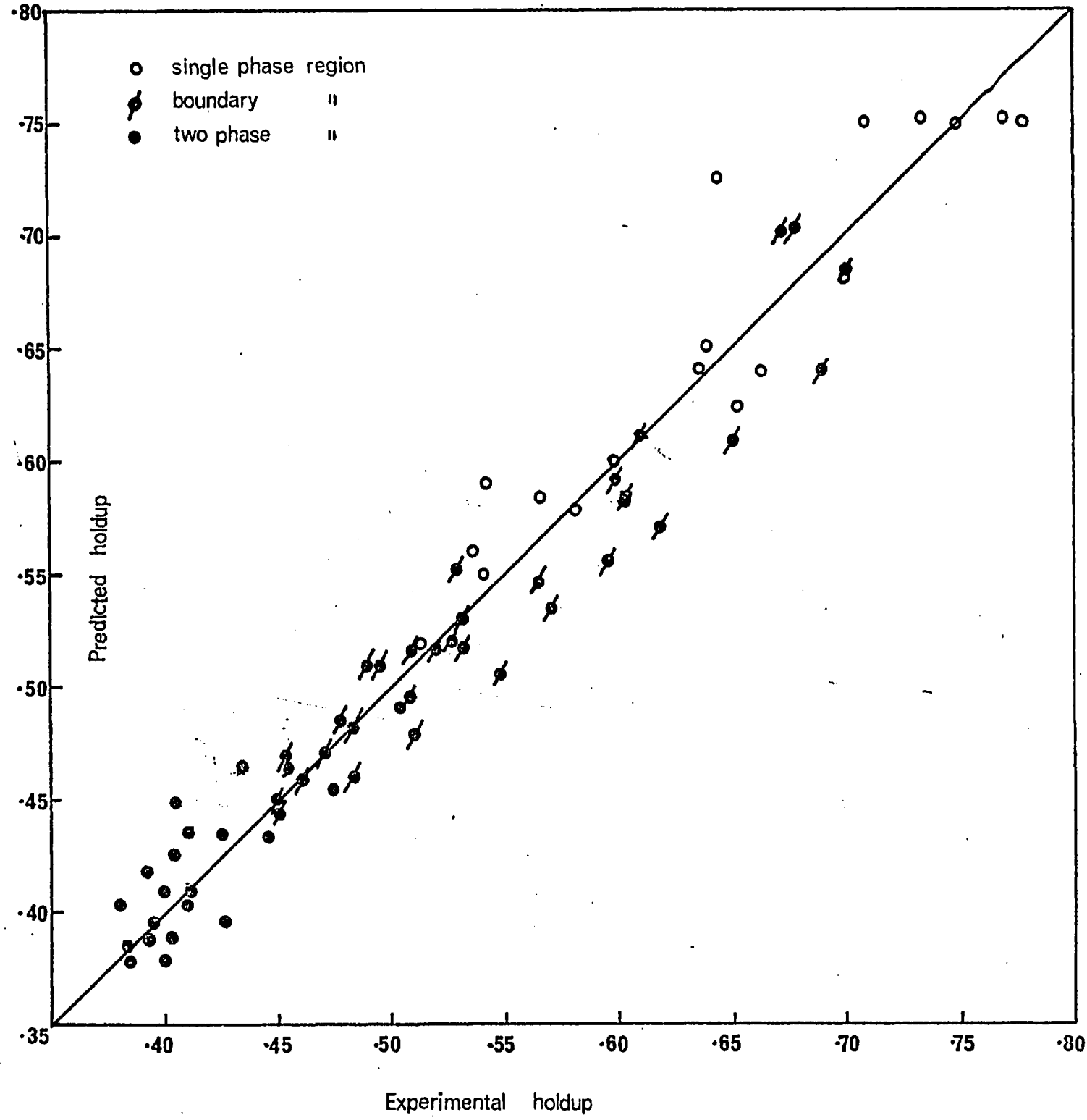

CORRELATION OF ALL LIQUID HOLDUP RESULTS SHOWING REGIONAL GROUPING

FIG 7.10

7.5 Analysis by the Liquid Stagnancy Model

The parameters of the liquid stagnancy model are listed in Appendix G. This model is characterised by three parameters but a search was also made to determine the liquid holdup. Since the liquid holdup results obtained from this model by Transfer Function minimisation are almost identical to those obtained from the Dispersion model they will not be discussed further. The Transfer Function for this model given in eq. 4.20 can be rearranged as:

$$F(p) = \exp\left\{\frac{-2\tau^* p\alpha\phi_L}{1 + (1+4\tau^* p\phi_L \alpha N_D)^{\frac{1}{2}}}\right\}$$

In this form it can be seen that there is no change in the numerical value of F(p) with changes in the Dispersion Number, for values of N_D $\left[10^{-16}\right]$ due to the limits of computer precision. All values of this order or less are recorded in Appendix G as zero. For the three runs at which $\gamma = 1$, the value obtained for the Number of Transfer Units is immaterial since there is no stagnant region with which to exchange fluid. The results suggest that with the parameters N_T and γ it is quite adequate to treat the flowing liquid phase as a plug flow region i.e. $N_D = 0$.

There are no discernable trends in the Number of Transfer Units, as a function of the gas or liquid Reynolds Numbers. The majority of the values obtained for the liquid flow fraction, γ, are within a relatively narrow range of 0.83 to 0.92 but again it is not possible to deduce a correlation with the gas and liquid flow rates. In contrast with the simpler 1 parameter basic axially dispersed plug flow model results, there is no simplification if the results are separated into the single phase pore flow and two phase pore flow regions.

It is concluded therefore that this model is not suitable for representing this two-phase system.

7.6 Analysis by the split flow model without stream interaction

The parameters of the split flow model are listed in Appendix H. As in the case of the liquid stagnancy model, the liquid holdup was also determined from the fitting procedure. The holdup results will not be discussed further since they are the same as those obtained from the Basic Dispersion Model.

It has not proved possible to obtain a satisfactory correlation of the model's parameters with either the liquid or gas flow rates. The liquid distribution model does not provide any insight into the trend of this model's parameters. As in the case of the stagnancy model, it must be concluded that this model is unsuitable for correlating the experimental residence time distribution data of this system.

7.7 Comparison with the results of previous studies

Compared with the considerable literature on dispersion in packed beds for single phase flow there are few two phase flow results published. It is convenient to separate those liquid mixing studies that have been reported for gas-liquid-particle operations on the basis of whether the bed was under trickle flow or bubble flow conditions. In trickle flow the liquid phase flows downwards and the continuous gas phase moves in either cocurrent or countercurrent flow. During bubble flow operation the gaseous phase moves upwards as discrete bubbles and the liquid phase may be either co- or countercurrent. The majority of the two phase studies found have been for countercurrent trickle flow conditions.

7.7.1 Liquid Dispersion Studies under cocurrent trickle flow conditions

The studies of SCHOENEMAN(65) in a trickle flow reactor used for butyndiol synthesis reported a residence time distribution approximating to 4 mixers. The residence time distribution in the 16m high and 800mm diameter reactor, packed with 4mm diameter silica pellets was unaffected by variations in the gas and liquid velocities for liquid velocities in the range 5×10^{-4} to 3×10^{-3} ms^{-1}. LAPIDUS(42) presented a few results for air water downward flow in a column 51mm diameter and 0.91m in height packed with 8.5mm glass beads. The results were taken to indicate a close approximation to plug flow for the liquid phase.

GLASER and LICHTENSTEIN(25) measured their residence time distributions in downward gas/liquid flow in columns of 19, 50 and 300 mm diameter containing 1.6 mm cylindrical packings. The fluid media were $CaCl_2$ solution and air in one set of experiments and kerosene and hydrogen in another. They characterised their results by variability defined as the standard deviation of the residence time divided by the average residence time.

For liquid flow rates ranging from 0.13 to 13 kg $s^{-1}m^{-2}$ the bulk flow variability was approximately constant at about 0.2. At liquid rates above 4 kg $s^{-1}m^{-2}$ the variability due to diffusion in and out of stagnant pools disappeared. (The current study covers a liquid range of 8 to 28 kg $s^{-1}m^{-2}$).

7.7.2 Liquid Dispersion Studies under Cocurrent Bubble flow conditions

SCHOENEMAN(65) reported qualitatively that the liquid residence time distribution for cocurrent upward bubble flow was narrower than that observed in trickle flow. WEBER(78) studied dispersion for air and water in upward cocurrent flow in a 1m high column of 50mm diameter.

For 5mm spheres the correlation given by WEBER(78) reduces to

$$N_D = 0.11_I Re_L^{-0.96} {}_I Re_G^{0.48}$$

in terms of the present study. Comparison with the coefficients listed in Table 7.1 shows similar dependencies on the gas and liquid Reynolds Numbers. Overall, however, the correlation predicts smaller values for the Dispersion coefficient than found in this study.

7.7.3 Liquid Dispersion studies under Countercurrent Flow Conditions

KRAMERS and ALBERDA(41) concluded that axial mixing increased with increasing gas flow rate and decreasing liquid rate, as found in this study. The results were not however adequately represented by the basic dispersion model. DUNN et al(18) also found the liquid mixing to increase with decreasing liquid rate but there was no gas rate effect over the range of flowrates studied. Details of the experimental systems for studies reported in this section are tabulated in Table 7.5. The reproducibility of the data was poor and it was proposed from these results that the Dispersion Number was proportional to $Re_L^{-0.5}$.

HOOGENDORN and LIPS(34) found a representation based on the basic Dispersion model using moments analysis was not possible due to the significant tailing effect. A negligible gas rate effect was found but there was a slight liquid rate effect on an approximately plug flow liquid phase.

Study	Liquid Rates kg $m^{-2}s^{-1}$	Gas Rates kg $m^{-2}s^{-1}$	Column Dia mm	Column Ht m	Particle size mm
DUNN(18)	2.71-14.9	0 - 1.49	610	1.82	2.54 Rings
KRAMERS(41)	-	-	150	0.66	10 Rings
HOOGENDORN(34)	2.13-5.18	.009-.09	410	3.04	12.7 Rings
De WAAL(77)	1.38-22.2	0-1.38	305	3.04	25.4 Rings
SATER(63)	.81-47.5	-	101.6	3.65	12.7 Rings
FURZER(23)	1.35-9.05	0-0.76	50.8	1.52	6.35 Rings
THIS WORK	7.9-27.7	.09-1.02	101.6	.835	5 Spheres

Table 7.5 Experimental conditions for countercurrent dispersion studies

De WAAL and VAN MAMEREN(77) in contrast found no tailing and decided that the effect of liquid residence time distribution can be neglected in tall columns.

SATER and LEVENSPIEL(63) correlated their Dispersion results as a function of the liquid Reynolds Number. In terms of the present study their correlation becomes:

$$N_D = 0.79\ Re_L^{-0.703}$$

The 95% confidence limit on the exponent was ±0.238.

In a later study FURZER and MICHELL(23) found the Dispersion model correlated their data well. The scatter reported by other workers, was attributed to the errors associated with the evaluation of the second moments of the response curve when tailing was present.

Their correlation, based on interstitial Reynolds Numbers, reduces to the following in terms of the present study:

$$N_D = 0.149_I Re_L^{-0.5}$$

During bubble flow conditions HOOGENDORN and LIPS(34) found the Dispersion model to be a good fit even though the Dispersion parameter was obtained using the second moment. The axial dispersion was largely independent of liquid flow rate and only slightly dependent on gas rate. Dispersion coefficients an order of magnitude greater than those obtained by WEBER(78) were reported.

To summarise it seems clear that in all modes of two-phase flow, there is little agreement as to

(i) the suitability of the basic Dispersion model for characterising liquid mixing and

(ii) the effect of the gas and liquid flowrates on the liquid residence time distribution.

CHAPTER 8 CONCLUSIONS

The following conclusions can be drawn from the theoretical and experimental studies undertaken in this work.

1 The liquid Dispersion results from the Axially Dispersed plug flow model are in agreement with the qualitative predictions of the liquid distribution model.

2 The Dispersion Numbers characterising the single phase pore flow regime are similar in magnitude to the values obtained when liquid alone flows through the packed bed and are not significantly influenced by variations in gas rate.

3 Dispersion Numbers in the two phase pore flow region are substantially higher than those in the single phase region, particularly at high gas to liquid ratios. In this region dispersion increases with gas Reynolds Number.

4 The Dispersion Numbers in the three regions can be correlated by:

$$N_D = 0.645\ {}_I Re_L^{-0.675} \qquad \text{for the single phase region}$$

$$N_D = 0.246\ {}_I Re_L^{-0.482} \qquad \text{for the boundary region}$$

$$N_D = 0.571\ {}_I Re_L^{-2.17}\ {}_I Re_G^{1.36} \qquad \text{for the two phase region}$$

5 If all the dispersion data are taken together, to facilitate comparisons with the results of previous studies, they can be correlated by:

$$N_D = 0.407\ {}_I Re_L^{-1.1}\ {}_I Re_G^{0.504}$$

6 The parameters of the stagnancy and split flow models cannot be correlated satisfactorily with gas and liquid Reynolds Numbers. These 3 parameter models are considered too complex for resolution by the experimental data available.

7 The liquid holdup data for all regions can be taken together and correlated by:

$$\phi_L = 1.33\ Re_L^{0.0752}\ Re_G^{-0.272}$$

8 The use of noise weighting functions gives consistent values for the Dispersion Number in the axially dispersed plug flow model when 1st and higher order modified moments are used.

9 The series solution technique will permit easier solutions to be obtained for the Transfer Functions of more complex flow models.

10 The series solution technique, applied to the problem of compressible flow in a packed bed, has shown that substantial errors in estimating the fluid Dispersion Number can arise if the commonly made assumption of fluid incompressibility is inappropriate.

APPENDIX A - APPLICATION OF THE SERIES SOLUTION TECHNIQUE IN DETERMINING THE TRANSFER FUNCTION FOR ISOTHERMAL FLOW OF A COMPRESSIBLE GAS IN A PACKED BED

In the past, solutions for gas flow within a packed bed have been obtained by considering the fluid within the system to be incompressible. Whilst this assumption is valid for the liquid systems it has little justification in packed bed systems when the gaseous phase can experience a considerable pressure drop.

The new technique for evaluating Transfer Functions outlined in eq.4.31 to eq.4.34 of the main text will be applied in this Appendix to analyse a system consisting of isothermal gas flow through a packed bed. The difficulties in determining accurately the true Dispersion Number for a compressible gaseous phase are clearly demonstrated.

For this system an unsteady state mass balance yields

$$u \frac{\partial C}{\partial z} + C \frac{\partial u}{\partial z} - D_L \frac{\partial^2 C}{\partial z^2} - \frac{\partial C}{\partial z} \cdot \frac{\partial D_L}{\partial z} + \frac{\partial C}{\partial t} = 0 \quad \ldots \quad (A.1)$$

For constant fluid velocity and dispersion coefficient eq.A.1 reduces to the incompressible dispersion eq.4.2 of the main text.

Setting $x = z/L$ as in the incompressible case the system is limited by $0 \leq x \leq 1$.

In the subsequent analysis the subscripts 0 and 1 refer to conditions at the upstream and downstream boundaries respectively.

The equation of continuity yields:

$$\rho u = \rho_o u_o = \rho_1 u_1 \quad \ldots\ldots\ldots \quad (A.2)$$

For isothermal flow:

$$\frac{P}{\rho} = \frac{P_o}{\rho_o} = \frac{P_1}{\rho_1} \quad \ldots\ldots\ldots \quad (A.3)$$

where P and ρ are the average fluid pressure and density at any axial position x.

From eq.A.2 and eq.A.3 it follows directly that:

$$u = \frac{P_o}{P} u_o \quad \ldots\ldots\ldots \quad (A.4)$$

The fluid pressure P can be expressed as a function of the dimensionless distance x from the upstream system boundary by the general expression:

$$P^2 = P_o^2 + k_1 x \qquad \ldots\ldots\ldots \qquad (A.5)$$

where k_1 is a constant depending on the mass flow rate, fluid properties and permeability of the porous mass. This linear dependence of the square of the pressure is applicable for isothermal flow at all subsonic velocities.

Setting $B = k_1/P_o^2$ eq.4.5 can be written

$$P = P_o (1 + Bx)^{\frac{1}{2}} \qquad \ldots\ldots\ldots \qquad (A.6)$$

For a convergent series expansion of P by the Binomial Theorem, Bx must be limited such that $-1 < Bx < 1$. On physical considerations P will always be less than P_o and greater than zero imposing the limits $-1 < Bx < 0$.

Combining eq.A.4 and eq.A.6 we obtain:

$$u = u_o (1 + Bx)^{-\frac{1}{2}} \qquad \ldots\ldots\ldots \qquad (A.7)$$

Eq. A.1 allows for a variation in the Dispersion Coefficient with axial position.

The Dispersion within any system at a particular Reynolds Number or mass flow rate is characterised by a particular value of the Dispersion Number. Since a constant mass rate may be achieved at various fluid velocities by varying the system pressure it is argued that the Dispersion coefficient must also vary with the fluid velocity.

Thus $\frac{D_L}{uL} = \frac{D_{Lo}}{u_o L}$ = constant is a reasonable assumption for a first approximation.

Then $D_L = D_{Lo} (1 + Bx)^{-\frac{1}{2}} \qquad \ldots\ldots\ldots \qquad (A.8)$

Substituting for D_L and u in eq. A.1, differentiating, taking Laplace transforms and dividing by u_o/L we obtain

$$N_{Do} (1+Bx) \frac{d^2\bar{C}}{dx^2} - (1+Bx+B/2\ N_{Do}) \frac{d\bar{C}}{dx} + (B/2 - (1+Bx)^{3/2}\ \tau_o p)\ \bar{C} = 0 \qquad \ldots\ldots\ldots \qquad (A.9)$$

where $N_{Do} = \frac{D_{Lo}}{u_o L}$ and $\tau_o = L/u_o$

The Dispersion Number N_{Do} and system mean residence time τ_o would alone characterise the system if it were treated incompressibly i.e. B = O.

Eq. A.9 can be written in the general form:

$$\frac{d^2\bar{C}}{dx^2} + R(x)\frac{d\bar{C}}{dx} + S(x)\bar{C} = O \qquad \ldots\ldots\ldots \qquad (A.10)$$

By inspection R(x) and S(x) are analytic at all x except when Bx = -1, which is not a feasible point since Bx > -1 as discussed previously.

Expanding $(1 + Bx)^{3/2}$ up to terms in $(Bx)^5$

$$(1+Bx)^{3/2} = 1 + {}^3/2\ Bx + {}^3/8\ (Bx)^2 - {}^1/16\ (Bx)^3 + {}^3/128\ (Bx)^4 - {}^3/256\ (Bx)^5 + \ldots\ldots \qquad (A.11)$$

From eq.4.31 and 4.32 of the main text we have :

$$\bar{C} = \sum_o^N a_k x^k \ ; \ \frac{d\bar{C}}{dx} = \sum_1^N k a_k x^{k-1} \ ; \ \frac{d^2\bar{C}}{dx^2} = \sum_2^N k(k-1) a_k x^{k-2} \ \ldots \qquad (A.12)$$

On substitution in eq. A.9 (dropping the o subscript for convenience) we obtain :

$$N_D \sum_2^N k(k-1)a_k x^{k-2} + BN_D \sum_2^N k(k-1)a_k x^{k-1} - (1+\frac{B}{2}N_D) \sum_1^N k a_k x^{k-1} - B\sum_1^N k a_k x^k$$
$$+ (\frac{B}{2} - \tau p) \sum_o^N a_k x^k - {}^3/2\ B\tau p \sum_o^N a_k x^{k+1} - {}^3/8\ B^2 \tau p \sum_o^N a_k x^{k+2} + \frac{3}{16}\tau p \sum_o^N a_k x^{k+3}$$
$$- {}^3/128\ B^4\ \tau p \sum_o^N a_k x^{k+4} + \frac{3}{256} B^5 \tau p \sum_o^N a_k x^{k+5} = O \qquad \ldots\ldots\ldots \qquad (A.13)$$

From eq. 4.34 of the main text the system Transfer Function $F(\bar{p})$ is given by:

$$F(p) = 1 + \sum_1^N b_k \quad \text{where} \quad b_k = {}^a k/a_o \qquad \ldots\ldots\ldots \qquad (A.14)$$

Each series in eq. A.13 can be rearranged into a more suitable computational form, as a series:

$$\sum_6^{N-1} K a_r x^k + \text{remaining terms}$$

where $K = K(k, N_D, \tau p, B)$

$r = r(k)$

For example the series $N_D \sum_{2}^{N} k(k-1)a_k x^{k-2}$ can be written as:

$$N_D \sum_{6}^{N-1} (k+2)(k+1)a_{k+2}x^k + N_D \left\{ 2a_2+6a_3x+12a_4x^2+20a_5x^3+30a_6x^4+42a_7x^5 - N(N+1)a_{N+1}x^{N-1} \right\}$$

Setting all the series terms in eq.A.13 in this form and collecting terms we obtain:

$$\sum_{6}^{N-1} \left\{ N_D(k+2)(k+1)a_{k+2} + (k+1)(BN_D(k-\tfrac{1}{2})-1)a_{k+1} - B(k-\tfrac{1}{2}+\tau p)a_k - \frac{3}{2} B\tau p a_{k-1} - \frac{3}{8} B^2\tau p a_{k-2} + B^3/16\ \tau p a_{k-3} - {}^3/128\ B^4\tau p a_{k-4} + {}^3/256\ B^5\tau p a_{k-5} \right\} x^k$$

$$+ \text{remaining terms} = 0 \qquad \ldots\ldots\ldots \qquad (A.15)$$

The remaining terms will consist of those terms outside the summation range. However it will only be necessary to deal with these terms in powers of x^j for $0 \leq j \leq 5$ in addition to those given by eq. A.15.

Thus equating coefficients of powers of x to zero:-

Terms in x^0

$$-(1 + \frac{B}{2} N_D)\ a_1 + 2N_D a_2 + ({}^B/2 - \tau p)a_o = 0$$

For a_o non zero we define $b_i = {}^a i/a_o$

$$\text{i.e. } (1 + {}^B/2\ N_D)\ b_1 - 2N_D b_2 = {}^B/2 - \tau p \qquad \ldots\ldots\ldots \qquad (A.16)$$

Terms in x^1

$$-({}^B/2+\tau p)b_1 + (BN_D-2)b_2 + 6N_D b_3 = {}^3/2\ \tau p\ B \qquad \ldots\ldots\ldots \qquad (A.17)$$

Terms in x^2

$$-{}^3/2\tau pBb_1 - ({}^3/2\ B+\tau p)b_2 + ({}^9/2\ BN_D-3)b_3 + 12N_D b_4 = {}^3/8\ \tau pB^2 \ldots \qquad (A.18)$$

Terms in x^3

$$\frac{3}{8}\tau pB^2 b_1 + {}^3/2\tau pBb_2 + ({}^5/2B+\tau p)b_3 - (10N_D B-4)b_4 - 20N_D b_5 = {}^1/16\tau pB^3 \ldots \qquad (A.19)$$

Terms in x^4

$${}^1/16\tau pB^3 b_1 - {}^3/8\tau pB^2 b_2 - {}^3/2\tau pBb_3 - ({}^7/2B+\tau p)b_4 + (\frac{35}{2}BN_D-5)b_5 + 30N_D b_6 = \frac{3}{128}\ \tau p\ B^4 \ldots\ldots\ldots \qquad (A.20)$$

Terms in x^5

$$\frac{3}{128}\tau pB^4 b_1 - {}^1/16\tau pB^3 b_2 + {}^3/8\tau pB^2 b_3 + {}^3/2\tau pB b_4 + ({}^9/2B+\tau p)b_5 - (27BN_D - 6)b_6$$

$$-42N_D b_7 = {}^3/256\ \tau pB^5 \qquad \ldots\ldots\ldots \qquad (A.21)$$

The general series eq. A.15 can also be divided by a_o to yield b_i coefficients. At the upper summation limit, k=N-1, the largest coefficient will be b_N since the first term in eq.A.15 is cancelled out by the term $-(N+1)Na_{N+1}$ which is a remainder term from the first term in eq.A.13.

We therefore have N coefficients to evaluate from N equations obtained by equating powers of x^k to zero for $0 \leq k \leq N-1$.

This set of linear equations in b; eqs. A.15 to A.21 may be concisely written as $\underline{\underline{E}}.\ \underline{b} = \underline{S}$ ..... (A.22)

where $\underline{\underline{E}}$ is the square N x N coefficient matrix

and $\underline{S}$ contains the elements of the forcing vector and

$S_i = 0$ for $6 \leq i \leq N-1$

This set of equations was successfully solved by Gaussian Elimination with row pivoting on the row with the largest magnitude leading element.

Reduction to Plug Flow Transfer Function when $N_D = B = 0$

Equations A.16 to A.19 become

$$b_1 = -\tau p$$

$$\tau p b_1 + 2b_2 = 0$$

$$\tau p b_2 + 3b_3 = 0$$

$$\tau p b_3 + 4b_4 = 0$$

Solving these equations we find:

$$b_1 = -\tau p\ ;\ b_2 = \frac{(\tau p)^2}{2}\ ;\ b_3 = \frac{-(\tau p)^3}{2.3}\ ;\ b_4 = \frac{(\tau p)^4}{2.3.4}$$

Using equation A.14 then

$$F(p) = 1 - \tau p + \frac{(\tau p)^2}{2} - \frac{(\tau p)^3}{2.3} + \frac{(\tau p)^4}{2.3.4}$$

$\therefore$ $F(p) = \exp\left\{-\tau p\right\}$ i.e. plug flow Transfer Function.

Value of the Transfer Function for p = 0

From the definition of the System Transfer Function eq. 4.3 we have:

$$F(p) = \frac{\int_o^\infty C_1(t)e^{-pt}dt}{\int_o^\infty C_o(t)e^{-pt}dt} \qquad \ldots\ldots\ldots \qquad (A.23)$$

$$\therefore F(o) = \frac{\int_o^\infty C_1(t)dt}{\int_o^\infty C_o(t)dt} \qquad \ldots\ldots\ldots \qquad (A.24)$$

The response curves at the two measurement points are related by a mass balance on the tracer.

If V_o and V_1 are the volumetric flow rates at the two measurement points then q the quantity of tracer in the system is given by:

$$q = V_o \int_o^\infty C_o(t)dt = V_1 \int_o^\infty C_1(t)dt \qquad \ldots\ldots\ldots \qquad (A.25)$$

Hence $F(o) = \frac{V_o}{V_1}$

Thus the Transfer Function as defined only has a value of unity at p = O for systems in which the volumetric flow rate remains constant.

For isothermal flow $\frac{V_o}{V_1} = P_1/P_o = (1 + B)^{\frac{1}{4}}$

$$\therefore F(o) = (1 + B)^{\frac{1}{4}} \qquad \ldots\ldots\ldots \qquad (A.26)$$

The effect of pressure drop as represented by B, on the plug flow Transfer Function is shown in Fig.A.1. For all values of $B \neq O$ there is a non unity intercept at $\tau p = O$ which obeys eq.A.26. This effect has been removed in Fig.A.2 by normalising each curve such that for any B F(o) = 1.0. It can be seen that for any given τp the Transfer Function increases as the pressure drop is increased. This is the same effect as occurs in an incompressible flow system when the system Dispersion Number is increased.

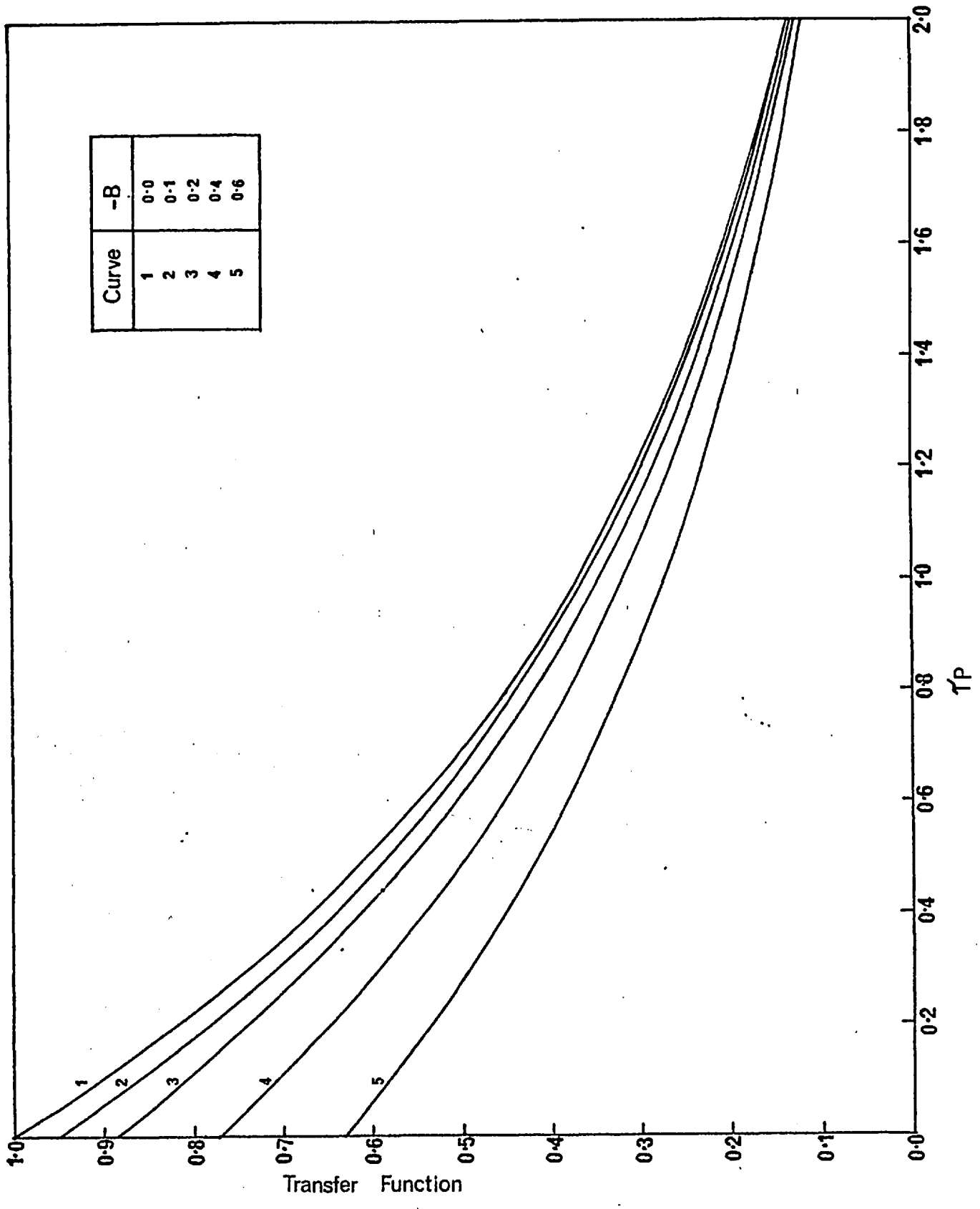

EFFECT OF PRESSURE DROP B ON UNNORMALISED PLUG FLOW TRANSFER FUNCTION

FIG. A.1

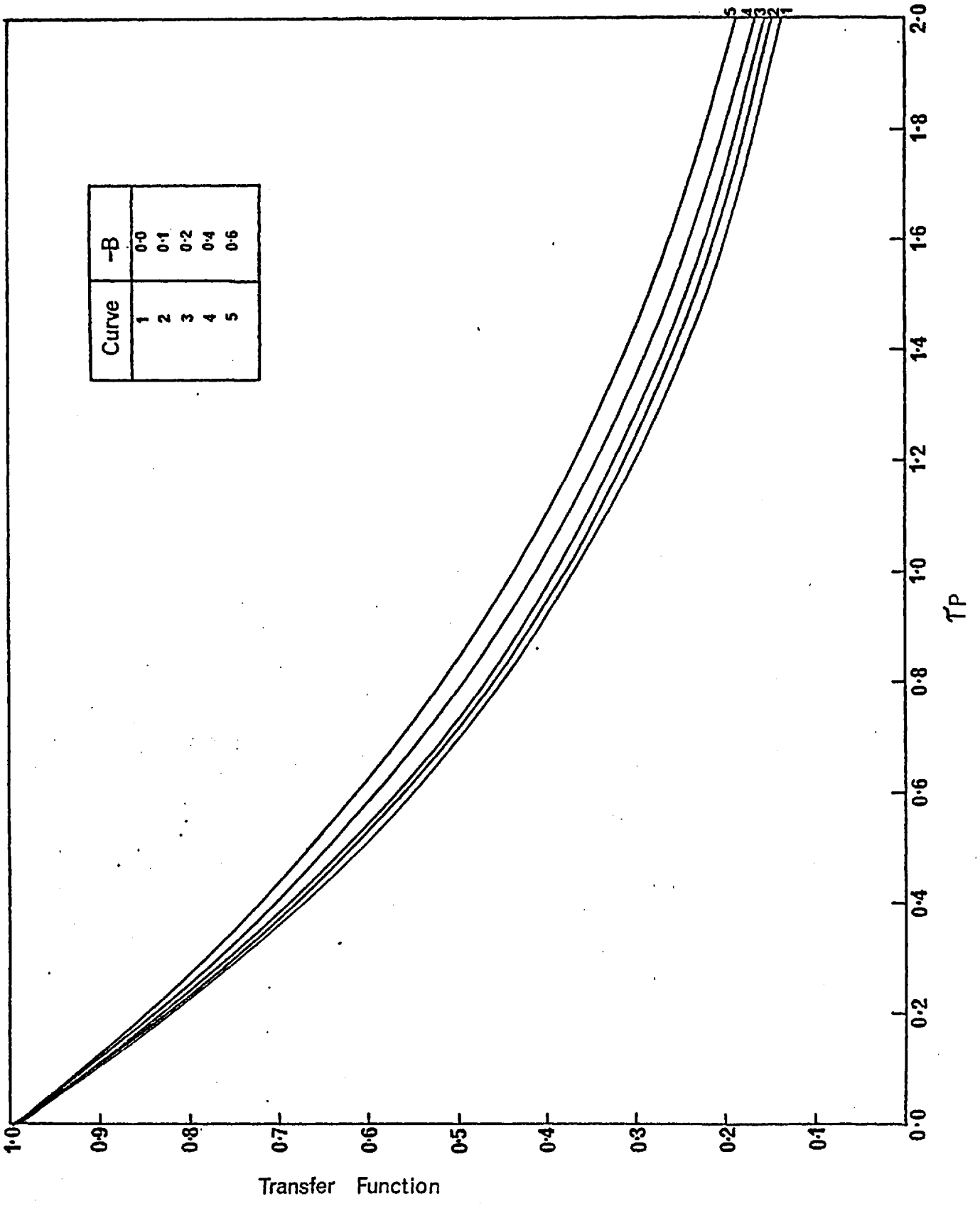

EFFECT OF PRESSURE DROP B ON NORMALISED PLUG FLOW TRANSFER FUNCTION

FIG. A.2

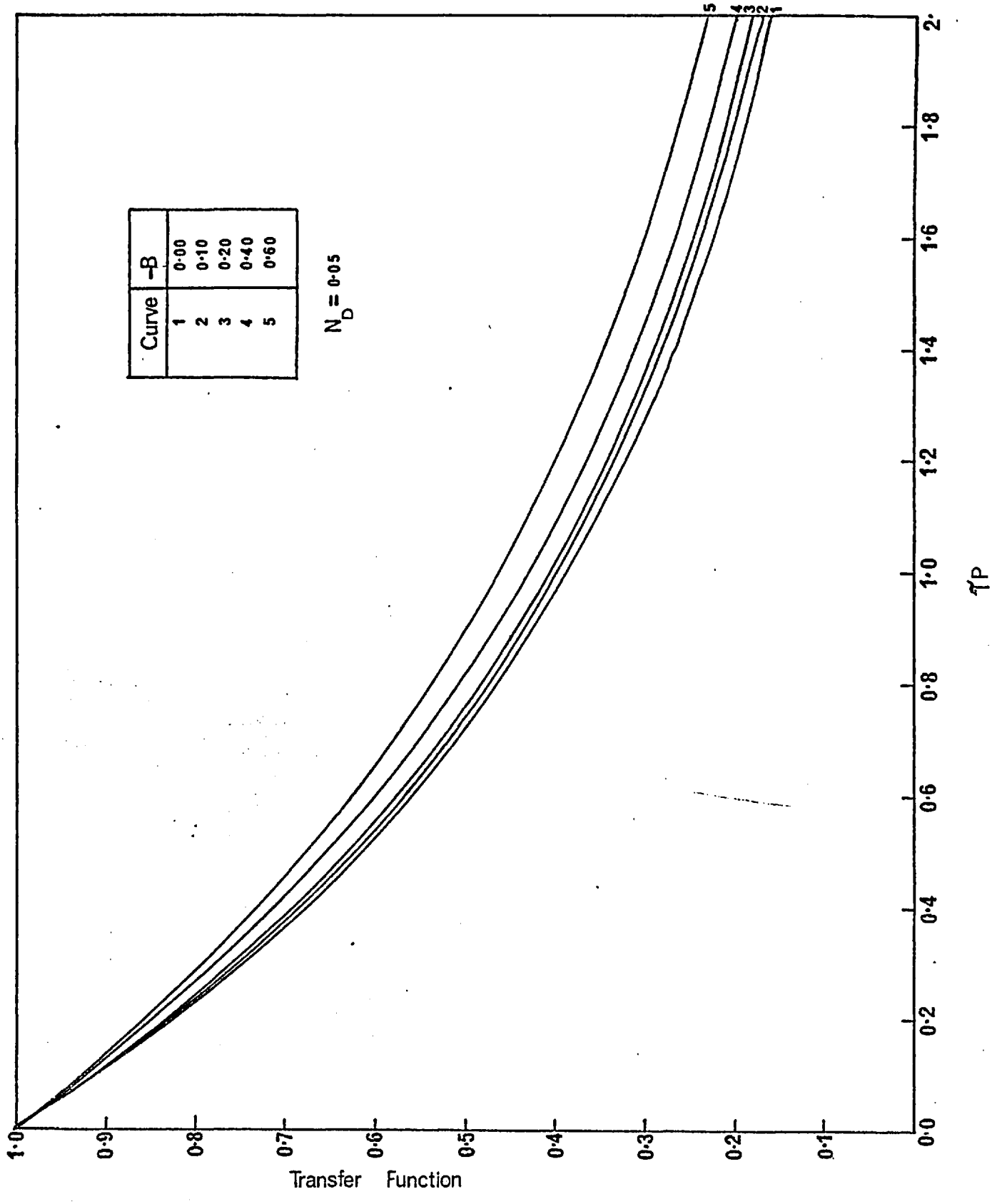

VARIATION IN NORMALISED TRANSFER FUNCTION WITH PRESSURE DROP B AT A GIVEN DISPERSION NUMBER N_D

FIG. A.3

Thus a system, which when treated incompressibly is characterised by a particular Dispersion Number, could in fact be a plug flow system with a certain pressure drop. Since this extreme case does not exist in reality, the more realistic case of pressure drop in systems where some fluid dispersion occurs is shown in Fig.A.3.

The combined effect of low dispersion and a fluid pressure drop is seen to be equivalent to a system exhibiting a higher Dispersion Number.

For a particular pressure drop, the behaviour of the system Transfer Function as the system Dispersion Number is increased, is identical to that found in incompressible systems, except for the displacement due to the pressure drop. This effect is illustrated in Fig.A.4.

The effect of pressure drop on the system response is in accord with the following qualitative assessment of the passage of a packet of tracer through a compressible system. As the fluid pressure decreases the tracer packet will expand giving an apparent dispersive effect. This will be in addition to the usual processes, e.g. diffusion and flow splitting around particles, which together are often characterised by a Dispersion coefficient.

For a compressible system the term $\tau_o p$, involving the incompressible mean residence time τ_o, becomes a system parameter. The relationship between the compressible mean residence time τ_c and τ_o is obtained from

$$dt = L\frac{dx}{u} \quad \text{and} \quad u = u_o (1 + Bx)^{-\frac{1}{2}}$$

$$\text{Thus } \tau_c = \frac{L}{u_o} \int_o^1 (1 + Bx)^{-\frac{1}{2}} dx$$

$$\therefore \tau_c = {}^2/_3 \, B \left\{ (1 + B)^{3/2} - 1 \right\} \tau_o \qquad \ldots\ldots\ldots \qquad (A.27)$$

The variation in the mean residence time with pressure drop B is shown in Fig.A.5.

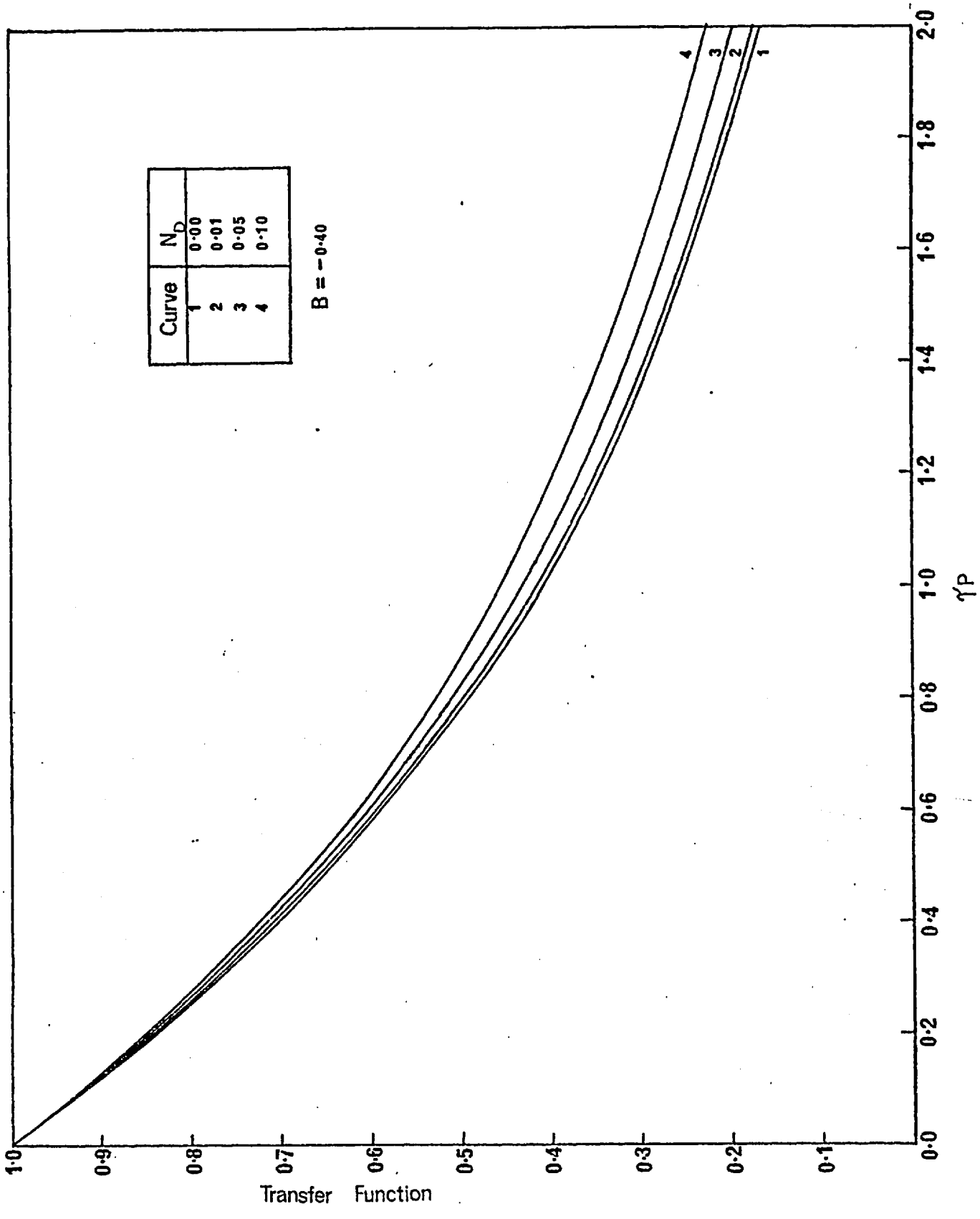

VARIATION IN NORMALISED TRANSFER FUNCTION WITH DISPERSION NUMBER N_D AT A GIVEN PRESSURE DROP B

FIG. A.4

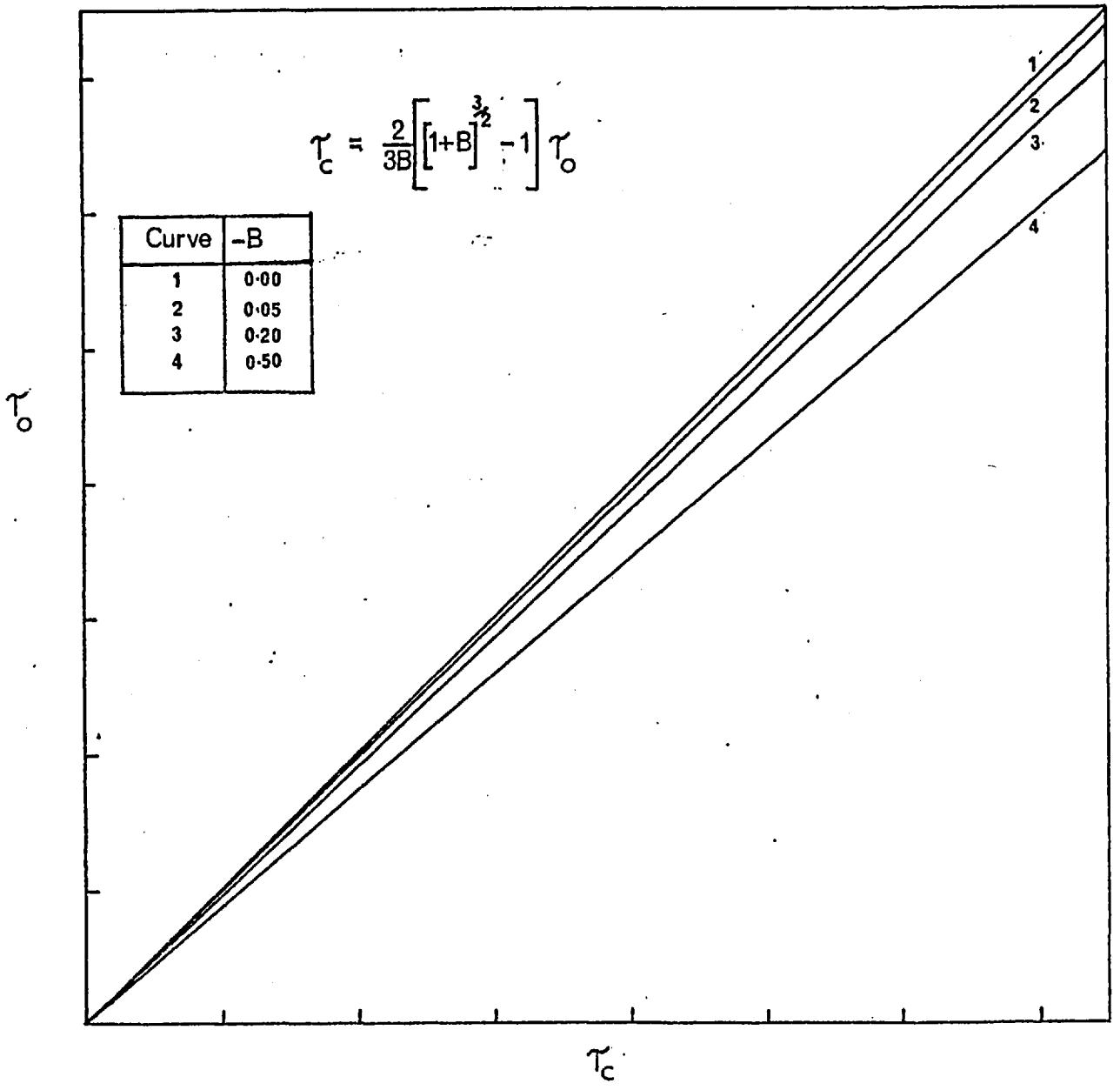

VARIATION IN MEAN RESIDENCE TIME WITH PRESSURE DROP B

FIG. A.5

APPENDIX B DETERMINATION OF THE NOISE WEIGHTING FUNCTIONS

To determine the optimum value of the Laplace Transform parameter for methods 1 and 2, the noise weighting functions $E_i(t)$ at the two measurement points must be evaluated.

From eq.5.22 of the main text, the error ΔN_D in the Dispersion Number is related to the noise $v_i(t)$ and the noise weighting function $E_i(t)$ by:

$$\Delta N_D = \int_o^\infty v_i(t)\, E_i(t)\, dt \qquad \ldots\ldots\ldots \quad (B.1)$$

To determine the weighting function at any time $t = T$, we consider the effect on the Dispersion Number when noise occurs only at time T. For noise at time T only we can express $v_i(t)$ by

$$v_i(t) = \Delta.\delta(t-T) \qquad \ldots\ldots\ldots \quad (B.2)$$

Δ will be small since the noise is assumed small in comparison with the recorded tracer concentration $c_i(t)$.

Using the properties of the delta function that:

$$\begin{aligned} &\delta(t-T) = 0 \quad \text{for } t \neq T \\ &\delta(t-T) = 1 \quad \text{for } t = T \end{aligned} \qquad \ldots\ldots\ldots \quad (B.3)$$

$$\text{and} \int_o^\infty \delta(t-T)\, E_i(t)\, dt = E_i(T)$$

we have $\Delta N_D = \Delta.E_i(T)$

$$\text{or } E_i(T) = \frac{\Delta N_D}{\Delta} \qquad \ldots\ldots\ldots \quad (B.4)$$

Thus the noise weighting function at time T is the ratio of the error in the Dispersion Number due to noise at time T, to the noise itself.

B.1 Weighting functions at the 1st measurement point i = 0

The response at the 2nd measurement point i = 1 is assumed error free.

Thus $${}_e C_o = {}_t C_o + v_o \qquad \ldots\ldots\ldots \quad (B.5)$$

and $${}_e C_1 = {}_t C_1 \qquad \ldots\ldots\ldots \quad (B.6)$$

where the presubscripts e and t denote the error and true values of the tracer concentration respectively.

If the response curves are assumed to be normalised such that

$$\int_o^\infty {}_t C\, dt = 1 \qquad \ldots\ldots\ldots \quad (B.7)$$

then the normalising ratio for the 1st measurement point will be $1 + \Delta$

In general therefore $${}_{t}\bar{M}_{o}^{r} = \int_{o}^{\infty} {}_{t}C_{o}\, e^{-pt}\, t^{r}\, dt \quad \ldots\ldots \quad (B.8)$$

and $${}_{e}\bar{M}_{o}^{r} = \frac{1}{1+\Delta} \int_{o}^{\infty} {}_{e}C_{o}\, e^{-pt}\, t^{r}\, dt \quad \ldots\ldots \quad (B.9)$$

For no noise at the 2nd measurement point

$${}_{e}\bar{M}_{1}^{r} = {}_{t}\bar{M}_{1}^{r} \quad \ldots\ldots \quad (B.10)$$

MICHELSEN and OSTERGAARD (50) expressed the error weighted moments in terms of the error free moments. In this study the expressions developed for $E_i(t)$ will contain only the error moments ${}_{e}\bar{M}_{i}^{r}$

Thus $${}_{e}\bar{M}_{o}^{o} = \frac{1}{1+\Delta}\left\{\int_{o}^{\infty} {}_{t}C_{o}\, e^{-pt} dt + \int_{o}^{\infty} \Delta.\delta(t-T)\, e^{-pt}\, dt\right\}$$

$$\therefore \quad {}_{e}\bar{M}_{o}^{o} = \frac{1}{1+\Delta}\left\{{}_{t}\bar{M}_{o}^{o} + \Delta e^{-pT}\right\}$$

On rearranging into the form suggested above:

$${}_{t}\bar{M}_{o}^{o} = (1 + \Delta)\, {}_{e}\bar{M}_{o}^{o} - \Delta.e^{-pT} \quad \ldots\ldots \quad (B.11)$$

Similarly we find:

$${}_{t}\bar{M}_{o}^{1} = (1 + \Delta)\, {}_{e}\bar{M}_{o}^{1} - T\Delta.e^{-pT} \quad \ldots\ldots \quad (B.12)$$

$${}_{t}\bar{M}_{o}^{2} = (1 + \Delta)\, {}_{e}\bar{M}_{o}^{2} - T^{2}\, \Delta.e^{-pT} \quad \ldots\ldots \quad (B.13)$$

B.1.1 Method 1 weighting functions

The Dispersion Number is given by eq.5.6 of the main text:

$$N_D = \frac{J + Qp}{J(J + 2Qp)}$$

Taking logs and differentiating:

$$\frac{dN_D}{N_D} = -\left\{\frac{1}{J} + \frac{1}{J+2Qp} - \frac{1}{J+Qp}\right\} dJ - p\left\{\frac{2}{J+2Qp} - \frac{1}{J+Qp}\right\} dQ \quad \ldots\ldots \quad (B.14)$$

Assuming $dN_D = {}_{e}N_D - {}_{t}N_D$; $dJ = {}_{e}J - {}_{t}J$; $dQ = {}_{e}Q - {}_{t}Q$

then from eq.5.20 $\dfrac{dN_D}{N_D} = \Delta N_D$.

$$\therefore E(T) = \frac{1}{\Delta}\frac{dN_D}{N_D}$$

$$\therefore E(T) = \frac{-dJ}{\Delta}\left\{\frac{1}{J} + \frac{1}{J+2Qp} - \frac{1}{J+Qp}\right\} - \frac{dQ}{\Delta}\left\{\frac{2}{J+2Qp} - \frac{1}{J+Qp}\right\} p \quad \ldots \quad (B.15)$$

Comparison with the work of MICHELSEN and OSTERGAARD (50) shows that the noise weighting function for the Dispersion Number is the negative of the noise weighting function for the Peclet Number.

From eq.5.8

$$t^J = \ell n\left\{\frac{t\bar{M}_1^o}{t\bar{M}_\phi^o}\right\} \quad \ldots\ldots\ldots \quad (B.16)$$

and $$e^J = \ell n\left\{\frac{e\bar{M}_1^o}{e\bar{M}_o^o}\right\} \quad \ldots\ldots\ldots \quad (B.17)$$

Substituting for $t\bar{M}_i^o$ from B.11

$$\therefore \quad t^J = \ell n\left\{\frac{e\bar{M}_1^o}{(1+\Delta)\,e\bar{M}_o^o - \Delta\bar{e}^{-pT}}\right\}$$

$$= \ell n\left\{\frac{e\bar{M}_1^o}{e\bar{M}_o^o}\right\} - \ell n\left\{1 + \Delta - \frac{\Delta e^{-pT}}{e\bar{M}_o^o}\right\}$$

$$\therefore \quad t^J = e^J - \ell n\left\{1 + \Delta\left[1 - \frac{e^{-pT}}{e\bar{M}_o^o}\right]\right\} \quad \ldots\ldots\ldots \quad (B.18)$$

$$\therefore \quad \frac{dJ}{\Delta} = 1 - \frac{e^{-pT}}{e\bar{M}_o^o} \quad \text{since} \quad \Delta << 1 \quad \ldots\ldots\ldots \quad (B.19)$$

This is the same expression as MICHELSEN and OSTERGAARD (50) except that their $t\bar{M}_o^o$ is now replaced by $e\bar{M}_o^o$.

From eq. 5.10 of the main text:

$$t^Q = \frac{t\bar{M}_b^1}{t\bar{M}_1^o} - \frac{t\bar{M}_o^1}{t\bar{M}_o^o} \quad \ldots\ldots\ldots \quad (B.20)$$

and $$e^Q = \frac{e\bar{M}_1^1}{e\bar{M}_1^o} - \frac{e\bar{M}_o^1}{e\bar{M}_o^o} \quad \ldots\ldots\ldots \quad (B.21)$$

From eq. B.11 and B.12 substituting for ${}_t\bar{M}_o^1$ and ${}_t\bar{M}_o^o$ into B.20

we find $dQ = {}_eQ - {}_tQ = \dfrac{(1+\Delta)\ {}_e\bar{M}_o^1 - T\Delta e^{-pT}}{(1+\Delta)\ {}_e\bar{M}_o^o - \Delta e^{-pT}} - \dfrac{{}_e\bar{M}_o^1}{{}_e\bar{M}_o^o}$

Simplifying we find on neglecting second and higher order terms in Δ

$$\frac{dQ}{\Delta} = \frac{e^{-pT}}{{}_e\bar{M}_o^o}\left\{ T - \frac{{}_e\bar{M}_o^1}{{}_e\bar{M}_o^o} \right\} \qquad \ldots\ldots\ldots \qquad (B.22)$$

Again comparison with MICHELSEN and OSTERGAARD (50) shows that ${}_e\bar{M}_o^o$ and ${}_e\bar{M}_o^1$ can be substituted for their ${}_t\bar{M}_o^o$ and ${}_t\bar{M}_o^1$ respectively.

The term ${}_e\bar{M}_o^o$ in the denominator is however missing from eq.49 of their paper.

On substituting for $\frac{dQ}{\Delta}$, $\frac{dJ}{\Delta}$, ${}_eJ$ and ${}_eQ$ into eq.B.15 we may obtain the noise weighting function E(T). This requires the zeroth and first weighted moments of the experimentally recorded concentration curves at a particular value of p.

B.1.2 Method 2 weighting functions

The Dispersion Number is determined from eq.5.14 of the main text:

$$N_D = \frac{H}{2Q^2}\left\{ 1 - \frac{2pH}{Q} \right\}^{-\frac{1}{2}} \qquad \ldots\ldots\ldots \qquad (B.23)$$

A similar analysis to that used for method 1 may be undertaken to yield:

$$E(T) = -\left\{ \frac{2}{Q} + \frac{pH}{Q^2}\left[1 - \frac{2pH}{Q} \right]^{-1} \right\} \frac{dQ}{\Delta} + \left\{ \frac{1}{H} + \frac{P}{Q}\left[1 - \frac{2pH}{Q} \right]^{-1} \right\} \frac{dH}{\Delta} \qquad \ldots\ldots\ldots \qquad (B.24)$$

where $$\frac{dH}{\Delta} = \frac{e^{-pT}}{{}_e\bar{M}_o^o}\left\{ \left[T - \frac{{}_e\bar{M}_o^1}{{}_e\bar{M}_o^o} \right]^2 + \frac{{}_e\bar{M}_o^2}{{}_e\bar{M}_o^o} + \left[\frac{{}_e\bar{M}_o^1}{{}_e\bar{M}_o^o} \right]^2 \right\} \qquad \ldots\ldots\ldots \qquad (B.25)$$

Comparison with eq.50 of MICHELSEN and OSTERGAARD (50) indicates differences in sign and also the ${}_e\bar{M}_o^o$ denominator term is again missing.

B.2 Weighting Functions for the 2nd measurement point i = 1

In an identical manner we can consider a noise free response at the first measuring point i = 0, whilst noise occurs at the second measurement point i = 1. This will yield the noise weighting functions at the 2nd measurement point.

If the analysis is undertaken it will be found that expressions similar to eq.B.15 and B.24 are obtained except that:

(i) the sign of the function is now positive

(ii) the weighted moments used in evaluating $\frac{dJ}{\Delta}$, $\frac{dQ}{\Delta}$ and $\frac{dH}{\Delta}$ now refer to the second measurement point i.e. ${}_e\bar{M}^r_1$ replaces ${}_e\bar{M}^r_o$.

APPENDIX C A QUALITATIVE ASSESSMENT OF THE FORM OF THE NOISE WEIGHTING FUNCTIONS

The following analysis which holds equally for positive or negative noise shows that the form of the noise weighting functions E(t) as illustrated in Fig.5.1 is correct. These noise weighting functions are nearly always positive at the second measurement point and negative at the first measurement point.

If we consider positive noise at the 1st measurement point alone, then the error integral given in eq.5.23 will be negative since E(t) is negative. Thus ΔN_D will be negative by eq.5.22, hence from eq.5.20 ${}_tN_D > {}_eN_D$.

It is well known e.g. BISCHOFF and LEVENSPIEL (5), that the Dispersion Number for the axially dispersed plug flow model when end effects are absent is proportional to the difference in variance between the tracer curves at the 2nd and 1st measurement points.

Thus $N_D \alpha (\sigma_1^2 - \sigma_o^2)$ ..... (C.1)

Assuming the true Dispersion Number ${}_tN_D$ is obtained when there is no noise on either input or output curves then:

$$\therefore {}_tN_D \alpha ({}_t\sigma_1^2 - {}_t\sigma_o^2) \quad \text{.....} \quad \text{(C.2)}$$

For positive error at the 1st measurement point the variance of this response curve will increase so that ${}_e\sigma_o^2 > {}_t\sigma_o^2$. Thus ${}_tN_D > {}_eN_D$ is in agreement with the predictions of the noise weighting functions.

For positive noise at the 2nd measurement point ${}_e\sigma_1^2 > {}_t\sigma_1^2$, hence from eq.C.2 it is clear that ${}_eN_D > {}_tN_D$. This result is also obtained from eq.5.22 since ΔN_D is now positive.

APPENDIX D BASIC EXPERIMENTAL DATA

Particle Diameter	dp	5 mm
Column Diameter	d_t	101.6 mm
Column Cross-Sectional Area	A_t	8.107×10^{-3} m^2
Test Section Length	L	0.835 m
Bed Voidage	e	0.356
Viscosity of air	μ_G	1.7×10^{-5} Nsm^{-2}
Viscosity of water	μ_L	1.0×10^{-3} Nsm^{-2}

Calculation of Reynolds Numbers based on Open Tower:

$$Re_L = \frac{L_M}{A_t} \frac{dp}{\mu_L}$$ where L_M = Liquid Mass Velocity $kg\,s^{-1}$

$$Re_L = 616.75\ L_M$$

$$Re_G = \frac{G_M}{A_t} \frac{dp}{\mu_G}$$ where G_M = Gas Mass Velocity $kg\,s^{-1}$

$$Re_G = 3.63 \times 10^4\ G_M$$

Limits of Experimental Universe

PHASE	UPPER LIMIT			LOWER LIMIT		
	Mass Velocity kgs^{-1}	Reynolds Number	Open Tower Velocity ms^{-1}	Mass Velocity kgs^{-1}	Reynolds Number	Open Tower Velocity ms^{-1}
GAS	0.00827	300.3	.783	0.00081	29.3	.076
LIQUID	0.225	138.8	.028	0.0639	39.4	.0079

APPENDIX E RESULTS OF SINGLE PHASE LIQUID DISPERSION RESULTS

The Dispersion Numbers are determined using the four methods derived for the Basic Axially Dispersed Plug Flow Model.

RUN NO.	LIQUID MASS RATE $X10^{-2}$ kgs^{-1}	REYNOLDS NUMBER Re_L	DISPERSION NUMBER N_D				LIQUID HOLD UP ϕ_L
			I	II	III	IV	
1	7.89	48.7	.0125	.0122	.0125	.0122	.990
2	11.17	68.9	.0086	.0085	.0087	.0085	1.000
3	12.00	74.0	.0089	.0089	.0089	.0088	1.008
4	12.00	74.0	.0089	.0089	.0089	.0089	.990
5	12.00	74.0	.0084	.0085	.0084	.0084	1.002
6	14.50	89.4	.0091	.0090	.0091	.0091	1.02
7	17.60	108.5	.0083	.0084	.0083	.0084	1.03
8	17.60	108.5	.0082	.0082	.0081	.0080	1.019
9	17.60	108.5	.0079	.0078	.0079	.0077	1.02
10	17.60	108.5	.0081	.0082	.0081	.0081	1.014
11	17.60	108.5	.0081	.0081	.0081	.0081	1.02

APPENDIX F RESULTS OF AXIALLY DISPERSED PLUG FLOW MODEL

Run Number	Re_L	Re_G	Dispersion Number N_D				Average holdup ϕ_L
			I	II	III	IV	
1	39.4	29.3	0.014	0.014	0.014	0.014	0.68
2	"	56.6	0.013	0.013	0.013	0.013	0.60
3	"	110.8	0.029	0.029	0.029	0.029	0.50
4	"	133.4	0.033	0.032	0.033	0.032	0.45
5	"	165.4	0.021	0.021	0.022	0.021	0.41
6	"	195.0	0.036	0.032	0.037	0.033	0.40
7	"	222.3	0.027	0.028	0.028	0.028	0.41
8	"	222.3	0.028	0.025	0.029	0.025	0.38
9	"	278.5	0.046	0.048	0.047	0.047	0.39
10	48.7	31.2	0.023	0.022	0.023	0.020	0.67
11	"	59.7	0.017	0.017	0.017	0.017	0.60
12	"	87.4	0.016	0.016	0.016	0.016	0.53
13	"	120.9	0.026	0.025	0.025	0.025	0.48
14	"	154.1	0.035	0.034	0.034	0.033	0.47
15	"	183.3	0.032	0.031	0.031	0.031	0.45
16	"	218.4	0.032	0.031	0.031	0.031	0.41
17	"	255.5	0.038	0.038	0.037	0.037	0.42
18	"	300.3	0.036	0.035	0.035	0.034	0.40
19	61.4	36.7	0.015	0.015	0.015	0.015	0.70
20	"	46.9	0.019	0.019	0.019	0.019	0.69
21	"	56.6	0.018	0.018	0.018	0.018	0.65
22	"	66.3	0.016	0.015	0.016	0.015	0.60
23	"	78.0	0.023	0.022	0.022	0.022	0.595
24	"	89.7	0.021	0.021	0.021	0.021	0.57
25	"	101.4	0.014	0.014	0.014	0.014	0.52
26	"	101.4	0.015	0.015	0.015	0.015	0.51
27	"	297.2	0.017	0.016	0.017	0.015	0.38
28	68.9	30.4	0.011	0.011	0.011	0.010	0.65
29	"	57.3	0.013	0.013	0.013	0.013	0.61
30	"	83.5	0.013	0.012	0.013	0.012	0.53
31	"	122.9	0.012	0.011	0.012	0.011	0.51
32	"	155.2	0.008	0.008	0.008	0.008	0.44
33	78.6	40.2	0.013	0.013	0.013	0.013	0.70
34	"	67.5	0.015	0.015	0.015	0.015	0.54
35	"	117.0	0.009	0.009	0.009	0.009	0.50
36	"	117.0	0.007	0.007	0.007	0.007	0.49

Run Number	Re_L	Re_G	Dispersion Number N_D				Average Holdup ϕ_L
			I	II	III	IV	
37	78.6	156.0	0.013	0.013	0.014	0.012	0.45
38	"	183.3	0.007	0.007	0.007	0.007	0.41
39	"	223.9	0.009	0.010	0.009	0.010	0.40
40	"	255.5	0.010	0.011	0.010	0.011	0.40
41	"	294.5	0.011	0.012	0.011	0.012	0.39
42	89.4	28.5	0.010	0.010	0.011	0.010	0.77
43	"	56.9	0.013	0.013	0.013	0.013	0.65
44	"	80.0	0.015	0.015	0.015	0.015	0.62
45	"	122.9	0.021	0.022	0.021	0.021	0.54
46	"	157.6	0.018	0.019	0.018	0.018	0.47
47	"	183.3	0.012	0.013	0.012	0.012	0.45
48	"	216.5	0.011	0.011	0.011	0.011	0.42
49	"	314.4	0.005	0.006	0.005	0.006	0.40
50	"	314.4	0.008	0.009	0.008	0.008	0.40
51	98.7	29.3	0.011	0.012	0.011	0.012	0.73
52	"	52.8	0.011	0.011	0.011	0.011	0.63
53	"	75.7	0.007	0.007	0.007	0.007	0.59
54	"	95.2	0.014	0.014	0.014	0.014	0.57
55	"	115.5	0.015	0.016	0.015	0.015	0.53
56	"	156.0	0.012	0.012	0.012	0.012	0.51
57	"	200.5	0.010	0.010	0.010	0.010	0.45
58	120.3	31.2	0.015	0.016	0.015	0.015	0.75
59	"	31.2	0.015	0.015	0.015	0.014	0.76
60	"	55.8	0.015	0.015	0.015	0.014	0.66
61	"	78.4	0.007	0.007	0.007	0.007	0.57
62	"	92.8	0.010	0.010	0.010	0.010	0.54
63	"	122.9	0.011	0.012	0.011	0.011	0.52
64	"	122.9	0.012	0.012	0.012	0.012	0.52
65	"	156.0	0.008	0.008	0.008	0.008	0.48
66	"	179.4	0.010	0.010	0.010	0.010	0.46
67	138.8	32.8	0.006	0.006	0.006	0.006	0.71
68	"	54.2	0.010	0.010	0.010	0.010	0.64
69	"	75.3	0.009	0.009	0.009	0.009	0.60
70	"	102.2	0.006	0.006	0.006	0.006	0.54
71	"	124.8	0.006	0.006	0.006	0.006	0.51
72	"	159.9	0.008	0.008	0.008	0.008	0.49
73	"	196.6	0.010	0.011	0.010	0.011	0.48

APPENDIX G RESULTS OF LIQUID STAGNANCY MODEL FROM TRANSFER FUNCTION FITTING

Run Number	Re_L	Re_G	Dispersion Number N_D	Number of Transfer Units N_T	Liquid Flow Fraction γ	Liquid Holdup ϕ_L	Mean Prediction Error %
1	39.4	29.3	0.0021	1.63	0.863	0.677	0.0159
2	"	56.6	0.0014	1.75	0.856	0.594	0.0040
3	"	110.8	0.0059	0.53	0.877	0.505	0.0025
4	"	133.4	0.0056	0.31	0.895	0.454	0.0087
5	"	165.4	0.0	0.889	0.852	0.411	0.0097
6	"	195.0	0.018	$4x10^{45}$	1.0	0.392	0.221
7	"	222.3	0.0	0.556	0.860	0.411	0.0139
8	"	222.3	0.0	0.285	0.898	0.380	0.0912
9	"	278.5	0.032	$4x10^{45}$	1.0	0.386	0.314
10	48.7	31.2	0.0	0.459	0.903	0.673	0.0178
11	"	59.7	0.0	1.245	0.846	0.597	0.0098
12	"	87.4	0.0	0.972	0.865	0.532	0.0155
13	"	120.9	0.0	0.537	0.864	0.484	0.0284
14	"	154.1	0.0086	0.186	0.899	0.475	0.0014
15	"	183.3	0.0	0.554	0.839	0.448	0.0182
16	"	218.4	0.0	0.451	0.849	0.414	0.0149
17	"	255.5	0.0058	0.459	0.849	0.426	0.0003
18	"	300.3	0.0051	0.327	0.871	0.401	0.0120
19	61.4	36.7	0.0	0.971	0.866	0.700	0.0077
20	"	46.9	0.0	1.272	0.833	0.691	0.0287
21	"	56.6	0.0	0.899	0.857	0.652	0.0087
22	"	66.3	0.0	0.653	0.884	0.603	0.0118
23	"	78.0	0.0013	0.867	0.846	0.597	0.0111
24	"	89.7	0.0	0.935	0.839	0.569	0.0107
25	"	101.4	0.0	0.902	0.871	0.520	0.0143
26	"	101.4	0.0	1.248	0.848	0.510	0.0067
27	"	297.2	0.0	0.316	0.905	0.386	0.0079
28	68.9	30.4	0.0	0.769	0.899	0.646	0.0111
29	"	57.3	$1.7x10^{-9}$	1.138	0.863	0.610	0.0275
30	"	83.5	0.0	0.430	0.910	0.532	0.0211
31	"	122.9	0.0	0.951	0.880	0.508	0.0132
32	"	155.2	0.0	2.244	0.855	0.436	0.0053
33	78.6	40.2	0.0	0.871	0.878	0.700	0.0089
34	"	67.5	0.0	1.245	0.849	0.541	0.0021
35	"	117.0	0.0	0.895	0.898	0.496	0.0043

Run Number	Re_L	Re_G	N_D	N_T	γ	ϕ_L	Error %
36	78.6	117.0	0.0	2.345	0.863	0.490	0.0140
37	"	156.0	0.0	0.557	0.895	0.454	0.0128
38	"	183.3	0.0	1.284	0.893	0.406	0.0101
39	"	223.9	0.0	0.696	0.906	0.404	0.0065
40	"	255.5	0.0	0.573	0.907	0.400	0.0124
41	"	294.5	0.0	0.237	0.928	0.395	0.0173
42	89.4	28.5	0.0	1.201	0.876	0.768	0.0052
43	"	56.9	0.013	2.174	0.831	0.651	0.0006
44	"	80.0	0.0086	2.030	0.818	0.619	0.0021
45	"	122.9	0.0	0.550	0.856	0.550	0.0245
46	"	157.6	0.0	0.697	0.863	0.472	0.0094
47	"	183.3	0.0	1.32	0.855	0.452	0.0095
48	"	216.5	0.0	0.492	0.907	0.426	0.0123
49	"	314.4	0.0	0.877	0.901	0.402	0.0070
50	"	314.4	0.005	0.0	1.00	0.394	0.0276
51	98.7	29.3	0.0	4.497	0.765	0.733	0.0052
52	"	52.8	0.0014	0.579	0.912	0.635	0.005
53	"	75.7	0.0014	0.376	0.942	0.586	0.009
54	"	95.2	0.0	1.21	0.852	0.567	0.0082
55	"	115.5	0.0	0.673	0.877	0.532	0.0093
56	"	156.0	0.0	0.637	0.893	0.507	0.013
57	"	200.5	0.0	0.156	0.936	0.450	0.021
58	120.3	31.2	0.0	0.677	0.875	0.752	0.016
59	"	31.2	0.0	0.742	0.873	0.776	0.011
60	"	55.8	0.0	0.811	0.868	0.663	0.010
61	"	78.4	0.0024	3.17	0.872	0.566	0.0033
62	"	92.8	0.0027	1.768	0.881	0.537	0.0097
63	"	122.9	0.0	0.774	0.887	0.527	0.0086
64	"	122.9	0.00035	1.795	0.842	0.524	0.0057
65	"	156.0	0.0	1.554	0.878	0.477	0.0077
66	"	179.4	0.0	0.455	0.912	0.464	0.019
67	138.8	32.8	0.004	6.704	0.886	0.707	0.0017
68	"	54.2	0.0	0.855	0.888	0.638	0.0101
69	"	75.3	0.0	1.867	0.855	0.597	0.0072
70	"	102.2	0.0048	5.204	0.904	0.538	0.0073
71	"	124.8	0.0013	2.056	0.890	0.512	0.0096
72	"	159.9	0.0024	2.57	0.877	0.487	0.0049
73	"	196.6	0.0	0.339	0.915	0.484	0.0257

APPENDIX H RESULTS OF SPLIT FLOW MODEL FROM TRANSFER FUNCTION FITTING

Run	Re_L	Re_G	Volume Flow Split X_1	Area Split X_2	Liquid only N_{D1}	N_{D2}	ϕ_L	Mean % Prediction Error
1	39.4	29.3	0.996	0.990	0.0103	1.92×10^{-7}	0.68	0.0147
2	"	56.6	0.998	0.992	0.0103	4.36×10^{-7}	0.60	0.0090
3	"	110.8	0.857	0.792	0.0101	0.0337	0.51	0.0005
4	"	133.4	0.883	0.826	0.0101	0.0858	0.45	0.0006
5	"	165.4	0.041	0.078	0.0122	0.0094	0.41	0.0005
6	"	195.0	0.974	0.927	0.0101	0.0077	0.40	0.003
7	"	222.3	0.963	0.918	0.0101	0.0020	0.41	0.0014
8	"	222.3	0.987	0.952	0.0102	4.0×10^{-7}	0.38	0.0988
9	"	278.5	0.903	0.807	0.0100	0.0109	0.39	0.0017
10	48.7	31.2	0.995	0.976	0.0097	9.0×10^{-7}	0.68	0.0270
11	"	59.7	0.424	0.498	0.0101	3.2×10^{-8}	0.60	0.0201
12	"	87.4	0.105	0.152	0.0107	0.0051	0.53	0.0153
13	"	120.9	0.932	0.885	0.0096	0.1113	0.49	0.0091
14	"	154.1	0.873	0.794	0.0095	0.0817	0.47	0.0005
15	"	183.3	0.907	0.834	0.0095	0.0452	0.45	0.0024
16	"	218.4	0.941	0.872	0.0095	0.0155	0.42	0.0017
17	"	255.5	0.834	0.739	0.0094	0.0382	0.43	0.0009
18	"	300.3	0.912	0.832	0.0095	0.0224	0.40	0.0123
19	61.4	36.7	0.025	0.049	0.0109	0.0085	0.70	0.0005
20	"	46.9	0.418	0.500	0.0096	6.9×10^{-9}	0.69	0.0362
21	"	56.6	0.037	0.070	0.0108	0.0090	0.65	0.0005
22	"	66.3	0.022	0.048	0.0113	0.0082	0.60	0.0003
23	"	78.0	0.868	0.814	0.0089	0.0460	0.60	0.0017
24	"	89.7	0.879	0.830	0.0089	0.0565	0.57	0.0006
25	"	101.4	0.012	0.030	0.0117	0.0945	0.52	0.0001
26	"	101.4	0.944	0.917	0.0905	0.0494	0.51	0.0004
27	"	297.2	0.116	0.185	0.0103	8.9×10^{-9}	0.39	0.0114
28	68.9	30.4	0.999	0.996	0.0088	4.0×10^{-7}	0.64	0.045
29	"	57.3	0.445	0.512	0.0092	1.5×10^{-7}	0.61	0.0340
30	"	83.5	0.995	0.982	0.0088	5.1×10^{-7}	0.53	0.0298
31	"	122.9	0.994	0.981	0.0088	3.7×10^{-7}	0.51	0.0027
32	"	155.2	0.433	0.477	0.0091	0.0013	0.44	0.0054
33	78.6	40.2	0.024	0.048	0.0102	0.0075	0.70	0.0006
34	"	67.5	0.367	0.443	0.0089	1.5×10^{-8}	0.54	0.0098
35	"	117.0	0.056	0.075	0.0092	0.0043	0.49	0.0151
36	"	117.0	0.999	0.999	0.0085	4.0×10^{-7}	0.49	0.0497

Run	Re_L	Re_G	Volume Flow Split X_1	Area Split X_2	Liquid only N_{D1}	N_{D2}	ϕ_L	Mean % Prediction Error
37	78.6	156.0	0.983	0.961	0.0085	0.0731	0.46	0.0013
38	"	183.3	0.424	0.469	0.0088	9.6×10^{-8}	0.41	0.0107
39	"	223.9	0.228	0.284	0.0091	1.8×10^{-4}	0.40	0.0080
40	"	255.5	0.997	0.983	0.0085	2.5×10^{-7}	0.40	0.0405
41	"	294.5	0.014	0.040	0.0112	0.0058	0.40	0.0009
42	89.4	28.5	0.995	0.986	0.0082	1.7×10^{-7}	0.77	0.0065
43	"	56.9	0.518	0.583	0.0085	2.0×10^{-6}	0.65	0.0017
44	"	80.0	0.458	0.533	0.0086	1.4×10^{-6}	0.62	0.0018
45	"	122.9	0.888	0.832	0.0081	0.1055	0.55	0.0012
46	"	157.6	0.928	0.881	0.0081	0.0378	0.47	0.0001
47	"	183.3	0.013	0.028	0.0102	0.0092	0.45	0.0002
48	"	216.5	0.016	0.037	0.0104	0.0067	0.43	0.0006
49	"	314.4	0.525	0.506	0.0082	3.6×10^{-8}	0.39	0.0204
50	"	314.4	0.373	0.427	0.0085	3.2×10^{-8}	0.40	0.0109
51	98.7	29.3	0.671	0.721	0.0082	6.8×10^{-9}	0.73	0.0058
52	"	52.8	0.988	0.974	0.0080	0.0429	0.64	0.0022
53	"	75.7	0.099	0.135	0.0087	0.0019	0.59	0.0095
54	"	95.2	0.593	0.656	0.0082	1.4×10^{-8}	0.56	0.0524
55	"	115.5	0.032	0.064	0.0097	0.0081	0.53	0.0005
56	"	156.0	0.015	0.036	0.0101	0.0075	0.51	0.0003
57	"	200.5	0.061	0.110	0.0094	3.5×10^{-4}	0.45	0.0256
58	120.3	31.2	0.019	0.046	0.0096	0.0095	0.75	0.0005
59	"	31.2	0.021	0.047	0.0094	0.0093	0.78	0.0002
60	"	55.8	0.030	0.060	0.0091	0.0086	0.66	0.0022
61	"	78.4	0.471	0.504	0.0077	0.0031	0.57	0.0044
62	"	92.8	0.976	0.967	0.0076	0.0923	0.54	0.0006
63	"	122.9	0.724	0.770	0.0077	1.0×10^{-7}	0.53	0.0543
64	"	122.9	0.989	0.959	0.0075	2.6	0.54	0.0379
65	"	156.0	0.440	0.490	0.0078	4.4×10^{-8}	0.48	0.0086
66	"	179.4	0.156	0.215	0.0083	5.9×10^{-5}	0.46	0.0218
67	138.8	32.8	0.517	0.507	0.0073	0.0041	0.71	0.0016
68	"	54.2	0.427	0.490	0.0076	3.6×10^{-8}	0.64	0.0287
69	"	75.3	0.980	0.970	0.0073	0.1072	0.60	0.0002
70	"	102.2	0.006	0.004	0.0067	0.0062	0.54	0.0067
71	"	124.8	0.377	0.411	0.0075	0.0025	0.51	0.0096
72	"	159.9	0.503	0.494	0.0073	0.0078	0.49	0.0118
73	"	196.6	0.013	0.038	0.0098	0.0069	0.49	0.0016

REFERENCES

1 ARIS R
Notes on the diffusion-type model for longitudinal mixing in flow
Chem.Eng.Sci. (1959), 9, 266

2 ASTARITA G
Mass Transfer with Chemical Reaction Elsevier 1967

3 BEIMESCH W E, KESSLER D P
Liquid-Gas Distribution Measurements in the pulsing regime of Two phase Concurrent flow in Packed Beds
A.I.Ch.E.J. (1971), 17, 1160

4 BISCHOFF K B
Notes on the diffusion type model for longitudinal mixing in flow
Chem.Eng.Sci. (1960), 12, 69

5 BISCHOFF K B, LEVENSPIEL O
Fluid dispersion - generalisation and comparison of mathematical models
Chem.Eng.Sci.(1962), 17, 245, 257

6 BRADLEY D
The Hydrocyclone - International Series of Monographs in Chemical Engineering. Pergamon Press 1965

7 BUCHANAN J E
Holdup in Irrigated Ring-Packed Towers below the loading point
Ind.Eng.Chem.Fund. (1967), 6, 400

8 BUFFHAM B A
On the residence-time distribution for a system with velocity profiles in its connections with the environment
Chem.Eng.Sci. (1972), 27, 987

9 BUFFHAM B A, GIBILARO L G
A Generalization of the Tanks in Series Mixing Model
A.I.Ch.E. (1968), 14, 805

10 BUFFHAM B A, GIBILARO L G, RATHOR M N
A Probabilistic Time delay Description of Flow in Packed Beds
A.I.Ch.E.J. (1970), 16, 218

11 CHARPENTIER J C, PROST C, LE GOFF P
Chute de pression pour des ecoulements a co-courant dans les colonnes a garnissage arrose : comparaison avec le garnissage noye
Chem.Eng.Sci. (1969), 24, 1777

12 CHUNG S F, WEN C Y
Longitudinal Dispersion of Liquid flowing through Fixed and Fluidised Beds
A.I.Ch.E.J. (1968), 14, 857

13 CLEMENTS W C
A note on determination of the parameters of the longitudinal dispersion model from experimental data
Chem.Eng.Sci. (1969), 24, 957

14 CLEMENTS W C
Correspondence on Comparison of Moments, S-Plane, and Frequency Response Methods for Analysing Pulse Testing Data from Flow Systems
Ind. Eng. Chem. Proc. Desg.Dev. (1972), 11, 461

15 CLEMENTS W C, SCHNELLE K B
Pulse Testing for Dynamic Analysis
Ind.Eng.Chem. P.D.D. (1963), 2, 94

16 DANCKWERTS P V
Continuous Flow Systems - Distribution of Residence Times
Chem.Eng.Sci. (1953), 2, 1

17 DANCKWERTS P V, SHARMA M M
The Absorption of Carbon Dioxide into solutions of Alkalis and Amines
Chem.Engineer (1966), No.202, 244

18 DUNN E W, VERMEULEN T, WILKES C R, WORD T T
Longitudinal mixing in packed gas absorption columns
Univ.California Radiation Lab. Report 10394 (1962)

19 EDWARDS M F
Gas flow patterns in beds of particles
University of Wales (1966) PhD Thesis

20 EISENKLAM P, FORD L H
Cocurrent Two-Phase Flow through Packed Beds
Proc of the Symp on the interaction between Fluids and Particles
Inst.Chem.Engs. June (1962), 333

21 ERGUN S
Fluid Flow through Packed Columns
Chem.Eng. Progr. (1952), 48, 89

22 FORD L H
Multiphase Flow through Porous Media, with Special Reference to the Turbulent Regime
PhD. Thesis (1960), University of London

23 FURZER I A, MICHELL R W
Liquid-Phase Dispersion in Packed Beds with Two-Phase Flow
A.I.Ch.E.J. (1970), 16, 380

24 GIANETTO A, SPECCHIA V, BALDI G
Absorption in Packed Towers with Concurrent Downward High-Velocity Flows - II : Mass Transfer
A.I.Ch.E.J. (1973), 19, 916

25 GLASER M B, LICHTENSTEIN I
Interrelation of Packing and mixed phase flow parameter with liquid residence time distribution
A.I.Ch.E.J. (1963), 9, 30

26 GLASER M B, LITT M
A Physical model for Mixed Phase flow through beds of porous particles.
A.I.Ch.E. (1963), 9, 103

27 GOTTSCHLICH C F
Axial Dispersion in a Packed Bed
A.I.Ch.E. (1963), 9, 88

28 GUNN D J
Mixing in Packed and Fluidised Beds
Chemical Engineer (1968), 46, CE153

29 HARRISON D, LANE M, WALNE J D
Axial Dispersion of liquid on a column of spheres
Trans.Inst.Chem.Engs. (1962), 40, 214

30 HARRISON R E,FELDER R M
Accuracy of parameter estimation by Frequency Response Analysis
Ind.Eng.Chem. Proc.Design Dev. (1974), 13, 389

31 HAYS J R, CLEMENTS W C, HARRIS T R
The Frequency Domain Evaluation of Mathematical Models for Dynamic Systems
A.I.Ch.E.J. (1967), 13, 374

32 HELSBY F W
Mass Transfer in Liquid/Gas Systems, with Special Reference to the Use of Foams.
PhD. Thesis, University of London (1958)

33 HOCHMAN J M, EFFRON E
Two phase Cocurrent Downflow in Packed Beds
Ind.Eng.Chem.Fund. (1969), 8, 63

34 HOOGENDORN C J, LIPS J
Axial Mixing of Liquid in Gas-Liquid flow through Packed Beds
Can.J.Chem.Eng. (1965), 43, 125

35 HOPKINS M J, SHEPPARD A J, EISENKLAM P
The Use of Transfer Functions in Evaluating Residence Time Distribution Curves
Chem.Eng.Sci. (1969), 24, 1131

36 HOUGAN J O, WALSH R A
Pulse Testing Method
Chem.Eng.Prog. (1961), 57, 69

37 HUTTON B E T, LEUNG L S
Cocurrent Gas-Liquid Flow in Packed Columns
Chem.Eng.Sci. (1974), 29, 1681

38 JEFFRESON C P
Dynamic testing - a unification
Chem.Eng.Sci. (1970), 25, 1319

39 JOHNSON J L, FAN L T
An observation concerning pulse testing of flow systems
A.I.Ch.E.J. (1966), 12, 1026

40 JOHNSON J L, FAN L T, WU Y S
Comparison of Moments, S-Plane, and Frequency Response Methods for Analysing Pulse Testing Data from Flow Systems
Ind.Eng.Chem. Proc.Design Dev. (1971), 10, 425

41 KRAMERS H, ALBERDA G
Frequency response analysis of continuous flow systems
Chem.Eng.Sci. (1953), 2, 173

42 LAPIDUS L
Flow Distribution and Diffusion in Fixed-Bed Two-Phase Reactors
Ind.Eng.Chem. (1957), 49, 1000

43 LARKINS R P, WHITE R R, JEFFREY D W
Two Phase Concurrent Flow in Packed Beds
A.I.Ch.E.J. (1961), 7, 231

44 LEVENSPIEL O, TURNER J C R
The interpretation of residence-time experiments
Chem.Eng.Sci. (1970), 25, 1605

45 LEVENSPIEL O, LAI B W, CHATLYNNE C Y
Tracer curves and residence time distribution
Chem.Eng.Sci. (1970), 25, 1611

46 LOBO W E, FRIEND L, HASHMALL L, ZENZ F
Limiting Capacity of Dumped Tower Packings
Trans A.I.Ch.E. (1945), 41, 693

47 LOCKHART R W, MARTINELLI R C
Proposed Correlation of Data for Isothermal Two Phase Two Component Flow in Pipes
Chem.Eng.Prog. (1949), 45, 39

48 LUCAS B R
An Experimental Development of a Gas Liquid Cyclone
August 1968 3rd Year Research Project. Imperial College

49 MCILVROID H G
Mass Transfer in Cocurrent Gas-Liquid Flow through a Packed Column
PhD. Thesis (1956), Carnegie Institute of Technology.

50 MICHELSEN M L, ØSTERGAARD K
The use of residence time distribution data for estimation of parameters in the axial dispersion model
Chem.Eng.Sci. (1970), 25, 583

51 MITAUCHI T, VERMEULEN T
Diffusion and Back Flow Models for Two Phase Axial Dispersion
Ind.Eng.Chem.Fund. (1963), 2, 305

52 MURTAGH B A, SARGENT R W H
A Constrained Minimisation Method with Quadratic Convergence.
Presented at the Institute of Mathematics and its Applications and British Computer Society Joint Conference on 'Optimisation' University of Keele, March 1968.

53 NAOR P, SHINNAR R
Representation and Evaluation of Residence Time Distributions
Ind.Eng.Chem.Fund. (1963), 2, 278

54 OTTO E, GESTRICH W
The Exponential tracer input signal for determining residence time distributions
Chem.Eng.Sci. (1974), 29, 1294

55 POWELL M D.
An Efficient Method for finding the minimum of a function of several variables without calculating derivatives.
Computer Journal (1964) 7, 155.

56 RAGHURAMAN J, VARMA Y B G
A model for residence time distribution in multistage systems with cross-flow between active and dead regions.
Chem.Eng.Sci. (1973), 28, 585

57 REISS L P
Cocurrent Gas-Liquid Contacting in Packed Columns
Ind.Eng.Chem. Process Design and Development (1967), 6, 486

58 REYNIER J P, CHARPENTIER J C
Holdup prediction in Packed Columns for Cocurrent Gas-Liquid Downflow
Chem.Eng.Sci. (1971), 26, 1781

59 ROSENBROCK H H, STOREY C
Computational Techniques for Chemical Engineers
Pergamon: 1st Edition 1966

60 SAADA M Y
Co-current Two-Phase Flow in Packed Beds, with special reference to Gas Absorption
PhD Thesis (1965) London University

61 SAADA M Y
Radiological assessment of liquid-phase mass transfer coefficients for cocurrent two phase flow in fixed beds
Chimie et Industrie-Genie Chimique (1969), 102, 1283

62 SAADA M Y
Assessment of Interfacial area in Cocurrent Two phase flow in Packed Beds
Chimie et Industrie-Genie Chimique (1972), 105, 1415

63 SATER V E, LEVENSPIEL O
Two Phase Flow in Packed Beds - Evaluation of Axial Dispersion and holdup by moments analysis.
Ind.Eng.Chem.Fundamentals (1966), 5, 86

64 SCHMALTZER D K, HOELSCHER H E
Detector Effects in Packed Bed Measurements
A.I.Ch.E.J. (1971), 17, 241

65 SCHOENEMANN K
Dechema Monograph (1952), 21, 203

66 SCHWARTZ J G, ROBERTS G W
An evaluation of models for liquid backmixing in Trickle Bed Reactors.
Ind.Eng.Chem.Process Design & Dev. (1973), 12, 262

67 SCOTT D S
Properties of Cocurrent Gas-Liquid Flow
Advances in Chemical Engineering (1963), 4, 199

68 SHENDE B W, SHARMA M M
Mass Transfer in Packed Columns : Cocurrent Operation
Chem.Eng.Sci. (1974), 29, 1763

69 SHESTOPALOV V V, KAGAROV V V, BLYAKHMAN L I
Longitudinal mixing in Packed Columns
Int.Chem.Eng. (1964), 4, 17

70 SPECCHIA V, SICARDI S, GIANETTO A
Absorption in Packed Towers with Concurrent upward flow
A.I.Ch.E.J. (1974), 20, 646

71 SWEENY D E
A correlation for Pressure Drop in Two-Phase Cocurrent flow in Packed Beds
A.I.Ch.E.J. (1967), 13, 663

72 TURNER J C R
The interpretation of residence-time measurements in systems with and without mixing
Chem.Eng.Sci. (1971), 26, 549

73 TURPIN J L, HUNTINGTON R L
Prediction of Pressure Drop for Two Phase Two Component Concurrent Flow in Packed Beds
A.I.Ch.E.J. (1967), 13, 1196

74 UFFORD R C, PERONA J J
Liquid Phase Mass Transfer with Concurrent Flow through Packed Beds
A.I.Ch . E.J. (1973), 19, 1223

75 VAN SWAAIJ W P M, CHARPENTIER J C, VILLERMAUX J
Residence Time Distribution in the liquid phase of trickle flow in Packed Columns.
Chem.Eng. Sci. (1969), 24, 1083

76 VILLERMAUX J, VAN SWAAIJ W P M
Modele representatif de la distribution des temps de sejour dans un reacteur semi-infini a dispersion axiale avec zones stagnantes. Application a l'ecoulement ruisselant dans des colonnes d'anneaux Raschig
Chem.Eng.Sci. (1969), 24, 1097

77 DE WAAL K J A, VAN MAMEREN A L
Pressure Drop, Liquid Holdup and Distribution, Residence time Distribution and Interfacial area between gas and liquid in one packed column.
A.I.Ch.E. I.Chem.E. (Symp.Ser) (1965), 6, 6

78 WEBER H H
Untersuchungen uber die Verweilzeitverteilung in Aufstromkolonnen
Diss.Tech.Hochschule, Darmstadt, Germany 1961.

79 WEEKMAN V M, MYERS J B
Fluid Flow Characteristics of Concurrent Gas-Liquid Flow in Packed Beds
A.I.Ch.E.J. (1964), 10, 951

80 WEN C Y, O'BRIEN W S, FAN L T
Mass Transfer in Packed Beds Operated Cocurrently
J Chem.Eng.Data (1963), 8, 42

81 WILLIAMS J A, ADLER R J, ZOLNER W J
Parameter Estimation of Unsteady-state Distributed Models in the Laplace Domain
Ind.Eng.Chem. Fund. (1970), 9, 193

82 YOSHIDA F, MIURA Y
Effective Interfacial area in Packed Columns for Absorption with Chemical Reaction
A.I.Ch.E.J. (1963), 9, 331

ERRATA AND ADDENDA

Page Number	Line Number	Amendment
16	Fig.2.5	In legend read Re_G^* for Re_G
53	eq. 4.20	$F(p) = \exp\left[\frac{1}{2N_D}\{1 - (1 + 4\tau p N_D \alpha)^{\frac{1}{2}}\}\right]$
69	20	... using the zeroth weighted moments.
86	29	Read Fig.6.2 for Fig.6.3.
108	19	insert the following after..... in Chapter 5.2. The values of the Laplace parameter used are listed in Appendix I.
115	Table 7.2	Confidence limits given for a and b constants are for b and c exponents respectively.
156	25	Read HOUGEN for HOUGAN in Reference 36.
158	9	Replace Reference 9 by .... MIYAUCHI T, VERMEULEN T Longitudinal Dispersion in Two Phase Continuous Operations. Ind.Eng.Chem.Fund. (1963), 2, 113.

APPENDIX I VALUES OF LAPLACE PARAMETER USED IN AXIALLY DISPERSED PLUG FLOW MODEL ANALYSIS

Run Number	τp values for methods I - IV			
	I	II	III	IV
1	.293	.195	.0976, .195, .293 .390, .488	.0976, .195, .293 .390, .488
2	.5	.4	.3, .4, .5, .6, .7	.2, .3, .4, .5, .6
3	.7	.5	.5, .6, .7, .8, .9	.3, .4, .5, .6, .7
4	.629	.449	.449, .539, .629 .719, .809	.269, .359, .449 .539, .629
5	.722	.516	.516, .619, .722 .825, .928	.309, .412, .516 .619, .722
6	.5	.4	.3, .4, .5, .6, .7	.2, .3, .4, .5, .6
7	.8	.5	.6, .7, .8, .9, 1.0	.3, .4, .5, .6, .7
8	.572	.477	.382, .477, .572, .668, .763	.286, .382, .477 .572, .668
9	.8	.5	.6, .7, .8, .9, 1.0	.3, .4, .5, .6, .7
10	.3	.3	0.1, .2, .3, .4, .5	.1, .2, .3, .4, .5
11	1.009	.606	.808, .909, 1.009, 1.211, 1.412	.404, .505, .606, .707, .808
12	.912	.608	.709, .810, .912, 1.013, 1.216	.405, .507, .608, .709, .810
13	.907	.605	.705, .806, .907, 1.007, 1.209	.403, .504, .605, .705, .806
14	1.009	.706	.807, .908, 1.009, 1.211, 1.413	.504, .606, .706, .807, .908
15	1.006	.704	.805, .905, 1.006, 1.207, 1.408	.503, .604, .704, .805, .905

Run Number	τp values for methods I - IV			
	I	II	III	IV
16	1.003	.702	.803, .902, 1.003, 1.204, 1.405	.502, .602, .702 .803, .902
17	1.048	.734	.838, .943, 1.048 1.258, 1.467	.523, .629, .734, .838, .943
18	.980	.686	.784, .882, .980 1.176, 1.372	.490, .588, .686 .784, .882
19	.995	.696	.796, .895, .995, 1.194, 1.393	.497, .597, .696, .796, .895
20	1.0	.7	.8,.9,1.0,1.2,1.4	.5, .6, .7, .8, .9
21	1.003	.702	.802, .903, 1.003, 1.204, 1.404	.502, .602, .702, .802, .903
22	1.006	.704	.804, .905, 1.006, 1.207, 1.408	.503, .603, .704, .804, .905
23	1.109	.776	.887, .998, 1.109, 1.331, 1.553	.555, .666, .776 .887, .998
24	1.203	.802	.902, 1.002, 1.203, 1.403, 1.603	.601, .702, .802, .902, 1.002
25	1.205	.803	.904, 1.004, 1.205, 1.406, 1.606	.602, .703, .803, .904, 1.004
26	1.137	.758	0.853, 0.948, 1.137, 1.327, 1.516	.569, .663, 0.758, .853, 0.948
27	1.132	.809	.809, .971, 1.132 1.294, 1.456	.647, .728, .809, .971, 1.132
28	1.0	.7	.8,.9,1.0,1.2,1.4	.5, .6, .7, .8, .9
29	1.211	.807	.908, 1.009, 1.211 1.413, 1.615	.606, .707, .807 .908, 1.009
30	1.203	.802	.902, 1.003, 1.203, 1.404, 1.604	.602, .702, .802, .902, 1.003

Run Number	τp values for methods I - IV			
	I	II	III	IV
31	1.404	.903	1.003, 1.203, 1.404, 1.604, 1.805	.702, .802, .903 1.003, 1.203
32	1.384	.889	.988, 1.186, 1.384 1.582, 1.782	.692, .791, .889, .988, 1.186
33	1.267	.845	.950, 1.056, 1.267 1.478, 1.689	.634, .739, .845, .950, 1.056
34	1.361	.875	.972, 1.167, 1.361, 1.556, 1.751	.681, .778, .875, .972, 1.167
35	1.393	.895	.995, 1.194, 1.393, 1.592, 1.790	.696, .796, .895, .995, 1.194
36	1.462	.853	1.097, 1.218, 1.462, 1.706, 1.949	.609, .731, .853, .975, 1.097
37	1.328	.854	.949, 1.138, 1.328, 1.518, 1.708	.664, .759, .854, .949, 1.138
38	1.396	.898	.997, 1.197, 1.396, 1.596, 1.795	.698, .798, .898, .997, 1.197
39	1.484	.848	1.059, 1.272, 1.484, 1.696, 1.908	.636, .742, .848, .954, 1.059
40	1.504	.859	1.074, 1.289, 1.504, 1.719, 1.934	.645, .752, .859, .967, 1.074
41	1.367	.781	.976, 1.171, 1.367, 1.562, 1.757	.586, .683, .781, .879, .976
42	1.404	.903	1.003, 1.204, 1.404, 1.605, 1.806	.703, .803, .903, 1.003, 1.204
43	1.6	1.0	1.2,1.4,1.6,1.8,2.0	.8, .9, 1.0,1.2,1.4
44	1.611	1.007	1.208, 1.409, 1.611 1.812, 2.014	.806, .906, 1.007 1.208, 1.409
45	1.623	.913	1.218, 1.420, 1.623, 1.826, 2.029	0.710, .812, .913, 1.015, 1.218

Run Number	τ_p values for methods I - IV			
	I	II	III	IV
46	1.560	.878	1.170, 1.365, 1.560, 1.755, 1.950	.683, .780, .878, .975, 1.170
47	1.619	.911	1.215, 1.417, 1.619, 1.822, 2.024	.709, .810, .911, 1.012, 1.215
48	1.614	.908	1.210, 1.412, 1.614, 1.815, 2.017	.706, .807, .908, 1.009, 1.210
49	1.687	.937	1.312, 1.499, 1.687, 1.874, 2.062	.750, .843, .937, 1.125, 1.312
50	1.642	.912	1.277, 1.460, 1.642, 1.825, 2.007	.730, .821, .912, 1.095, 1.277
51	1.546	.994	1.104, 1.325, 1.546, 1.766, 1.987	.773, .883, .994, 1.104, 1.325
52	1.575	.875	1.225, 1.400, 1.575, 1.750, 1.926	.700, .788, .875, 1.050, 1.225
53	1.549	.968	1.162, 1.355, 1.549, 1.743, 1.936	.775, .871, .968, 1.162, 1.355
54	1.702	.957	1.277, 1.489, 1.702, 1.915, 2.128	.745, .851, .957, 1.064, 1.277
55	1.594	.897	1.196, 1.395, 1.594, 1.793, 1.993	.697, .797, .897, .996, 1.196
56	1.621	.912	1.216, 1.419, 1.621, 1.824, 2.027	.709, .811, .912, 1.013, 1.216
57	1.584	.863	1.150, 1.342, 1.584, 1.725, 1.917	.671, .767, .863, .959, 1.150
58	1.605	.903	1.204, 1.405, 1.605, 1.806, 2.007	.702, .803, .903, 1.003, 1.204
59	1.526	.954	1.145, 1.336, 1.526, 1.717, 1.908	.763, .859, .954, 1.145, 1.336
60	1.610	1.006	1.207, 1.409, 1.610, 1.811, 2.012	.805, .906, 1.006, 1.207, 1.409

Run Number	τp values for methods I - IV			
	I	II	III	IV
61	1.8	1.0	1.4, 1.6, 1.8, 2.0, 2.2	.8, .9, 1.0, 1.2, 1.4
62	1.785	1.020	1.275, 1.530, 1.785, 2.040, 2.295	.765, .892, 1.020, 1.148, 1.275
63	1.851	.926	1.481, 1.666, 1.851, 2.037, 2.222	.741, .833, .926, 1.111, 1.296
64	1.736	.964	1.350, 1.543, 1.736, 1.928, 2.121	0.771, .868, .964, 1.157, 1.350
65	1.900	.950	1.520, 1.710, 1.900, 2.090, 2.280	.760, .855, .950, 1.140, 1.330
66	1.772	.886	1.378, 1.575, 1.772, 1.969, 2.166	.689, .788, .886, .984, 1.181
67	1.793	.996	1.394, 1.594, 1.793, 1.992, 2.191	.797, .896, .996, 1.195, 1.394
68	1.8	1.0	1.4, 1.6, 1.8, 2.0, 2.2	.8, .9, 1.0, 1.2, 1.4
69	1.794	.997	1.396, 1.595, 1.794, 1.994, 2.193	.798, .897, .997, 1.196, 1.396
70	1.963	.976	1.562, 1.757, 1.963, 2.148, 2.343	.781, .879, .976, 1.172, 1.367
71	2.030	1.015	1.624, 1.827, 2.030, 2.233, 2.436	.812, .913, 1.015, 1.218, 1.421
72	2.004	1.002	1.603, 1.803, 2.004, 2.204, 2.405	.802, .902, 1.002 1.202, 1.403
73	1.888	.944	1.469, 1.678, 1.888, 2.098, 2.308	.734, .839, .944, 1.049, 1.259